WRC Report No. 209

IN SITU BIORECLAMATION OF CONTAMINATED GROUNDWATER

by

Bruce E. Rittmann
Albert J. Valocchi
Joseph E. Odencrantz
Wookeun Bae

Environmental Engineering and Science Department of Civil Engineering
University of Illinois at Urbana-Champaign

Project No. S-109-ILL
Jointly published as HWRIC Research Report No. 031

Water Resources Center
2535 Hydrosystems Laboratory
Urbana, IL 61801
December 1988

The work on which this report is based was supported in part by funds provided by the United States Department of the Interior as authorized under the Water Resources Research Act of 1984. The contents of this report do not necessarily reflect views and policies of the U.S. Department of the Interior, nor does mention of trade names or commercial products constitute their endorsement by the United States Government.

CONTENTS

LIST OF TABLES

LIST OF FIGURES

LIST OF ABBREVIATIONS

BAZ	biologically active zone
BF	bromoform
cpm	counts per minute
CTC	carbon tetrachloride
DCB	dichlorobenzene
EDB	ehtylene dibromide
SOC	soluble organic carbon
SMP	soluble microbial product
TeCE	tetrachoroethene
TCE	trichloroethene
1,1,1-TCA	1,1,1-trichloroethane
1,2-DCB	1,2-dichlorobenzene
1,3-DCB	1,3-dichlorobenzene
1,4-DCB	1,4-dichlorobenzene

ABSTRACT

This report summarizes the results of a research project aimed at developing a better mechanistic understanding of the phenomena controlling in situ biological activity. A methodology involving laboratory-column experiments and computer modeling was utilized to investigate the formation of biologically active zones (BAZs) when a limiting electron acceptor (NO_3^-) is injected along the flow path and the secondary utilization of trace-level pollutants contained in the water flowing through the BAZ. Laboratory experiments conducted in a unique one-dimensional porous-medium column demonstrated the relationship between lateral injection of NO_3^- and the location and extent of BAZs when acetate was present as the sole carbon source. BAZs established and sustained by acetate and NO_3^- were able to degrade trace-level halogenated compounds. Carbon tetrachloride was nearly completely removed, while bromoform, dibromomethane, trichloroethene, and tetrachloroethene were removed to lesser degrees. Trichloroethane was slightly removed. Dichlorobenzenes, previously thought to be refractory in denitrifying conditions, were removed by 20-30% during their passage through the BAZ.

The fundamental phenomena of BAZ formation and the utilization of limiting, nonlimiting, and secondary substrates were expressed quantitatively in a computer model that coupled principles of one-dimensional solute transport and steady-state-biofilm kinetics. A new, highly efficient solution algorithm was developed to solve directly for the steady-state profiles of the limiting substrate and biofilm mass, as well as for non-limiting and secondary substrates. The predictive ability of the model was verified by successful simulation of the laboratory experiments using independently determined kinetic parameters. The verified model was used to illustrate two possible strategies for field bioreclamation. First, the use of multiple injection points can decrease aquifer clogging potential by spreading out the extent of the BAZ. Second, injection of a supplementary carbon source can extend the length of the BAZ in order to achieve greater removals of secondary substrates.

In Situ Bioreclamation of Contaminated Groundwater

EXECUTIVE SUMMARY

In situ bioreclamation of contaminated groundwater is a promising new technique for enhancing the clean-up rate of aquifers contaminated with organic pollutants, such as chlorinated solvents, gasoline constituents, and pesticides. In situ bioreclamation involves injecting the materials necessary to significantly increase the microbiological activity in the subsurface. The injected material is a component that limits the growth of the desired microorganisms and is usually an electron acceptor (e.g., oxygen or nitrate), a carbon source, or a macro-nutrient (e.g., nitrogen or phosphorus). Injecting the proper amount of the limiting material creates a region of increased microbiological activity, called the Biologically Active Zone (BAZ).

Creation of a BAZ offers major advantages for aquifer clean-up because the removal agents, the bacteria, are in close proximity to all the contaminants, including those in the water, those sorbed to aquifer materials, and those in a nonaqueous liquid phase. Thus, the relatively slow mechanism of flushing by water flow is replaced by a degradation reaction very near the source of contaminants.

The direction of this study is towards an increased ability to understand and quantitatively describe the key phenomena affecting the formation of and reactions within a BAZ. The specific objectives are:

1. Develop a laboratory-scale, porous-medium column that can be used to create and study BAZs under well-defined conditions.

2. Evaluate the formation of one or more BAZs within the laboratory-scale column when the electron acceptor, nitrate, is injected into the flow path.

3. Using the laboratory-scale columns, evaluate the fate of commonly found halogenated solvents as they passed through the BAZs.

4. Develop and test an efficient computer model for the formation of BAZs and the utilization of substrates by the BAZs.

5. Apply the model to describe and interpret the formation of the BAZ and the fates of the various substrates in the column experiments.

6. Employ the model to evaluate strategies for <u>in situ</u> bioreclamation in the field.

The laboratory-scale, porous-medium columns were constructed of 2.5-cm inside diameter by 22.5-cm long glass tubes and were filled with 3-mm glass beads. Ports were placed every 2.5 cm to allow for sampling and/or injection. Special injection assemblies were designed to allow for uniform planar injection of substrate into the flow path. The systems gave an excellent approximation of one-dimensional flow.

The organic source was sodium acetate, which was available as a ^{14}C-radio-labelled tracer. It was fed continuously to the inlet end of the column from an elevated reservoir. In most experiments, the injected material was the electron acceptor, NO_3^-. One or two BAZs were established at and downstream of the injection ports. In order to ensure that NO_3^- was limiting, no other electron acceptors were added to the feed medium, and extreme measures were taken to preclude O_2 entry in the reservoir, feed lines, and columns.

Well-defined BAZs developed from the injection ports and up to 7.5 cm downstream of the injection ports. Photography of the intact columns and of the beads in the columns demonstrated that the bacterial growth was present as biofilms on the glass beads. Photography and measurements of biofilm mass on the beads confirmed that the amount of accumulated biofilm was greatest right after the injection port, and it gradually declined downstream.

Acetate (expressed as soluble organic carbon, SOC) and NO_3^- declined across the BAZs according to the expected stoichiometry, 0.67 mg NO_3^--N/mg SOC. For the column with two BAZs, removal of SOC was partial in the BAZ after the first injection port, because NO_3^- was depleted; however, SOC removal was essentially complete in the

second BAZ, as sufficient NO_3^- was supplied in the second injection. These results demonstrated that stoichiometric addition of an electron acceptor could be used to remove an electron-donor substrate to the degree desired.

Formation of N_2 gas bubbles occurred as a result of the denitrification of NO_3^-. These bubbles tended to accumulate in the BAZs and caused some short-circuiting, which led to a deterioration of SOC removal. Removal of the bubbles restored the SOC removal and demonstrated the possible deleterious effects of gas evolution within a confined aquifer.

Eight trace-concentration halogenated solvents were applied to the feed of the column having one BAZ. Two dichlorobenzenes were added together as a mixture, and six one- or two-carbon halogenated aliphatics were added as another mixture. Of the halogenated aliphatics, carbon tetrachloride was removed the most completely by the denitrifying BAZ. Tetrachloroethene, bromoform, ethylene dibromide, and trichloroethene were removed to lower degrees. Trichloroethane was slightly removed. 1,2 and 1,3 dichlorobenzene also were 20-30% removed during passage through the BAZ. Significant increases in the fractional removal were effected as the liquid flow velocity was decreased, which increased the contact time in the BAZ. These results are especially significant for two reasons. First, they show that common groundwater contaminants were degradable in the BAZs induced by NO_3^- injection. Most interesting are the removals of the dichlorobenzenes and trichloroethene, which were thought previously to be refractory under denitrifying conditions. Second, the results show that the removals of each compound depended upon the degradation kinetics of the particular compound and the contact time in the BAZ.

Modeling of the formation of a BAZ was based on application of biofilm kinetics to solute transport in porous media. The steady-state-biofilm model, developed originally by Rittmann and McCarty (1980a) and improved recently by Sáez and Rittmann (1988), was incorporated into a one-dimensional, steady-state, solute-transport equation. The equation was transformed from the differential form to one using discrete finite differences and solved numerically directly for the steady-state profiles of substrate concentration and

biofilm accumulation. Major modeling advancements were the ability to have lateral injection sources at any point along the column and the use of quasilinearization to give a highly efficient and direct solution for the steady state. The quasilinearization technique, which involves substituting a first-order Taylor series approximation for the highly nonlinear reaction term, made the convergence to steady state approximately ten times faster than by conventional methods. Even greater improvements are expected for more complicated geometries.

The modeling also was advanced by explicit coupling of the steady-state-biofilm model solution, which solves for the concentration profile of the limiting substrate and the amount of biofilm, to models for a non-limiting substrate and for secondary substrates. An example of a non-limiting substrate is $NO3^-$ when SOC is limiting; the flux of $NO3^-$ into the biofilm was set equal to the flux of SOC multiplied by a stoichiometric coefficient. Although the flux of the non-limiting substrate was determined by the flux of limiting substrate, it had its own rates of advection, dispersion, and injection. A secondary substrate is, in this context, a trace-level contaminant that is removed in the BAZ, even though its utilization provides negligible or no benefit to the microorganisms. The flux of secondary substrate was determined by its own kinetic characteristics and by the amount of biofilm accumulated through utilization of the SOC.

The steady-state, solute-transport model for the limiting substrate and the coupled transport model for the non-limiting substrate were used to evaluate the experiments on the formation of BAZs. Kinetic parameters for the utilization of the SOC were determined independently; thus, model results were true predictions. SOC, $NO3^-$, and biofilm profiles matched the experimental results very well for columns with one and two BAZs. Model predictions and experimental results agreed quantitatively that removals of SOC and $NO3^-$ and accumulation of biofilm were greatest in the first 2.5 cm beyond the injection port. Removal rates and biofilm accumulation declined gradually in the next 5.0 cm, and substrate concentrations attained a steady plateau value thereafter. Predictions and experimental results also concurred that injection of more of the limiting material ($NO3^-$ in this case) allowed formation of a second BAZ and renewed removal of SOC. The model predictions correctly described all trends,

and absolute deviations between predicted and experimental results were small in all cases.

The coupled transport model for secondary substrates also was used successfully for describing the removal of the halogenated aliphatic solvents. Since the kinetic parameters for each secondary substrate could not be determined independently, one set of results from the column experiments was used to obtain a best-fit set of kinetic parameters. These parameters were then used to predict the removal across the BAZ for experiments with different liquid flow velocities. Model and experimental results agreed well on the effect of liquid flow velocity. When the flow velocity was decreased, the contact time for the secondary substrates in the BAZ was increased proportionally. This increase in contact time allowed greater removal. For example, experimental and modeling results agreed that the removal of carbon tetrachloride through a BAZ should increase from 18% to 55% to 92% as the post-injection detention time increased from 50 minutes to 125 minute to 500 minutes, respectively.

The steady-state models were applied to investigate possible strategies to be used in field bioreclamations. The use of multiple injection wells was studied for its ability to decrease aquifer clogging potential by spreading out the distance over which limiting substrate is added. Modeling results verified that the strategy of multiple injections could reduce high densities of biofilm accumulation near the injection well. Also investigated was the strategy of adding a supplemental carbon source to extend the length of a BAZ. The modeling illustrated that such an extension of the BAZ could be accomplished and could result in longer contact times of a secondary substrate with the BAZ, thereby increasing the removal of the secondary substrate.

CHAPTER 1. INTRODUCTION

Contamination of groundwater by organic materials -- such as chlorinated solvents, petroleum products, and landfill leachates -- is widely recognized as one of the most critical environmental problems of recent times. Currently, clean-up efforts usually involve extraction of the contaminated water, followed by physical, chemical, or biological treatment. Because the organic contaminants can adsorb onto aquifer solids or can be trapped in regions of relatively low permeability, the volume of water required to be extracted is many times larger than the pore volume that is contaminated; thus conventional clean-up is very expensive and time-consuming.

In situ biological degradation is being proposed as a promising alternative for aquifer restoration. In situ projects typically involve a set of extraction and injection wells, which establishes a defined flow field and permits inputs of seed microorganisms, electron acceptor, carbon source, or other nutrients at one or more points along the flow path. Being a very new technology, in situ bioreclamation designs have been based on only a few simple microbiological experiments aimed at testing biodegradation potential and nutrient requirements. Incorporation of realistic biodegradation kinetics and groundwater hydraulics has not been accomplished.

An initial requirement of any in situ decontamination technology is that the flow field be defined. Otherwise, contaminants can escape treatment by migrating out of the treatment site or by remaining in isolated portions of the aquifer. For in situ bioreclamation, however, more than a defined flow field is required: the water in that flow field must pass through a biologically active zone before it is extracted or leaves the treatment site. The biologically active zone in an aquifer is made up almost completely by microorganisms attached as biofilms to the large amount of surface area presented by the aquifer solids. Even in uncontaminated aquifers, bacteria are found attached to aquifer solids; however, their densities are very low (10^6/gram of soil), and their metabolic capabilities are largely undefined (Ghiorse and Balkwill, 1983). Successful in situ bioreclamation requires that the attached biomass be increased greatly from that normally found on aquifer solids. In some cases, different types of microorganisms, having capabilities not found in

the natural community, should be added as seed. In almost every situation, however, success requires that the microorganisms grow to attached densities a hundred or more times that naturally present.

Cell growth and accumulation in an aquifer depend on the availability of an electron donor, an electron acceptor, and several other nutrients, such as nitrogen, phosphorous, and sulfur. Usually, one factor is rate limiting and controls how much cell mass can be accumulated. The growth-limiting factor can be called the limiting substrate (McCarty et al., 1981). Enhanced in situ bioreclamation usually involves adding the limiting substrate in such a manner that the growth limitation is eliminated and significant quantities of biomass are generated in the aquifer.

What the limiting substrate must be varies with the contaminating situation. For instance, a leak or spill that creates high organic-contaminant concentrations probably is limited by the electron acceptor or a nutrient. On the other hand, low-level contamination of a drinking water supply by a distant source creates a situation in which an organic electron donor is needed to allow significant growth.

The objective of enhanced in situ bioreclamation is to establish a biologically active zone by supplying the limiting substrate in such a manner that no contaminant escapes biodegradation. However, biodegradable material added via an injection well to enhance in situ biodegradation often is consumed very rapidly near the injection well (Rittmann and McCarty, 1980a; Rittmann et al., 1980), creating two significant problems: (1) biological growth is limited to only a region very near the injection well, and (2) well clogging can occur. The first problem is quite serious, since localization of biological activity prevents adequate contaminant/microorganism contact throughout most of the aquifer. The second problem also is serious because clogging retards the input of the limiting substrate and may force the groundwater flow to go around the biologically active zone.

The problem of localized biological activity can be solved, at least in principle, by providing multiple injection wells perpendicular to and/or along the flow path. Figure 1.1a depicts the case where multiple injection wells are placed laterally along the flow path to create a saw-tooth pattern of nutrient concentration, which allows

(a) enhancement of in situ biodegradation along the groundwater flow path

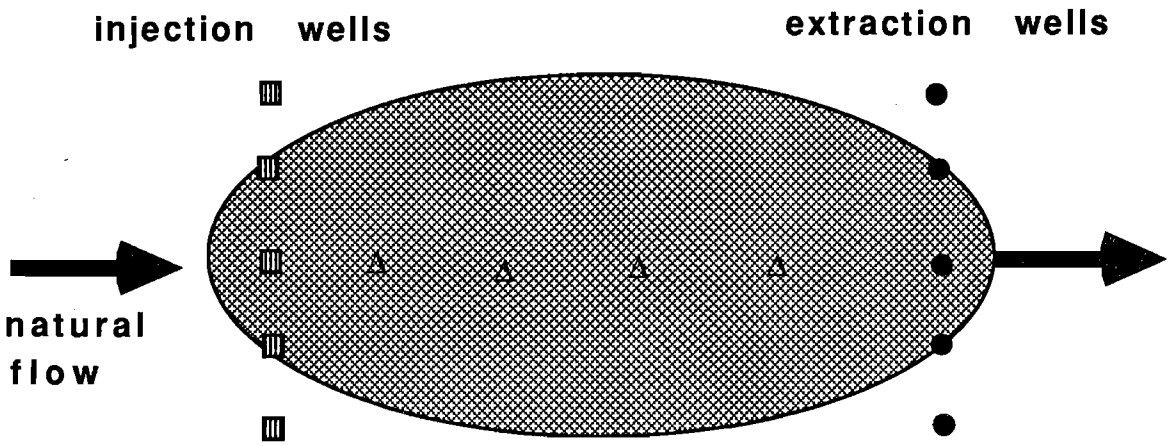

■ ● injection/extraction wells for hydraulic control of plume migration

Δ injection wells for stimulation of in situ biological activity

biologically active zone

(b) enhancement of in situ biodegradation perpendicular to groundwater

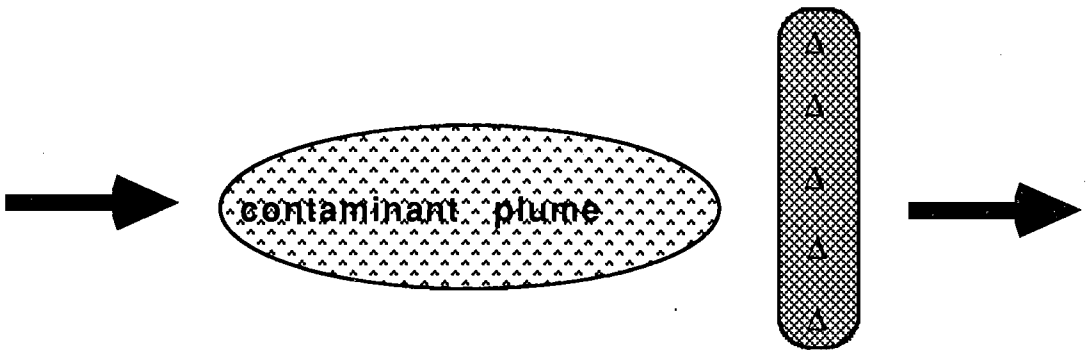

Figure 1.1. Strategies for in situ bioreclamation of contaminated groundwater.

the biological activity to extend the necessary distance to assure adequate contaminant removal. Figure 1a also demonstrates the concept of coupled hydraulic/biological reclamation, since a network of injection/extraction wells is utilized to hydraulically isolate the contaminant plume from the natural groundwater flow regime. To date, all reported cases of in situ bioreclamation have included hydraulic control measures; in fact, several projects did not utilize multiple injection wells along the flow path and, thus, biological activity was most likely concentrated in the vicinity of the hydraulic-control injection wells (Nagel et al., 1982; Werner, 1985; Flathman et al., 1983, 1984).

The need for multiple injection wells along the flow path is most acute for two commonly encountered situations. The first occurs when the limiting substrate is oxygen, a common electron acceptor. Because of the low solubility of dissolved oxygen (about 9 mg/l when exposed to the atmosphere) and its reactivity with reduced materials, supplying dissolved oxygen from one injection point cannot maintain sufficient dissolved oxygen throughout the flow path when the amount of organic material to be degraded is more than a few mg/l. Since degradation of certain common classes of compounds, especially including benzene derivatives, appears to occur best (and likely exclusively) when oxygen is available, the application of oxygen is likely to be a major vehicle for enhanced in situ bioreclamation. Other oxygen sources are ozone and hydrogen peroxide; although application of these materials overcomes some of the solubility problems of dissolved oxygen, they are reactive with reduced materials and are toxicants to microorganisms. Thus, they cannot be applied in unlimited amounts.

The second common occasion when multiple injections are needed along the flow path occurs when an electron donor, usually an organic compound, must be applied to allow increased growth of microorganisms that bring about contaminant removal through secondary utilization or co-metabolism (McCarty et al., 1981; Kobayashi and Rittmann, 1982; Stratton et al., 1983). Because the electron donor can be utilized quickly near the injection well, small input concentrations do not penetrate far into the aquifer, but large concentrations cause well clogging through biomass plugging or gas binding (in methanogenic or denitrifying cases). Thus, the electron

donor input must be spread out along the flow path to give a sufficient amount of microorganisms without plugging the aquifer.

Figure 1.1b shows the case in which multiple injection wells are placed perpendicular to the groundwater flow path to create a biologically active zone through which all of a contaminant plume must pass. This bioreclamation scheme is probably less expensive than that shown in Figure 1.1a, since hydraulic control measures are not utilized. Creating a biologically active zone perpendicular to the natural groundwater flow path is a novel concept in the field of aquifer restoration.

CHAPTER 2. PROJECT OBJECTIVES

The overall objective of the project is to develop, evaluate, and demonstrate a predictive modeling approach that combines realistic phenomena for biofilm degradation and groundwater hydraulics and that is suited to in situ bioreclamation schemes. The primary focus is to investigate the fundamental mechanisms that act when an electron acceptor is injected along the flow path of an electron-donor-rich groundwater to establish a biologically active zone (BAZ). The most important mechanisms considered in this project are the development of the biological activity within the porous medium and the biodegradation of primary and secondary substrates in the flowing water. To accomplish the overall objective, the following specific tasks have been performed:

1. A unique one-dimensional biofilm reactor was designed and developed to provide for substrate injection and sampling along the flow path.

2. Experiments evaluating the formation of BAZs were conducted with the biofilm reactors. Acetate was fed as the sole carbon source and nitrate was injected as the limiting electron acceptor.

3. Secondary substrate utilization in BAZs was studied by conducting experiments where various chlorinated solvents at low concentration were fed into columns with established BAZs.

4. A new, highly-efficient numerical model that couples solute transport mechanisms and biofilm kinetics was developed. The model is capable of solving directly for the steady-state profiles of primary limiting and non-limiting substrates, secondary substrates, and biomass.

5. The predictive ability of the model was verified by application to the laboratory experiments.

6. The model also was used to conduct numerical studies of the impact of various hypothetical lateral injection schemes on the overall efficiency of in situ bioreclamation.

CHAPTER 3. EXPERIMENTAL METHODS AND RESULTS

3.1 Porous-Medium Experimental System

3.1.1 Experimental Columns

In order to accomplish the research objectives defined in Chapter 2, a unique experimental set-up was designed with the following characteristics:

a. to provide a porous matrix having surface for biofilm growth
b. to provide a well-defined, one-dimensional water flow
c. to feed electron donor (organic matter) and electron acceptor (e.g., nitrate) in an independent manner
d. to have multiple electron-acceptor injection ports to create biologically active zones (BAZs)
e. to take liquid samples along the length of the flow path
f. to measure the pressure drop along the length of the column

Figure 3.1 is a schematic of the experimental system. A 2.5-cm diameter by 22.5-cm long glass column packed with 3-mm diameter glass beads was used to provide one-dimensional flow in a porous matrix. Bulk flow was established by pumping in the electron-donor feed solution at one end. A key feature was that injection and sampling ports were located along the length of the reactor. Two injection sites were arranged to satisfy purposes (c) and (d) above. Six sampling ports and the effluent line provided syringe sampling for substrate concentration (purpose (e)) and could also be used as manometers to measure headlosses which arise when the biofilm accumulated on the porous medium (purpose (f)). An injection port also could be utilized as a sampling port or a manometer when it was not used for injection.

The peristaltic, bulk-flow pump had a wide range of dispensing rates (0.02 ml/min to 22 ml/min), such that the bulk flow velocity could be manipulated to satisfy different experimental purposes. A multiple-channel syringe pump or a low-speed peristaltic pump was used for electron acceptor injection; thus, independent application of electron donor and electron acceptor was achieved.

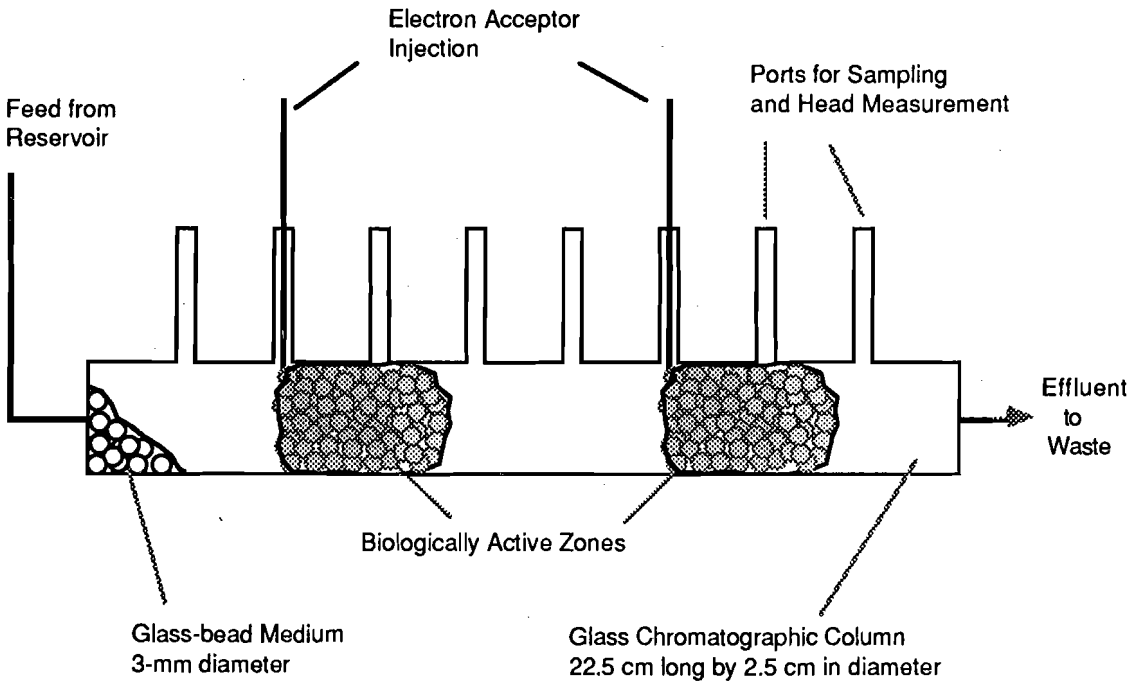

Figure 3.1. Schematic of column reactor to establish Biologically Active Zones (BAZs).

3.1.2 Injection System and Dye Tracer Tests

In order that the mechanisms of biofilm accumulation, substrate utilization, and clogging could be studied quantitatively, it was necessary to eliminate complications arising from spatial variations in concentration of injected material. To preclude creating concentration gradients perpendicular to the flow path and, thus, to provide a satisfactory one-dimensional regime, the injection arrangement was designed to give a uniform distribution of the injected material across the cross-section of the column.

Dye tests were carried out to asses the hydrodynamic dispersion of material injected from injection ports. A typical bulk flow rate of 0.5 ml/min (which corresponds to 0.1 cm/min of superficial flow velocity or 0.25 cm/min of interstitial velocity) was adopted for these tests. An alkaline thymol-blue dye solution was introduced through one injection port at a flow rate of one percent of the bulk flow rate. When the alkaline thymol-blue solution, which was yellow at acidic pH, mixed with the bulk flow, the thymol blue was exposed to a pH higher than 9, and it turned to a blue color.

3.1.2.1 Point-Source Injection

Dye solution was injected through a stainless steel needle to the exact center of the column. Figure 3.2 shows that the effect of cross-sectional hydrodynamic dispersion (mechanical mixing + molecular diffusion) was slow compared to advection (bulk flow); thus, a long, funnel-shaped dye distribution was observed. Clearly, the point source did not provide a satisfactorily uniform injection.

3.1.2.2 Line-Source Injection

To provide a more uniform dye distribution, a line-source injection was tested by using a closed teflon tube that had thirteen 0.2-mm dia. orifices evenly spaced along the length of the tube. Although the dye distribution was strikingly improved in the vertical transverse direction (see Figure 3.3a), Figure 3.3b demonstrates that the horizontal transverse distribution was nearly as poor as the case of a point-source injection. Thus, line-source injection was inadequate for establishing uniform input across the column's cross-section.

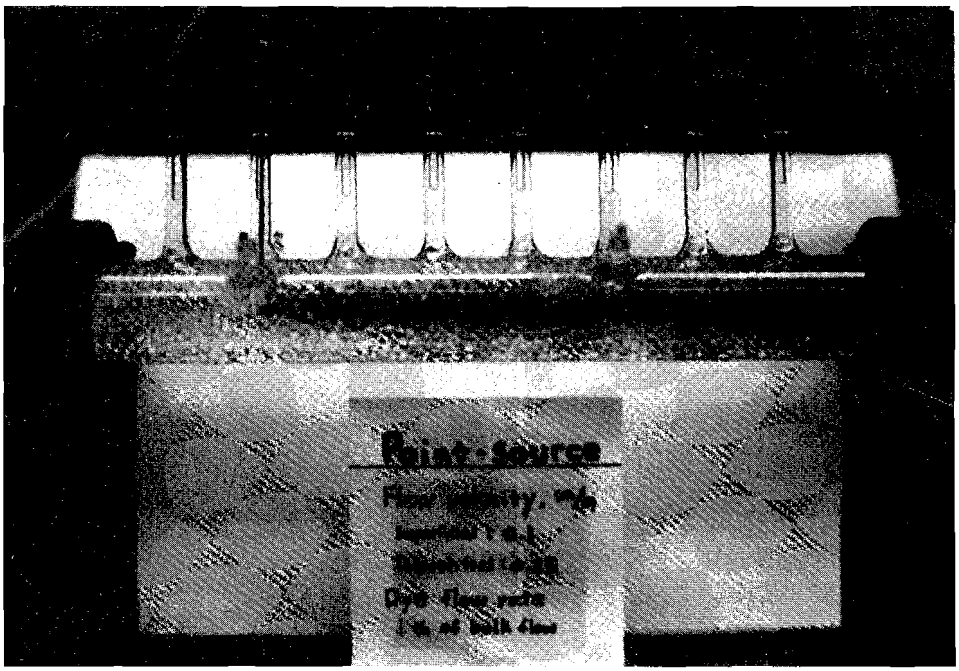

Figure 3.2. Point-source injection of thymol-blue dye solution. Flow characteristics were: superficial velocity = 0.1 cm/min, interstitial velocity = 0.25 cm/min, and dye flow rate = 1% of bulk flow rate.

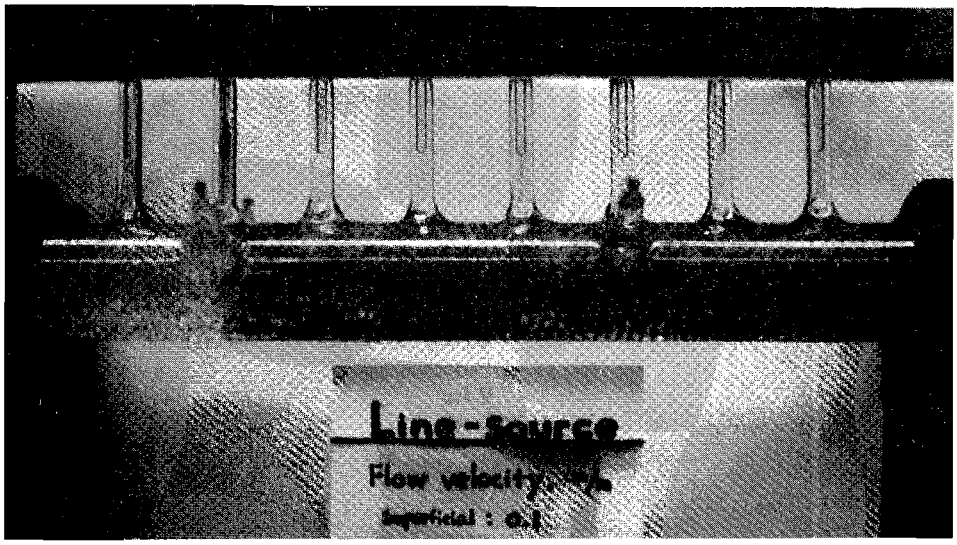

(a)

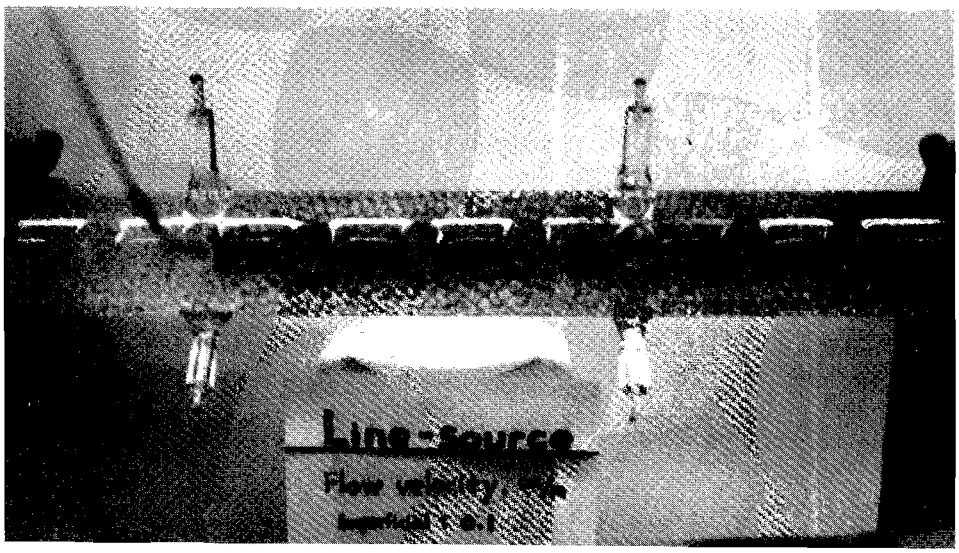

(b)

Figure 3.3. Line-source injection of thymol-blue dye solution; (a) vertical transverse direction, (b) horizontal transverse direction. The flow characteristics were the same as in Figure 3.2.

3.1.2.3 Planar Injection System

Since a uniform distribution of electron acceptor from the point of injection was essential, a planar-source modification of the injection system was designed. A triplet of injection ports, each of which was an injection needle, was provided. The system is shown schematically in Figure 3.4. Small orifices, 0.1 mm in diameter, were spaced along the length of the injection needle. Since the goal of the planar-injection system was to ensure uniform cross-sectional mixing, the orifices along each needle were spaced so as to provide an equal injection rate per unit cross-sectional area (see Figure 3.4). The orifice spacing along the needle was determined by two factors. The first was the unequal distribution of areas occupied by successive annular segments in the cross-section. In other words, the outer annular segments had greater area per unit of radius than did annular segments near the center, since area is a function of the radius squared. Second, the injection pressure at the top of the needle was controlled by the injection pump, but frictional losses caused the fluid pressure to decrease along the needle. Thus, orifice flow rate diminished from the top to the bottom of the needle, because orifice flow rate is a function of the pressure on the inner side of each orifice.

An iterative calculation procedure was devised to compute the spacing that guaranteed uniform cross-sectional injection. The Darcy-Weisbach equation (Daugherty and Franzini, 1977) for laminar flow was used to compute the pressure loss along the needle. The flow rate through each orifice was calculated from the remaining pressure at the location of each orifice, using the same Darcy-Weisbach equation. The areas of the annular segments in Figure 3.4 were determined in such a way that they were proportional to the flow rates of corresponding orifices. The flow out of each orifice was assumed to immediately and completely mix with its annular segment of the cross-section, as shown in Figure 3.4.

The final design of the planar source is shown in Figure 3.5. In order to avoid an overlap of orifices at the center of the cross section, only the vertical needle (type A) had a center orifice. Stainless steel syringe needles having 0.84-mm inside diameter (18-gage) and 0.22-mm wall thickness were utilized. Punctures with 0.1-mm-diameter holes with an exact spacing were possible by using an

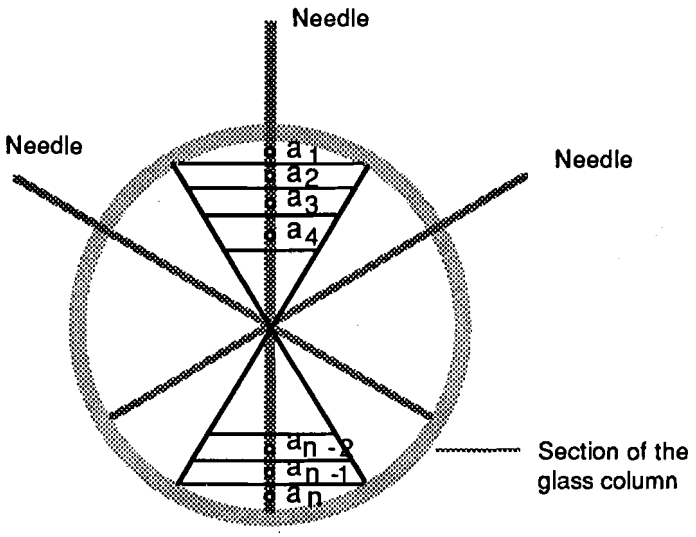

Figure 3.4. Planar injection system with hypothetical segments of area assumed to be completely mixed with each orifice discharge.

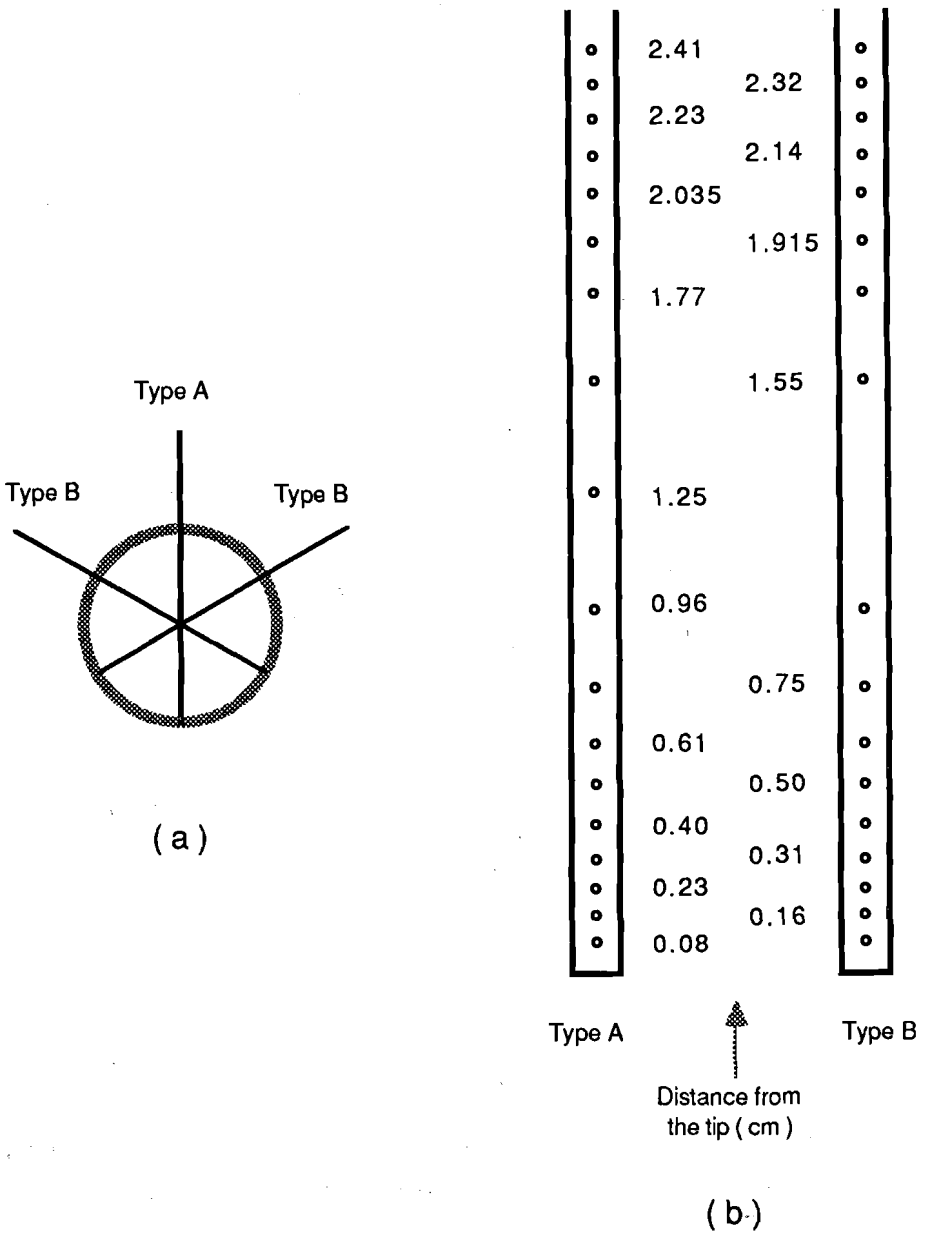

Figure 3.5. Final design of planar injection system: arrangement of needles (a), and orifices (b).

electrical discharge machine with the help of the Materials Research Lab at the University of Illinois.

Several dye tests were performed to assess the mixing properties of the planar-injection system. As before, a thymol-blue dye solution was used as the injection fluid; several experiments, at the flow rates given in Table 3.1, were performed. Figures 3.6 , 3.7a and 3.8 show the dye distribution in the vertical transverse direction of Runs 1, 2, and 3, respectively, and Figure 3.7b shows the horizontal transverse dye distribution for Run 2. All combinations showed very uniform cross-sectional dye distributions in all directions. Thus, the planar source was successful for achieving a uniform cross-sectional injection.

Table 3.1. Flow Rates Used for Dye Test

Run	Bulk flow rate per unit cross-sectional area (cm^3/cm^2-min)	Planar injection flow rate (% of bulk flow)
1	0.05	2.0
2	0.1	1.0
3	0.2	0.5

3.2 Biologically Active Zone (BAZ) Experiments

3.2.1 Experimental Methods

3.2.1.1 Experimental Set-Up

Two columns were run for the biologically active zone (BAZ) experiment: Column 1 and Column 2. Column 1 had one planar injection port for electron-acceptor input. One injection source led to one BAZ. Column 2, on the other hand, had two sets of planar injection ports, which led to two BAZs. In practice, one goal of having multiple injections is to evenly distribute the biomass, which prevents excessive build-up of biomass in one location and reduces

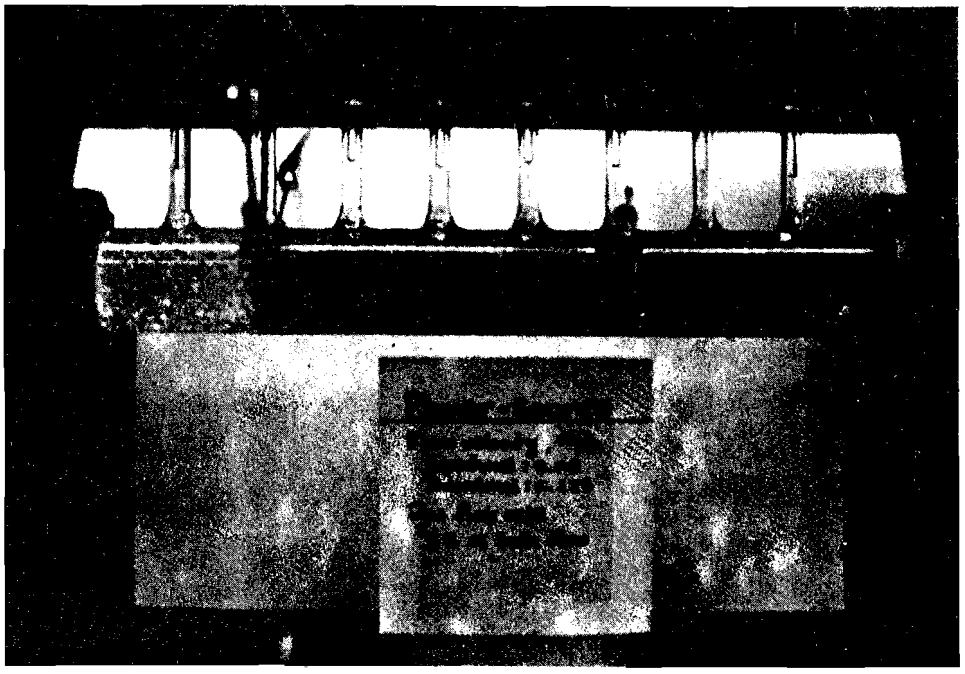

Figure 3.6. Planar injection of thymol-blue dye solution at the defined flow characteristics in Table 3.1 (Run 1).

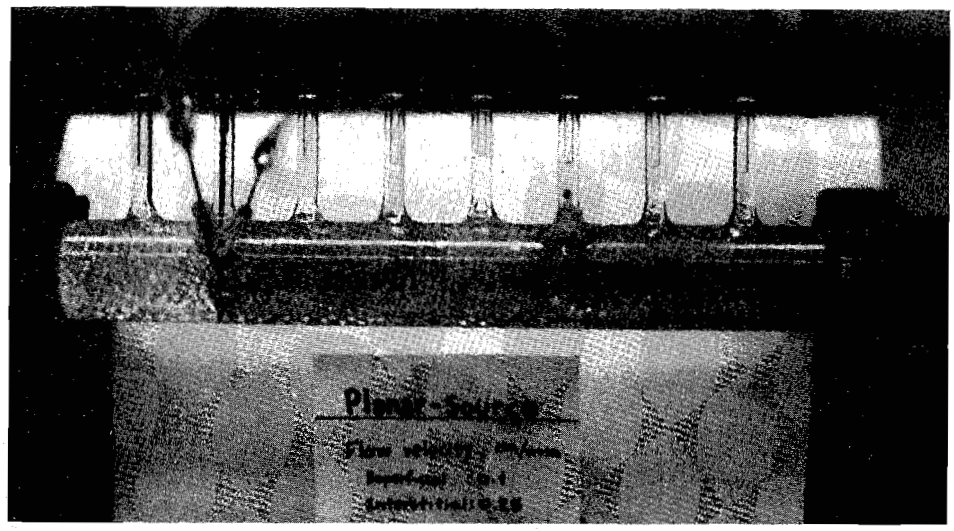

(a)

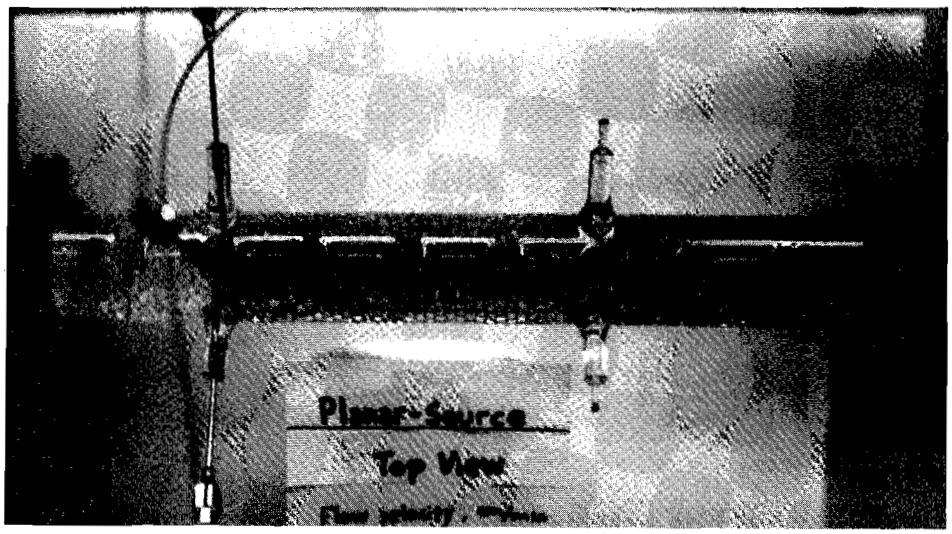

(b)

Figure 3.7. Planar injection of thymol-blue dye solution at the defined flow characteristics in Table 3.1; (a) Run 2-vertical transverse direction, (b) Run 2-horizontal transverse direction.

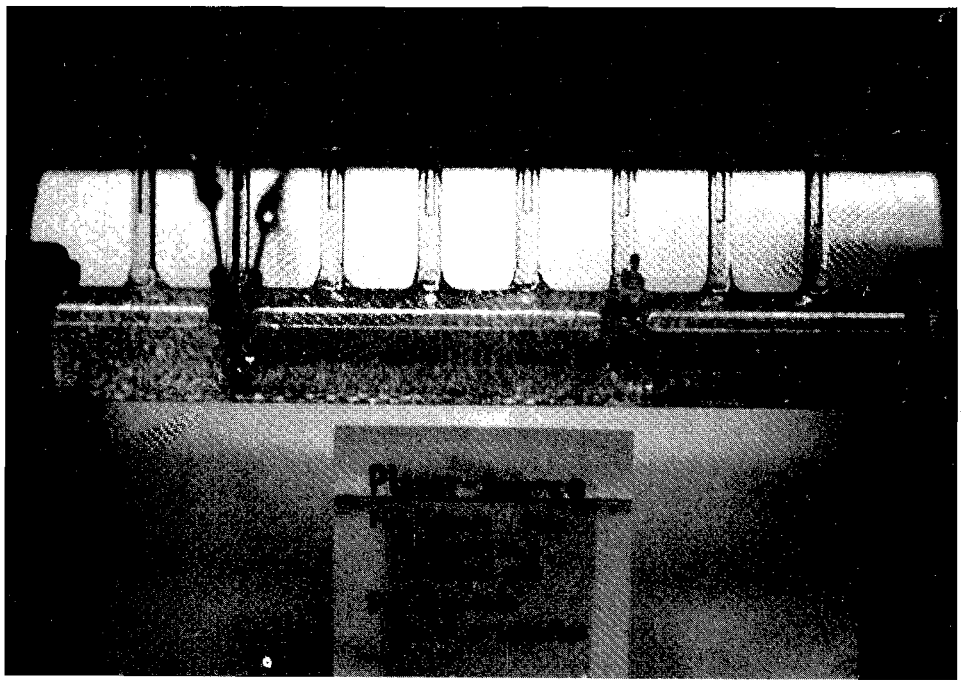

Figure 3.8. Planar injection of thymol-blue dye solution at the defined flow characteristics in Table 3.1 (Run 3).

the hydraulic headloss which arises as the biofilm growth clogs the pore space. Having two BAZs was a means to distribute the biomass more evenly.

The locations of the injection ports in Column 1 and 2 are shown in Figure 3.9. All the other substrates and nutrients were fed with the bulk flow from the feed reservoir, which was deoxygenated by a combination of boiling and nitrogen-gas purging before use.

Special efforts were needed to prevent reoxygenation of the prepared feed solution. First, the feeding peristaltic pump was located at the column outlet, and the connection tubing between the feed reservoir and the column was shortened as much as possible. Placement of the pump after the column was required, because the flexible peristaltic-pump tubing was oxygen permeable. Second, a slight positive nitrogen gas pressure (about 103% of the ambient pressure) was applied to the feed reservoir to prevent penetration of oxygen from the air and to replace the volume of liquid dispensed by the peristaltic pump. Third, all the sampling ports were capped with serum caps. The columns were set in a vertical direction, and the feed solution was pumped in from the bottom to the top. The overall experimental set-up is shown in Figure 3.10.

3.2.1.2 Characteristics of Column and Feed Composition

Characteristics of the column reactors and liquid flow are shown in Table 3.2. The flow rate of the electron-acceptor injection at each injection port was adjusted to about one percent of the bulk-flow rate, and this was not taken into account in detention time calculations.

The feed composition is shown in Table 3.3. Acetate (CH_3COO^-) was fed as the sole carbon source. The concentration was 20 mg/L as COD, 18.4 mg/L as acetate, or 7.5 mg/l as SOC. A small amount of ^{14}C-acetate was added to label the feed carbon. Denitrifying one mole of nitrate with acetate destroys up to one mole of H^+, potentially causing a pH increase. Thus, phosphate compounds were added in such a way that the medium had sufficient buffering capacity to maintain the pH between 6.9 and 7.1. Sodium molybdate (Na_2MoO_4) was added at 0.25 mM to prevent the growth of the sulfate-reducing bacteria (Bouwer, 1987).

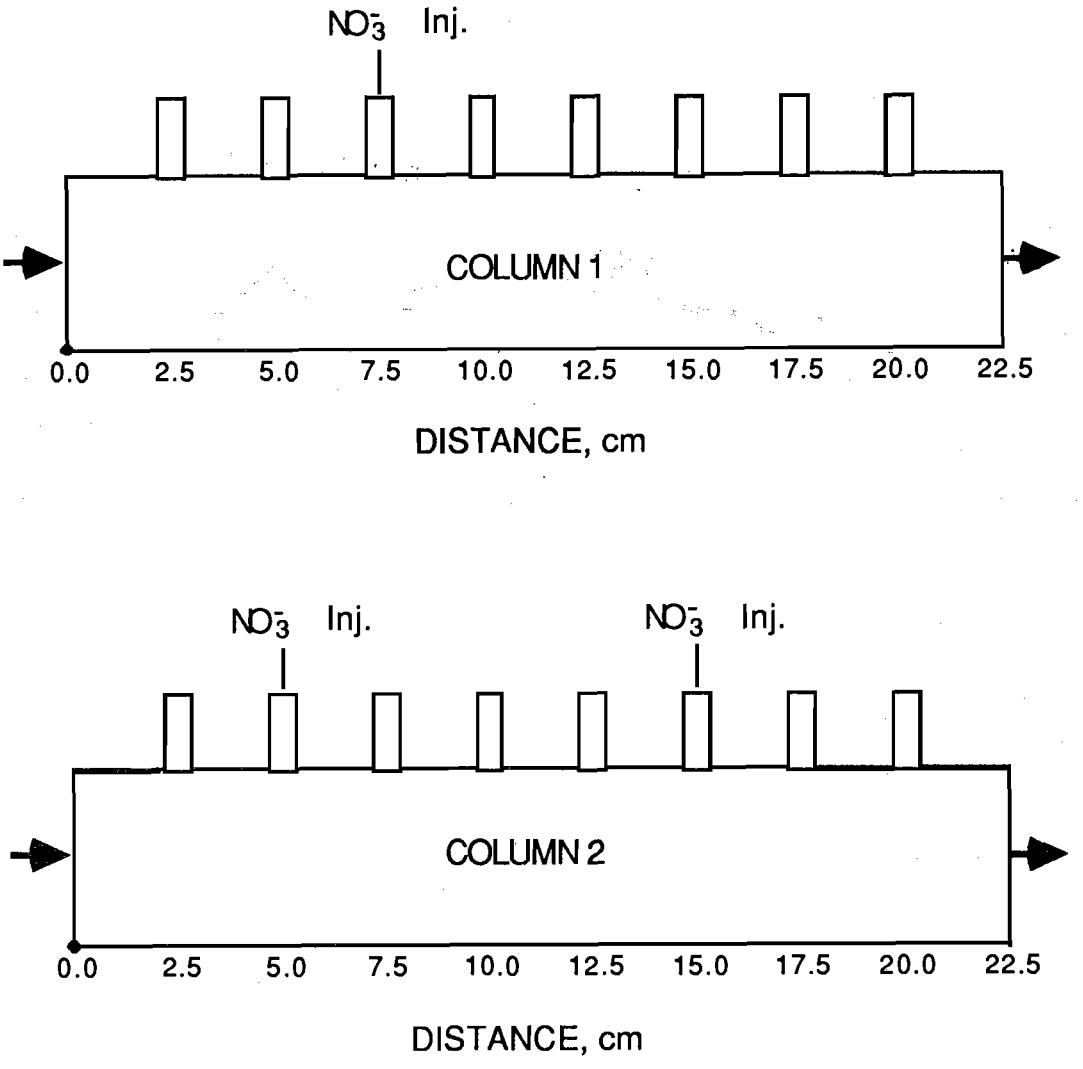

Figure 3.9. Locations of injection ports in Columns 1 and 2.

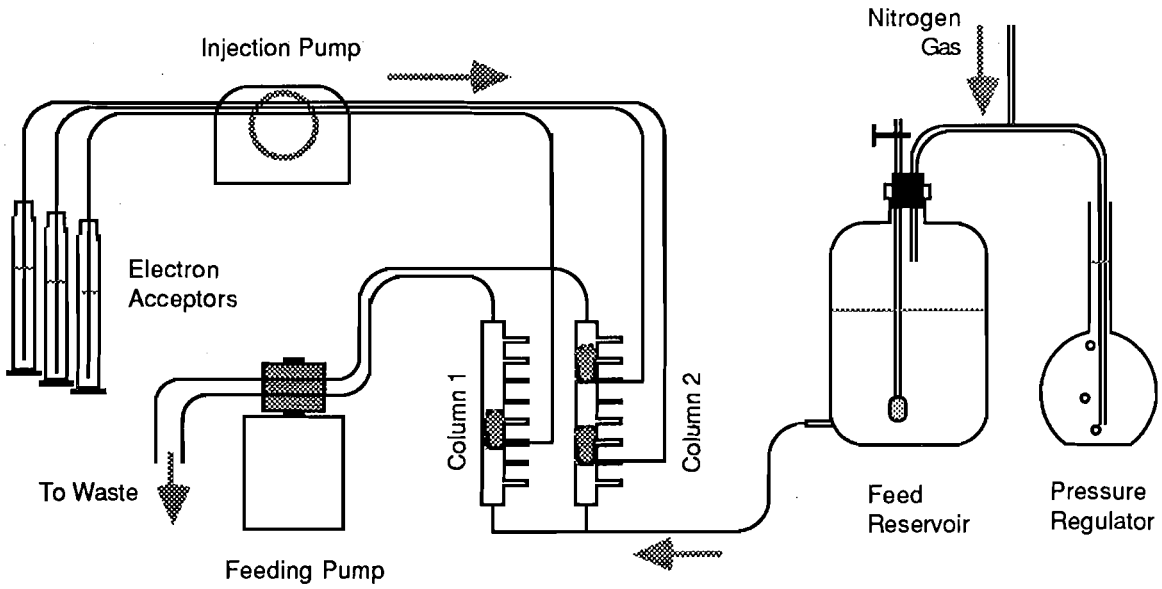

(a)

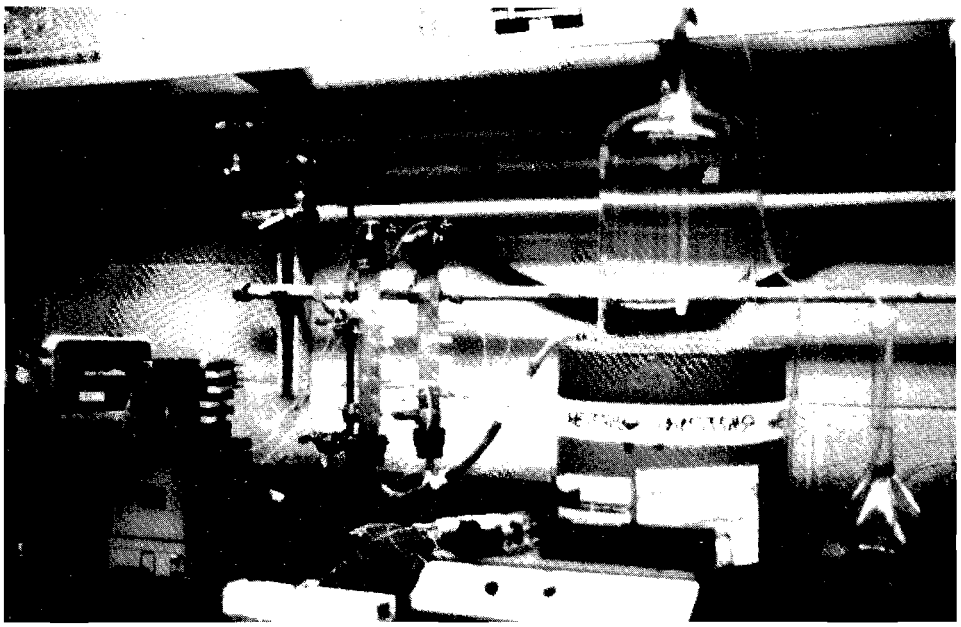

(b)

Figure 3.10. Experimental set-up for biologically active zone (BAZ) experiments; (a) a schematic, (b) a picture, from left: injection pump, feeding pump, column 1, column 2, feed reservoir, and nitrogen-gas pressure regulator.

Table 3.2. Characteristics of Column Reactor

Parameter	Unit	Value
Column Reactor:		
Length	cm	22.5
Diameter	cm	2.5
Volume	cm^3	110
Glass-bead diameter	cm	0.3
Porosity		0.4
Liquid flow:		
Feed-flow rate	mL/min	0.49
Feed-flow velocity		
- Superficial	cm/min	0.10
- Interstitial	cm/min	0.25
Nitrate-injection rate	mL/min	0.006 for Column 1 0.012 for Column 2
Detention time		
- Total	min	90
- After 1st injection	min	60 for Column 1 70 for Column 2

Table 3.3. Composition of Feed Solution for Denitrifying Columns

Compound	Concentration, mg/L
Acetate (CH_3COO^-)	7.5 as SOC
KH_2PO_4	170.0
K_2HPO_4	108.75
Na_2HPO_4	88.5
NH_4Cl	3.4
$MgSO_4$	11.0
$CaCl_2$	27.5
$FeCl_3$	0.15
Na_2MoO_4	51.5

The columns were inoculated with a 1% dilution of denitrification-reactor effluent from another study. Feeding started on March 12, 1987 for Column 1 and on June 18, 1987 for Column 2.

3.2.1.3 Sampling and Analytical Methods

Samples the soluble organic carbon (SOC) determination of the feed solution and effluent stream were taken twice a week. Samples for the determination of the SOC and nitrate profiles along the flow path of the column were taken when the SOC removal in the column reached a steady state.

All samples, except for the feed solution, were taken with a peristaltic pump collecting sample at a rate equal to the feed-flow rate. When taking samples from the sampling ports, a syringe needle was inserted into the center of the cross section of the column. Samples for the feed solution were taken by hand using a syringe. For each sample, approximately 10 mL of liquid was collected.

The SOC concentrations in the samples taken from the sampling ports, effluent stream, or feed reservoir were measured by counting ^{14}C. The liquid sample was passed through a 0.45-μm membrane filter to remove the suspended portion of organic carbon. Then, CO_2 was driven off by acidifying the sample to pH 2 or less with one drop of 1N HCl and shaking the vial for 10 minutes in a shaker. ^{14}C was counted with a Beckman liquid scintillation counter (Model LS-100). Thus, a filtered and acidified sample contained only soluble organic carbon.

The biomass in the liquid sample was estimated by taking the difference between the filtered and unfiltered organic carbon concentrations from acidified samples.

The total carbon concentration in the sample--SOC, biomass, and CO_2-- was estimated by counting the total ^{14}C in the sample. In this case, the sample was collected in an airtight syringe which contained a small amount (2.5% after sampling) of Carbo-Sorb II (United Technologies Packard), a strong base that absorbed CO_2 for scintillation counting. The difference between the total carbon and the unfiltered organic carbon was the CO_2.

Nitrate was measured using the chromotropic-acid method as described in Standard Methods (American Public Health Association, 1981). Nitrite was also determined following Standard Methods.

3.2.2 Results for Column 1

Column 1 was operated by injecting a stoichiometrically sufficient amount of nitrate through a single injection port. The performance data for the entire column are shown in Figure 3.11. The feed concentration was the SOC in the feed reservoir, and the influent SOC concentration was measured from the samples taken at the port immediately upstream from the injection port. Therefore, the difference between the feed and influent samples was aerobically degraded SOC. Its utilization was caused by residual oxygen in the feed or oxygen that diffused through the connection tubing between the reservoir and column. The SOC decrease from the influent sample to the effluent sample was achieved by a denitrification reaction.

The location of the feeding peristaltic pump was changed from column inlet to outlet, as described in Section 3.2.1.1 on day 71. Also, feed solution was boiled during the N_2-gas purging to enhance the deoxygenation after this day. These provisions drastically improved the quality of the influent, maintaining it almost at the original feed concentration throughout the experiment.

The effluent SOC showed a gradually decreasing tendency for about 120 days, after which it maintained a very low, steady-state concentration, except for a few cases of fluctuations which were caused by occasional system disturbances, e.g. gas removal from the column. The average effluent SOC after day 120 was about 0.2 mg/L, which corresponds to 97% removal of the influent SOC.

The relative carbon concentrations of SOC, biomass-C, CO_2-C, and total-C in the effluent are presented, together with the input-C, in Figure 3.12. Although there were a few irregular datum points, the overall pattern was that 67% and 20% of the input C were converted to CO_2 and biomass, respectively, while 3% of input C exited the column as unused SOC. One tenth of the input C was not recovered in the effluent carbon measurement and was retained biomass. Thus, most input C was mineralized, but a significant fraction was

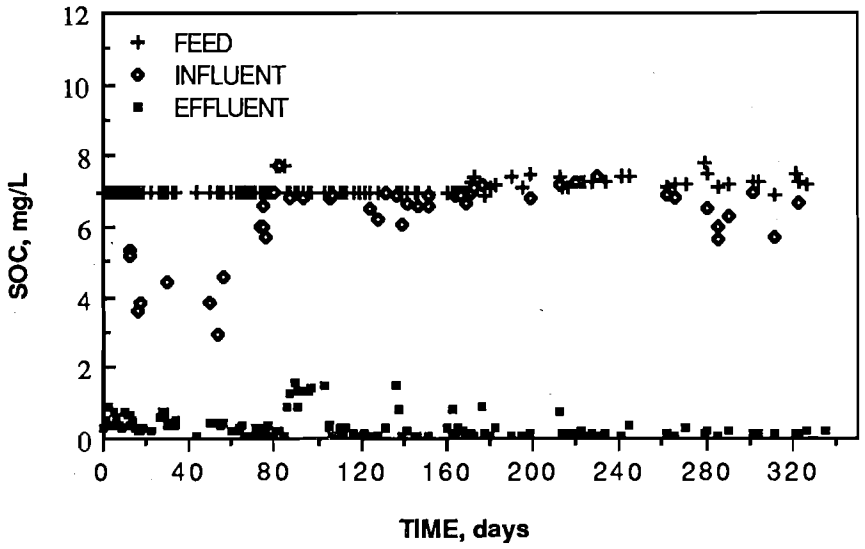

Figure 3.11. Soluble organic carbon concentrations in Column 1.

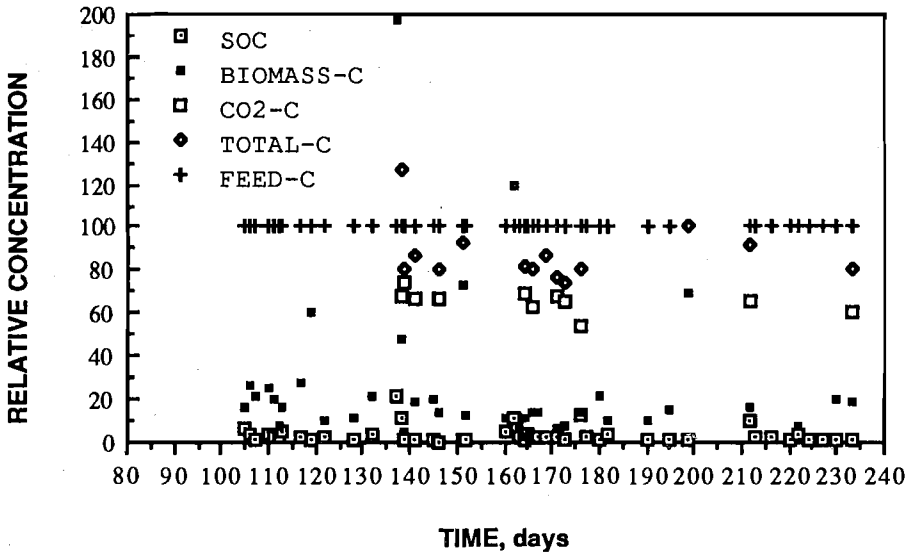

Figure 3.12. Relative effluent carbon concentrations, with reference to input carbon, in Column 1.

converted to biomass that could be transported in the fluid flow or retained in the column.

Figure 3.13 shows several SOC profiles along Column 1. Because the SOC concentration at the nitrate injection port could not be measured, it was assumed to be the same as the SOC of the immediate upstream port. The results were quite reproducible, suggesting that the BAZ was approximately at steady state. The majority of the SOC removal took place in the 2.5-cm region immediately downstream from the nitrate injection port; then the rate of removal diminished toward the column outlet. Thus, the BAZ was mainly contained within about 7.5 cm of the injection.

Figure 3.14 is a photograph of Column 1 at day 351. The back-lighting emphasizes that most of the BAZ was located between the injection port and the third sampling port, a distance of 7.5 cm. The slight dark coloration throughout the reactor is evidence of some attached biological activity, but the dense area shows where the main BAZ was located.

Figure 3.15 superimposes the NO_3^--N profile over the SOC profile. Figure 3.15 shows that the SOC was the limiting substrate after the injection, because nitrate was always present at concentrations of at least 2.8 mg N/L. The upstream port (5-cm location) before nitrate injection showed a substantial nitrate concentration. Since the dye tests (see Figures 3.6-3.8) did not show any back diffusion of the injected material, it should be attributed to a sampling error. Subsequent samples which were taken at a reduced sampling flow rate and did not show any significant nitrate concentration at this port.

A considerable amount of nitrogen gas should be produced during the denitrification energy reaction (McCarty, 1972). Stoichiometrically, a complete oxidation of 1 mg of acetate-C by nitrate produces 0.747 mL of N_2 gas. As the feed solution was already saturated with nitrogen gas, most of the nitrogen gas produced should have been released to the gas phase. The photograph shown in Figure 3.16 demonstrates that nitrogen gas was released and trapped in the column. Gas trapped in the pore space was measured by removing the liquid from the sampling and injection ports before and after gas accumulation. The volume

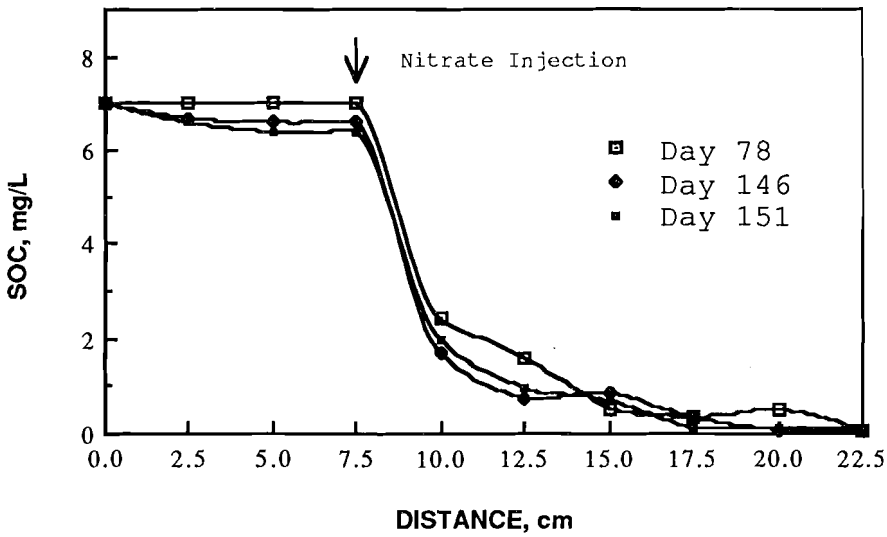

Figure 3.13. SOC profile at different times in Column 1.

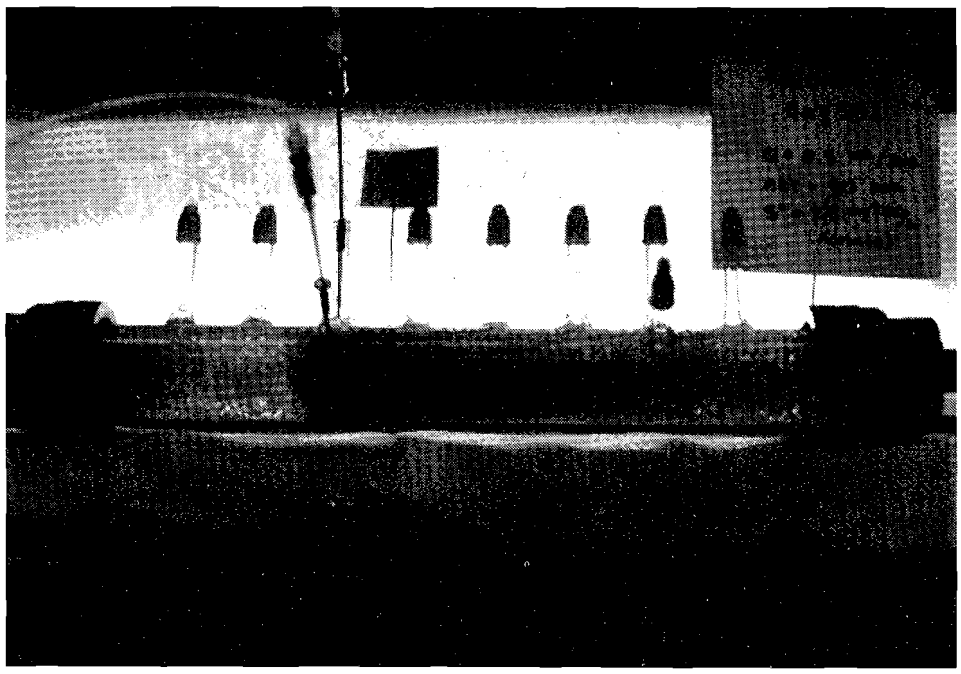

Figure 3.14. BAZ distribution in Column 1 at day 351. The reactor conditions were as defined in Table 3.2 and Table 3.3.

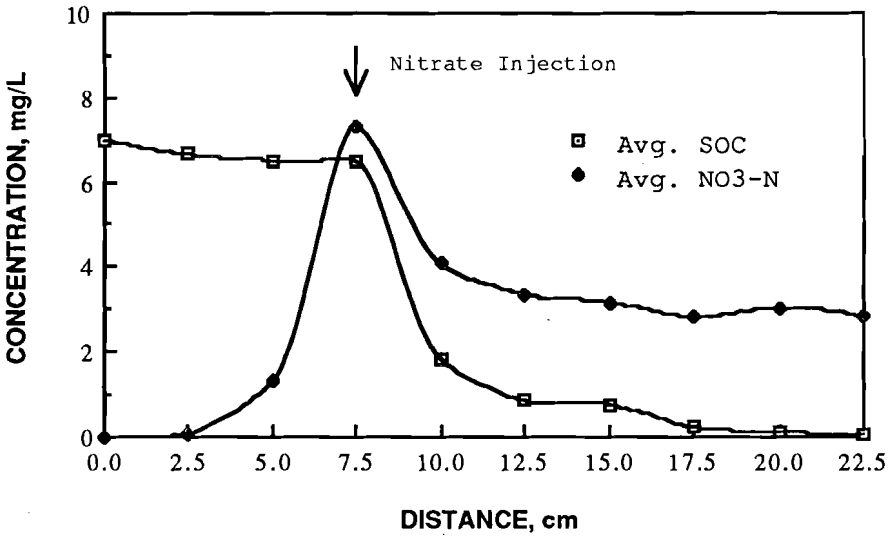

Figure 3.15. Average SOC and NO_3^- concentration profiles in Column 1 (data from day 146 and day 151).

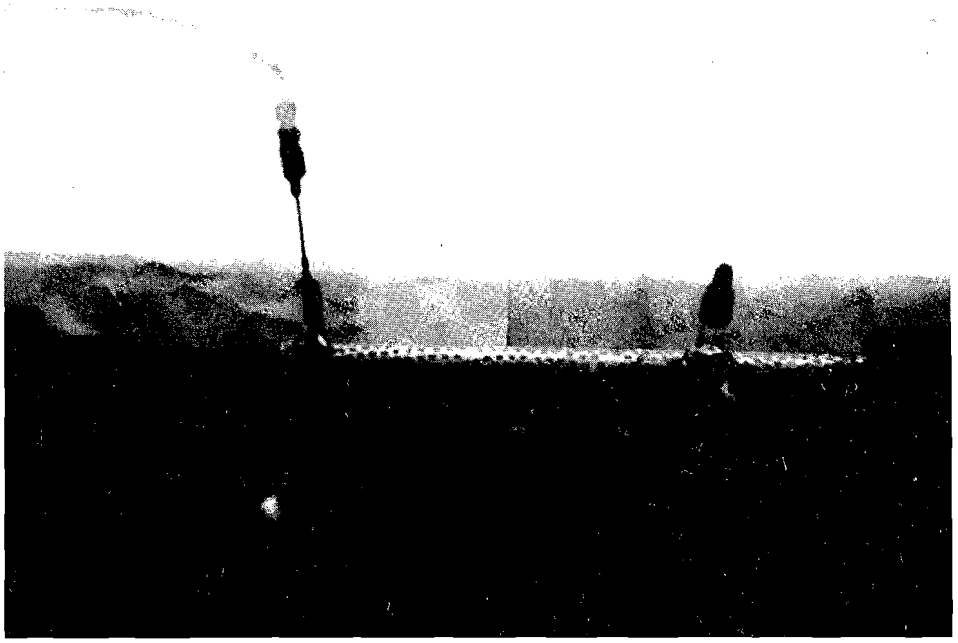

Figure 3.16. N_2-gas accumulation in Column 1. The reflections at the top side of the column were produced as a result of gas-bubble accumulation.

difference of the drained liquid was assumed to be equal to the gas volume trapped in each segment of the column. Gas analysis with a gas partitioner (Fisher Gas Partitioner, Model 1200) repeatedly showed that N_2-gas was the only detectable component in the collected gas samples.

Figure 3.17 shows the gas distribution in Column 1 at day 233, which was 72 days after the gas removal. Total gas accumulated in the column was 11.1 mL, which corresponded to 38% of the total pore volume after the injection port. Even though the denitrification reaction occurred mainly in the first two segments after the injection, there was not much gas in those two segments. More than half of the gas was trapped in the 3rd and 4th segments after injection. No gas accumulation occurred before the nitrate injection, confirming that the gas was produced by denitrification in the BAZ.

The location of nitrogen-gas accumulation can be explained by the following scenario. First, nitrogen gas was produced in the BAZ, but it was in the liquid phase. Second, as more liquid-phase nitrogen gas accumulated, it was gasified to small bubbles. Third, the gas bubbles agglomerated together, growing to larger bubbles as the water and bubbles flowed downstream. Finally, the large bubbles were trapped and accumulated in the pore space. Probably, a steady state occurred from a balance between gas bubble transport from upstream and bubble shear-off to downstream.

The overall removal of SOC in Column 1 did not deteriorate in spite of the gas accumulation, because the gas accumulation was not significant in the BAZ. Thus, the residence time in the BAZ was not affected significantly by the gas accumulation.

3.2.3 Results for Column 2

Column 2 was operated by injecting nitrate in such a manner that about one half of the SOC fed was removed in the first BAZ, and the other half was removed in the second BAZ. The total nitrate injection was the stoichiometrically sufficient amount required to completely oxidize the fed acetate. Initially, an equal amount of nitrate was injected at the two ports. Later, the ratio was adjusted so that the upstream port injected 25% of the total and the downstream injected 75%.

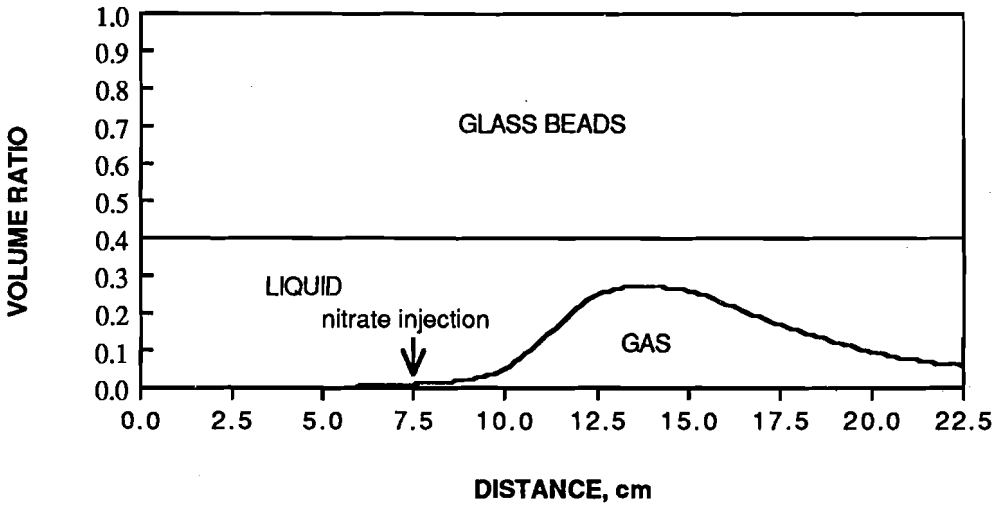

Figure 3.17. Gas accumulation and distribution in Column 1 (day 233, or 72 days after gas removal).

The overall performance of the entire column is shown in Figure 3.18. The effluent SOC reached an apparent steady-state within a week and maintained a good removal until the injection ratio was changed. The average SOC concentration between 8 to 25 days was 0.09 mg/L, corresponding to 98.6% removal of the influent SOC. When the nitrate injection ratio was changed, the average effluent SOC concentration increased to about 1 mg/L, which corresponded to 86% removal efficiency.

An important phenomenon observed from days 26 to 106 was a cyclic fluctuation of the effluent quality. Gas bubbles were also observed during this period. On day 107, the gas bubbles in the column were removed by draining the liquid from the column. Then, the column was refilled with liquid as the N_2 gas was put under negative pressure. Throughout this procedure, every precaution was taken to minimize system disturbance and biofilm loss. Figure 3.18 shows that the substrate removal was greatly enhanced almost immediately after the gas removal. The effluent SOC decreased within 3 days to 0.14 mg/L, which was comparable to the Column 1 effluent (0.2 mg/L). However, the SOC began to increase after 15 days of operation, and it reached a maximum effluent value after 50 days (2.4 mg-SOC/L). After that, it decreased again to the previous low level. The dynamic effects of gas accumulation caused the changes in SOC removal, which are discussed in detail below.

Typical SOC profiles obtained at different operational conditions in Column 2 are shown in Figure 3.19. Profile 1 represents the reactor performance when an equal amount of nitrate was injected through each port. Most of SOC removal took place right after the first injection, and the remaining SOC was removed after the second injection. The overall removal efficiency of this injection was excellent, but it failed to create a balanced SOC removal, which was necessary for balanced BAZ development. Profile 2 was obtained 66 days after the injection scheme was adjusted. The distribution of SOC removal between the two BAZs was satisfactory, but the overall efficiency deteriorated considerably. Profile 3 was obtained on day 116, which was 9 days after gas removal. The distribution of SOC removal and the overall removal efficiency were satisfactory after gas removal.

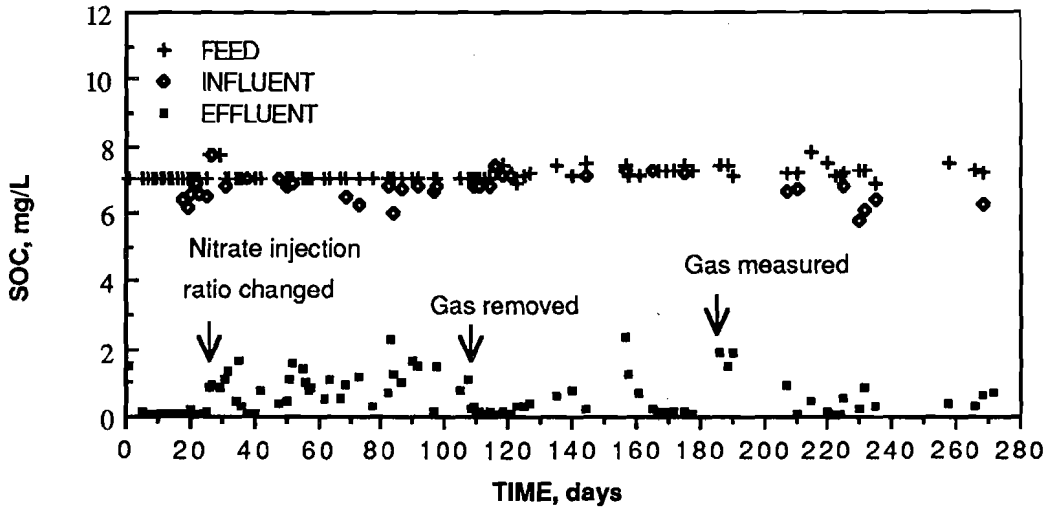

Figure 3.18. Soluble organic carbon concentrations in Column 2.

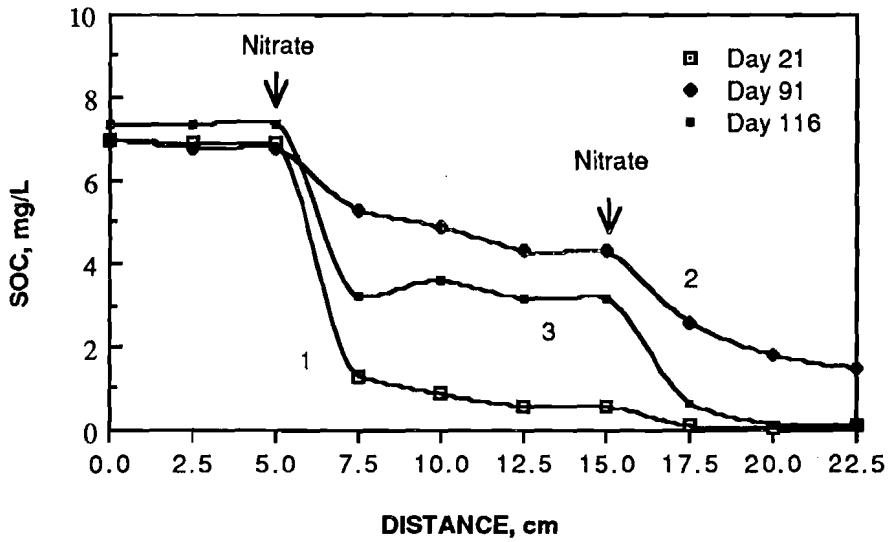

Figure 3.19. SOC profiles in Column 2.

The effluent SOC concentrations and the SOC profiles make it clear that gas accumulation was a key factor controlling SOC removal. Therefore, the gas trapped in the pore space was measured using the technique described in Section 3.2.2. Figure 3.20 shows the gas distribution in Column 2 at day 179, which was 72 days after the gas removal. The total gas accumulated in the column was 14.4 mL, which corresponded to 42% of the total pore volume after the first injection port. As for Column 1, relatively little gas was trapped near the first injection port, although it was greater than in Column 1. Accumulation was very large 2.5-7.5 cm downstream of the first injection. Gas distribution after the second injection was relatively even, and the volume constituted about 30% of the pore volume. Figure 3.21 demonstrates the gas accumulation photographically. Again, no gas was accumulated before the first injection.

Two features are particularly important in Figure 3.20. First, a considerable volume of gas was trapped in the BAZs (compare the gas accumulations within 5 cm from the injections with Column 1 in Figure 3.17). Since the BAZs were the location of SOC removal, gas accumulation in the BAZs seemed to cause the relatively poor performance of Column 2. Gas accumulation caused a reduction in liquid detention time in the BAZs and a loss of substrate/biofilm contact. Second, much gas was contained between the first and second BAZs; the peak gas volume amounted to 87% of pore volume. If such a "body" of gas were to move downstream toward the outlet, the second BAZ would be severely affected as the gas peak passed through it. In such a case, the removal efficiency would be expected to deteriorate temporarily. It seems plausible that movement of gas "bodies" may have caused the large effluent-quality fluctuations (see Figure 3.18).

Figure 3.22 shows a typical correlation between SOC and nitrate concentrations in Column 2. Although nitrate was the rate-limiting substrate after the first injection, it was in surplus after the second injection, making SOC the rate-limiting substrate.

Characteristics of the biofilm in Column 2 were determined. After 297 days of operation, the column was taken apart, and 10 glass beads from each injection or sampling-port section, including the inlet and outlet, were taken out to measure the biofilm dry weight and thickness. The procedures were described previously (Namkung,

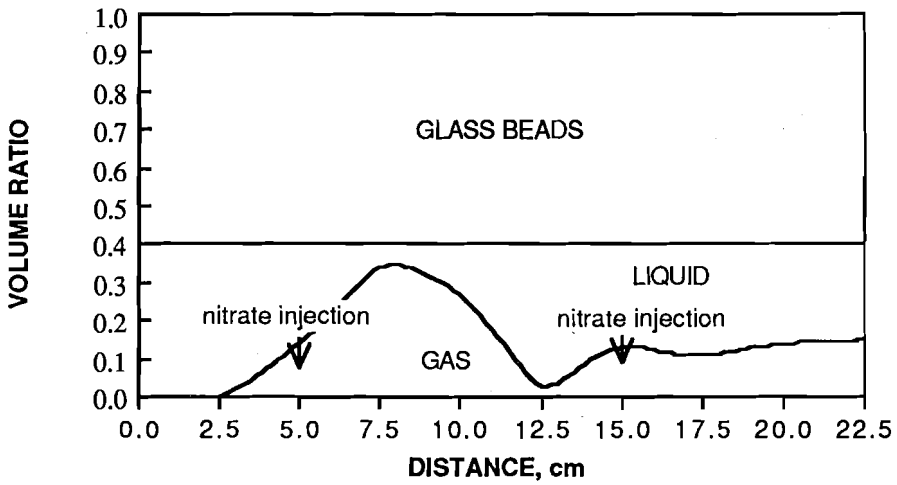

Figure 3.20. Gas accumulation and distribution in Column 2 (day 170, or 72 days after gas removal).

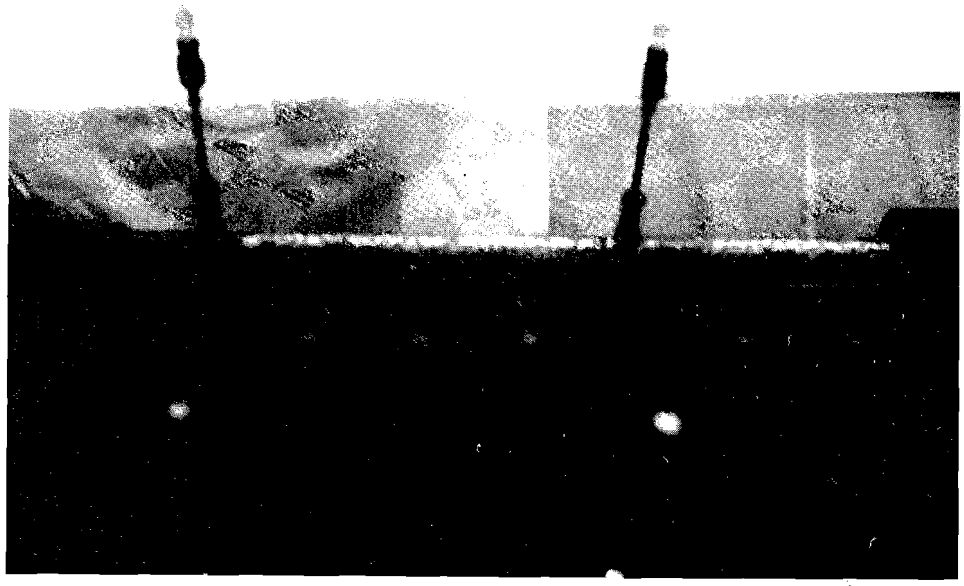

Figure 3.21. N_2-gas accumulation in Column 2.

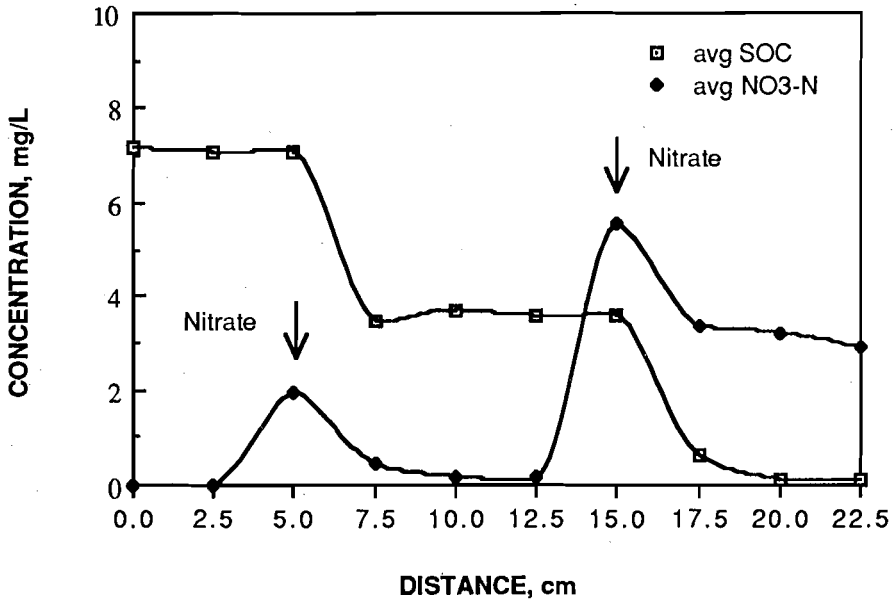

Figure 3.22. Average SOC and NO_3^--N concentration profiles in Column 2 (data from day 114 and day 116).

1985). The results are shown in Figure 3.23. The distribution of dry cell mass per glass bead along the length of the column clearly visualizes the concept of the BAZ (see Fig 3.23-a). The amount of cell mass on the glass beads increased sharply at each injection port and decreased slowly downstream. A photograph of BAZ distribution in Column 2 is shown in Figure 3.24. A striking resemblance is observed between Figures 3.24 and 3.23-a. The decrease in cell mass with distance from the injection was slower than might be expected from the SOC profile (see Figure 3.22). This suggests that a significant portion of downstream cell mass was sheared biofilm that was transported from upstream and deposited on the glass beads. The small amount of biofilm at the inlet was grown on oxygen which was not removed from the feed solution or which permeated into liquid through the connection tubing.

Biofilm thickness (see Figure 3.23-b) showed a similar tendency of increase and decrease along the column, but its distribution corresponded more closely to the SOC distribution than did the dry cell mass. The biofilm-density distribution in Figure 3.23-c was almost a mirror image of the biofilm thickness distribution. Its values at the first and second injection ports, 11.9 mg-cell/cm^3 and 8.8 mg-cell/cm^3, respectively, were not very far from other results in glass-bead columns (Namkung, 1985). However, the density greatly increased downstream from the injection ports. It appears that the increased density was caused by gas accumulation, which partially dried the biofilms.

3.2.4 Headloss Through the BAZs

No measurable headloss was observed for either column. A calculated headloss by the Kozeny-Carmen equation (Freeze and Cherry, 1978), assuming a 75 μm-thick biofilm in a 2.5-cm-long BAZ, was 0.07 mm, which also was immeasurable.

3.2.5 Determination of Kinetic Parameters

Four kinetic parameters--namely, the maximum specific substrate utilization rate (k), the half-maximum rate concentration (K_s), the cell-yield coefficient (Y), and the cell-decay coefficient (b)--were determined in one batch reactor. To consider potential physiological differences of cells grown at different locations along the column,

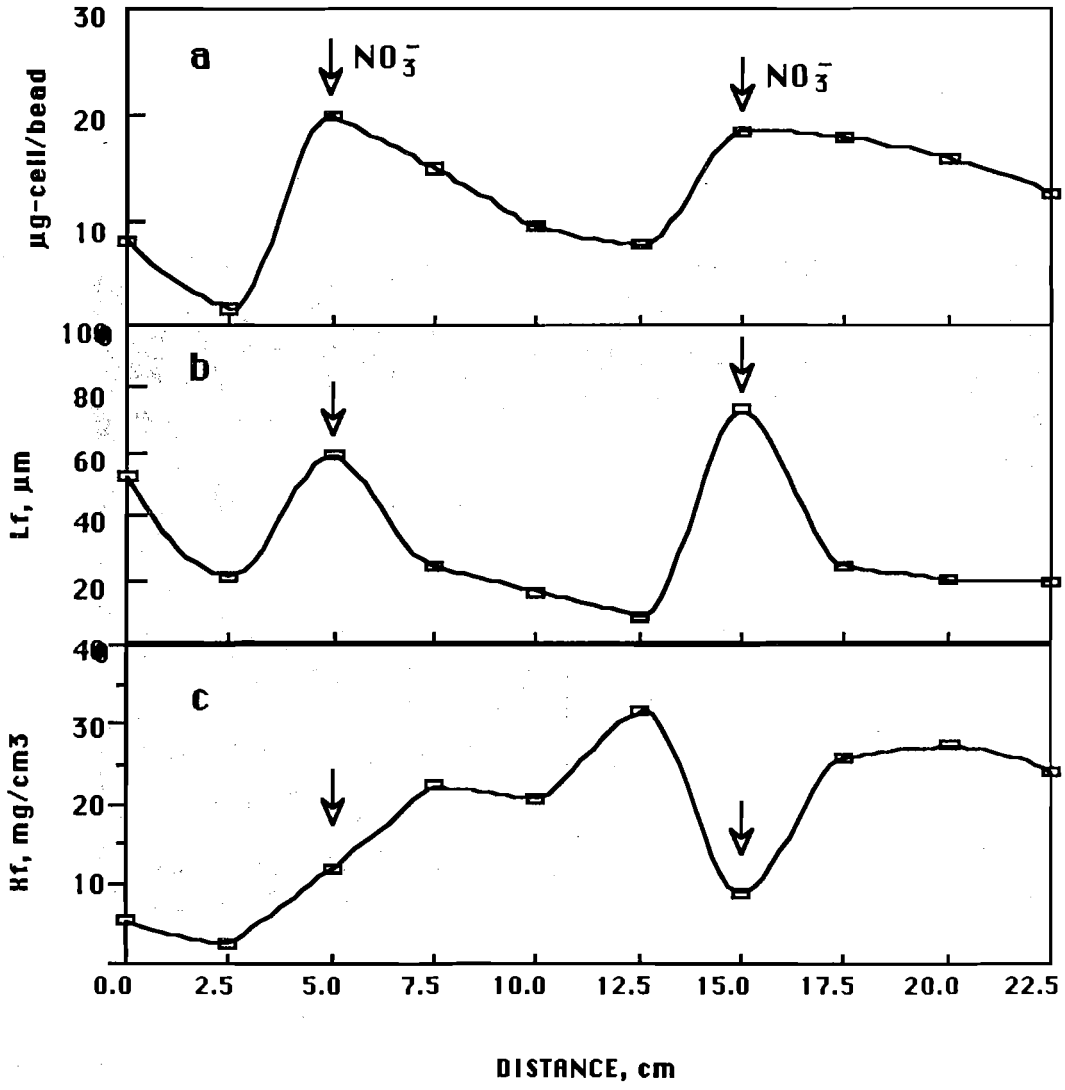

Figure 3.23. Biofilm distribution in Column 2 after 297 days of operation: distribution of dry cell mass (a), biofilm thickness ,L_f (b), and biofilm density, X_f (c).

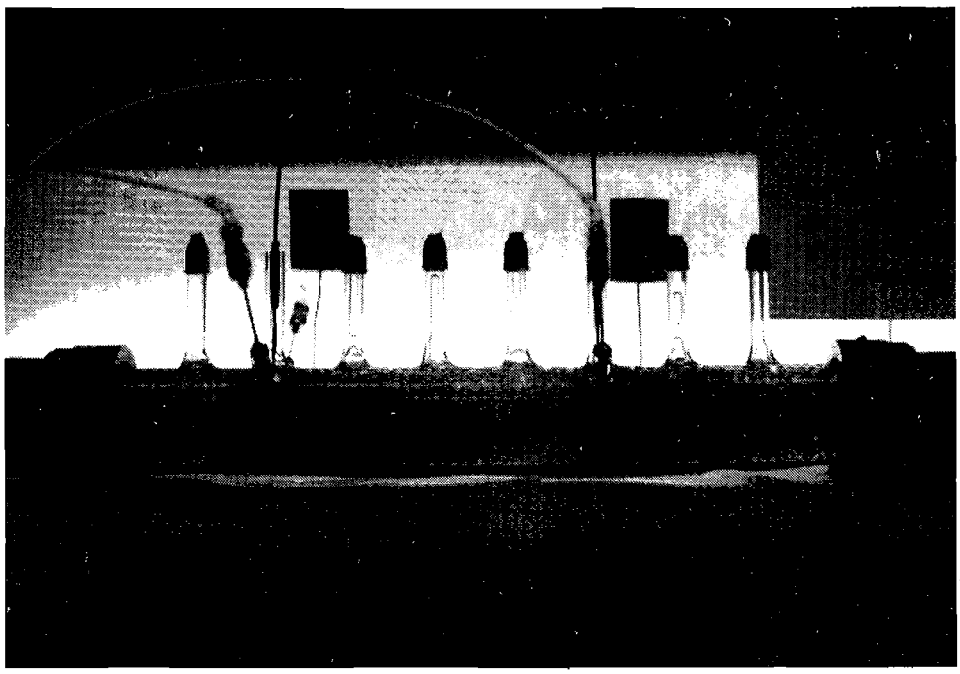

Figure 3.24. BAZ distribution in Column 2 at day 296. The reactor conditions were as defined in Table 3.2 and Table 3.3.

five batch reactors were run in parallel with five different inocula, as indicated in Figure 3.25. Batch I1 and Batch I2 used cells from the first and second injection sites in Column 2, where the cell activity was high. Both electron donor and acceptor were relatively abundant compared to other locations in the column, but each site had a different donor/acceptor ratio (see Figure 3.22). Batch 1-2 used cells from the second sampling-port after the first injection, where cells were under nitrate limitation. Batch 2-2 used cells from the second sampling-port after the second injection, where cells were under SOC limitation. Batch 5 used cells from the fifth sampling-port after injection in Column 1, where most of the easily-biodegradable SOC was used up and the cells were under extremely SOC-limited conditions.

Five 120-mL vials, equipped with air-tight rubber caps, were used as batch reactors. An aliquot of 100 mL of oxygen-free feed solution which had the same mineral composition as the BAZ-experiment feed filled the vials. The initial concentrations of acetate (^{14}C labeled) and nitrate were doubled to ensure exponential growth. The headspace was filled with N_2 gas. The batch reactors were shaken continuously in a shaker. Samples were taken out by a syringe, replacing the liquid volume with N_2 gas. ^{14}C in filtered and unfiltered samples was counted to determine SOC and cell concentrations.

The changes in SOC and cell concentrations with time from the five reactors are shown in Figure 3.26. SOC and cell concentrations are denoted by S and X, respectively.

3.2.5.1 Determination of Y

The cell yield coefficient, Y, was determined from

$$Y = - \Delta X/\Delta S \qquad (3.1)$$

during the exponential-growth phase. Y was calculated at each sampling time, using cumulative ΔX and ΔS, and an average value was taken. For example, Batch 5 computations of Y are shown in Figure 3.27, which illustrate the convergence of Y to 0.36 mg cell-C/mg SOC. The Y values for Batches I1, 1-2, I2, and 2-2 were 0.37, 0.36, 0.375, and 0.36 mg cell-C/mg SOC, respectively. The data clearly show that Y was not a function of sampling location.

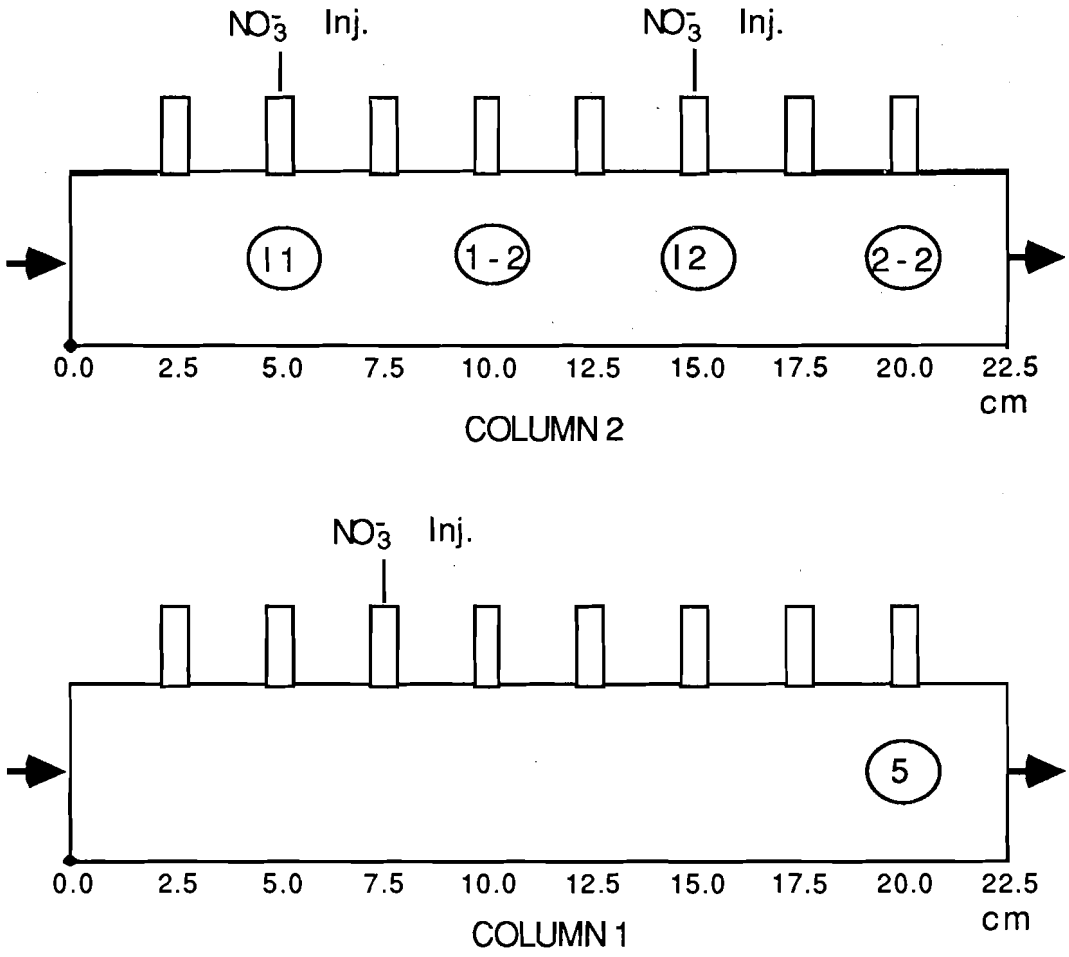

Figure 3.25. Locations of harvested cells for kinetic-parameter determination

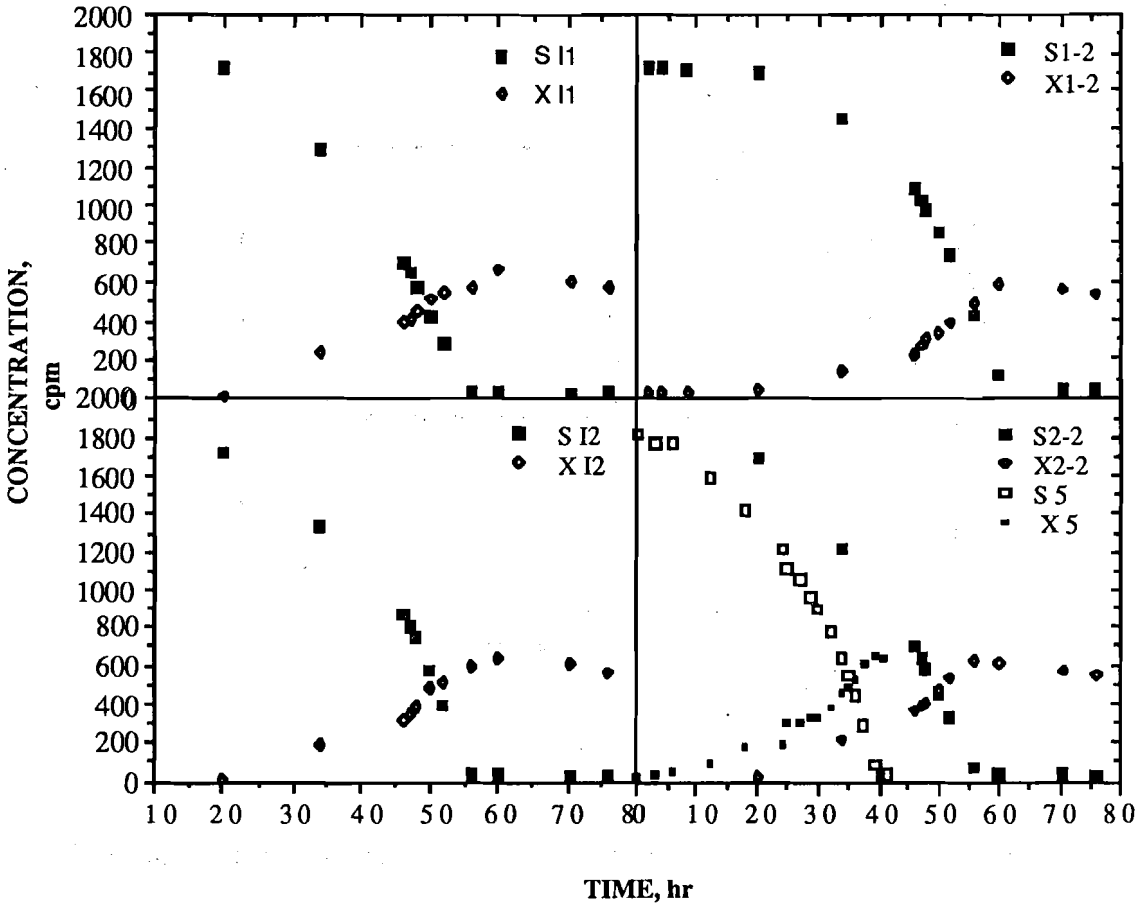

Figure 3.26. SOC utilization and cell growth in batch reactors. SOC and cells are denoted by S and X, respectively.

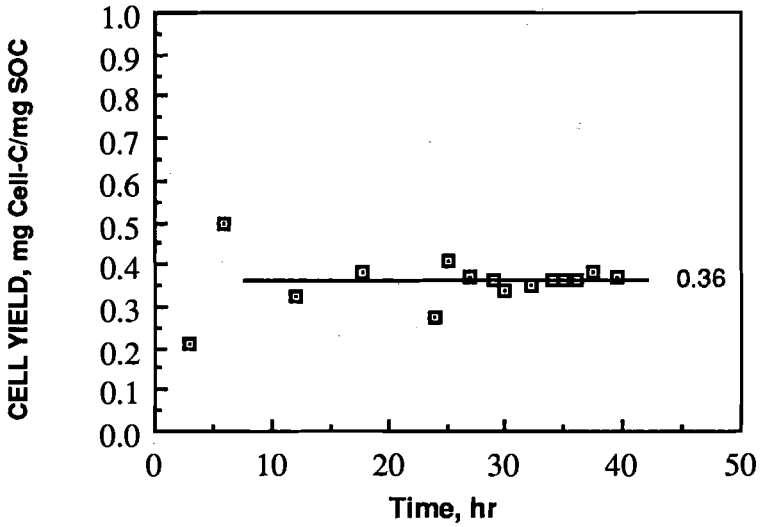

Figure 3.27. Determination of average cell yield in Batch 5.

3.2.5.2 Determination of k

The maximum specific substrate utilization rate, k, was determined for the exponential growth phase with

$$k = \mu_m / Y \qquad (3.2)$$

in which μ_m is a maximum specific cell growth rate which, in turn, was computed using

$$\mu_m = \ln(X_t/X_0)/t \qquad (3.3)$$

The measured X values, shown in Figure 3.26, gave reasonably good estimation for μ_m, but the experimental deviations in cell-concentration measurements caused some scatter in the μ_m values. Thus, a different cell-mass estimating method, utilizing SOC concentrations, was devised to smooth out the μ_m values. The method utilized the fact that removed SOC was incorporated into cell mass with proportionality of Y. Thus,

$$X_t = X_0 + Y(S_0 - S_t) \qquad (3.4)$$

The X_t estimated from SOC data did not alter the shape of the cell-mass curve, but gave a smoother profile from which to compute μ_m. A comparison of the methods, presented in Figure 3.28 for Batch 5 data, shows that the new computation method did not alter the X curve.

Cell-concentration vs. time was plotted on a semi-log coordinate to compute μ_m. Figure 3.29 shows the semi-log plots for the exponential growth phase. The k values were determined from the slopes of straight lines and from Y for each batch run. The k values were 2.00, 2.24, 2.16, 1.83, and 2.22 mg-SOC/mg-cell,day for Batches I1, 1-2, I2, 2-2, and 5, respectively. The variations among batches did not reflect any significant physiological differences among the cells from different sampling locations.

3.2.5.3 Determination of K_s

K_s was determined from a μ (specific cell growth rate) vs. S curve. The μ values were calculated based on

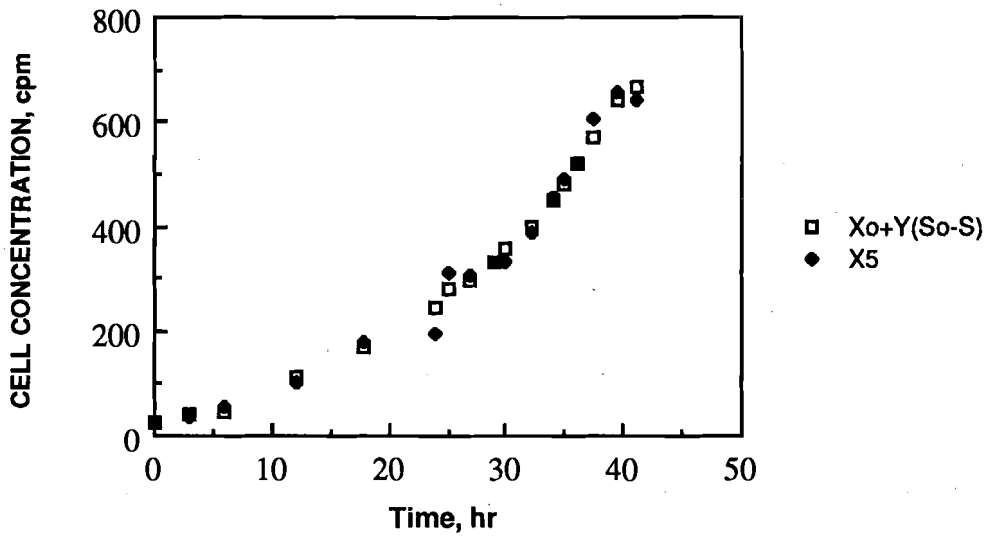

Figure 3.28. Comparison of estimated biomass (Xo + Y(So - S)) and measured biomass (X5) in Batch 5.

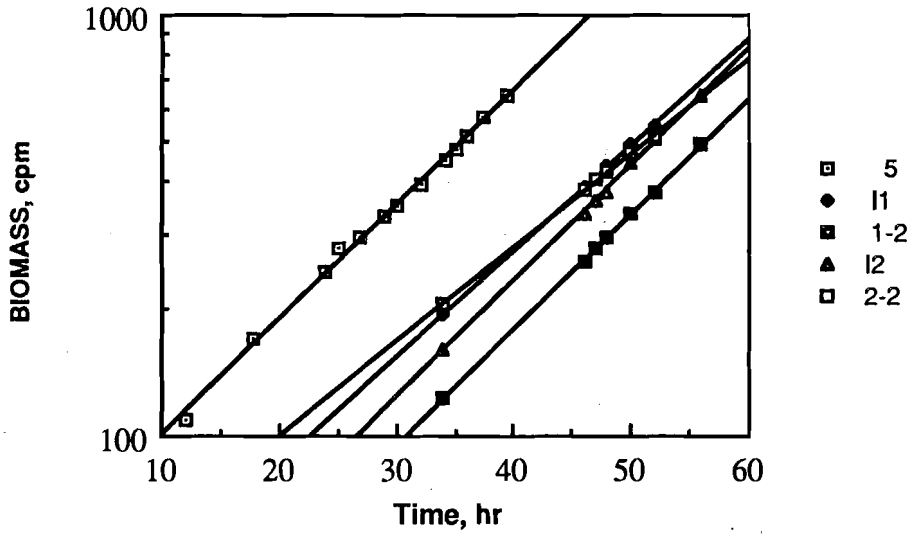

Figure 3.29. Exponential growth semi-log plot for five batch reactors.

$$\mu = (dX/dt)(1/X) \quad (3.5)$$

The dX/dt was estimated as $\Delta X/\Delta t$. A typical μ vs. S curve is shown in Figure 3.30. K_s was estimated by finding the S value when μ was half of μ_m. Because a small fraction of SOC (less than 2% of input C; 0.23-0.25 mg/L) was refractory in all batches, that fraction of SOC was subtracted from S values in the K_s determination. The K_s values determined for Batches I1, 1-2, I2, 2-2, and 5 were 0.78, 1.20, 0.78, 0.82, and 0.22 mg SOC/L, respectively. Perhaps the relatively low K_s value in Batch 5 reflected a cell adaptation to low SOC. That Batch 1-2 showed a relatively high K_s value may indicate that a high carbon affinity was not needed under nitrate limitation.

3.2.5.4 Determination of b

The cell decay coefficient, b, was determined for the declining phase with

$$dX/dt = - bX \quad (3.6)$$

Integrating Equation (3.6) yields

$$\log X_t = bt/2.303 + \log X_0 \quad (3.7)$$

X vs. t curves were constructed on a semi-log coordinate for the declining phase. A typical curve is shown in Figure 3.31, in which Batch 1-2 data are plotted. A characteristic of the cell-decay curves was a continuous decrease of the decay rate; thus, the curves look almost diphasic, as is emphasized by the two curves in Figure 3.31. The decay rate ranged from 0.07 to 0.12 day^{-1} for the first phase, and it decreased by at least one order of magnitude in the second phase. A similar phenomenon was observed, or discussed by other workers (Chang 1985, Casolari 1988). One explanation of a diphasic response is heterogeneity of the microbial population. A fraction of cells decays quickly, but the other fraction decays very slowly and remain to establish the second phase. A gradual adaptation of cells to nutrient limitation can be a second explanation.

3.3 Secondary Utilization of Halogenated Organic Compounds in BAZs

The goal during <u>in situ</u> bioreclamation is usually expressed in terms of specific hazardous contaminants which often constitute only

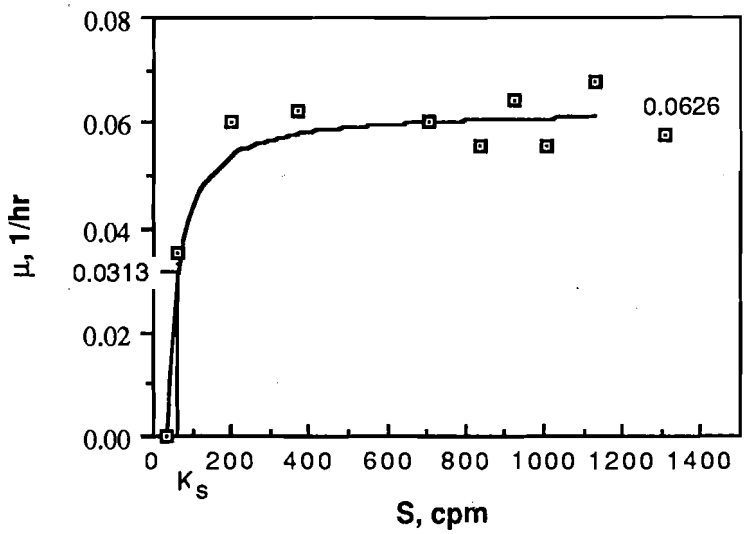

Figure 3.30. Determination of K_s from μ vs. S curve (Batch 5).

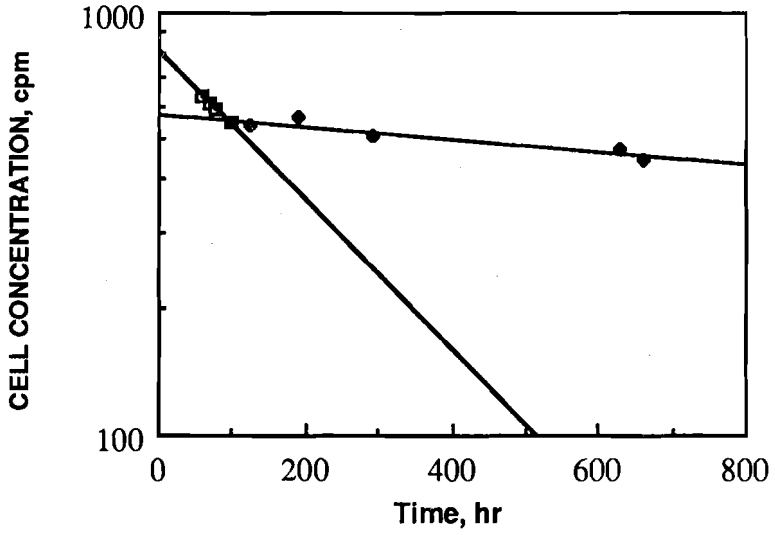

Figure 3.31. Cell decay in declining phase for Batch 1-2. Lines represent the initial rapid and later slow decay rates.

a small fraction of the soluble organic carbon (SOC). These compounds can be efficiently degraded as secondary substrates (Namkung et al., 1983) in the BAZ when the amount of accumulated biomass and the compound/biomass contact time are sufficiently large. Since the hazardous compounds frequently have slower biodegradation kinetics than a compound such as acetate, removals of the specific secondary compounds can be less than for general SOC.

The experiments reported in this section investigate the removal of several common halogenated solvents by the BAZs established through utilization of acetate as the primary substrate and electron acceptors injected along the flow path. The relative rates of degradation in the BAZs and the effect of contact time are emphasized.

3.3.1 Experimental Methods

3.3.1.1 Selection of Halogenated Organic Compounds

Six halogenated aliphatics and three chlorinated aromatics were tested. The halogenated aliphatics contained three sub-groups: carbon tetrachloride (CTC) and bromoform (BF), which were substituted methanes; 1,1,1-trichloroethane (1,1,1-TCA) and ethylene dibromide (EDB), which were substituted ethanes; and trichloroethene (TCE) and tetrachloroethene (TeCE), which were substituted ethenes. The chlorinated aromatics included 1,2-dichlorobenzene (1,2-DCB), 1,3-dichlorobenzene (1,3-DCB), and 1,4-dichlorobenzene (1,4-DCB). According to previous work by Bouwer and McCarty (1983) and Bouwer (1987), the substituted methanes (CTC and BF) should be relatively rapidly degraded under denitrifying conditions, the substituted ethanes (1,1,1-TCA and EDB) should be relatively slowly degraded, and the substituted ethene (TeCE) and the dichlorobenzenes should be refractory. Under aerobic conditions, on the other hand, the halogenated aliphatics were refractory, while the dichlorobenzenes were degradable (Bouwer and McCarty 1985, Bouwer 1987).

3.3.1.2 Experimental Set-up

Column 1 and Column 2 were used initially to test the removal of halogenated organic compounds by a secondary utilization mechanism in primary-substrate-grown BAZs (Run 1a and Run 2 in

Table 3.4). The six halogenated aliphatics and three DCBs were dissolved in the feed reservoir at a concentration of about 100 μg/L each. The feeding started on January 23, 1988 for the compounds except TCE and BF, which started on February 18, 1988, and for EDB, which started on March 7, 1988. All the other experimental conditions were maintained the same as the previous BAZ experiments.

Table 3.4. Secondary Utilization Experiments for Halogenated Organic Compound Removal

Run	Electron Acceptor	Primary Substrate	Secondary Substrate	Flow Velocity (cm/min)	Detention Time after Injection (min)	Experimental Period
1a	NO_3^-	Acetate	X-aliphatics and DCBs	0.1	50	1988 1/23-3/23
1b	"	"	"	0.04	125	3/23-4/27
1c	"	"	"	0.01	500	4/27-6/11
1d	"	"	"	0.1	50	6/11-6/16
2	"	"	"	0.1	50	1/23-3-23
3	H_2O_2	"	DCBs	0.1	50	4/27-6/16

The effect of liquid detention time was tested by reducing the flow rate in Column 1 to 40% and then to 10% of the original flow rate. Thus, the liquid detention time in the column was increased by 2.5 and 10 times, respectively. When the 10%-flow-rate experiment was over, the flow rate was increased back to the original flow rate to check for any additional cell adaptation to the halogenated compounds. The series of experiments is summarized as Runs 1b to 1d in Table 3.4.

An aerobic column which had hydrogen peroxide injected as electron acceptor was operated (Run 3 in Table 3.4) to test for aerobic removal of dichlorobenzenes in the BAZ. The reactor characteristics were identical to the BAZ-experiment column which was shown in Table 3.2. A 0.3% H_2O_2 solution was injected to an

injection port located at 5.0 cm from the inlet (the first injection port in Figure 3.9-Column 2). Acetate was fed as a primary substrate at a concentration of about 7.5 mg-SOC/L as before. The mineral constituents are given in Table 3.5.

The column was inoculated with a 1% dilution of settled primary effluent obtained from Urbana Sewage Treatment Plant. The inoculum was adopted to DCBs for three weeks before use. The operation started on April 27, 1988.

Table 3.5. Composition of Feed Solution for Hydrogen Peroxide Injection Column

Compounds	Concentration, mg/L
Acetate (CH_3COO^-)	7.5 as SOC
KH_2PO_4	34.0
K_2HPO_4	21.75
Na_2HPO_4	17.7
NH_4Cl	3.4
$MgSO_4$	11.0
$CaCl_2$	27.5
$FeCl_3$	0.15

3.3.1.3 Sampling and Analytical Methods

Samples were taken by syringe pump from the sampling ports at the rate equal to the input feeding rate. Approximately 12 mL of liquid was collected from each sampling port. Syringe-pump sampling had two advantages: keeping the exact upstream flow rate and preventing volatilization during sampling.

Exactly 10 mL of sample was extracted with 1 mL of dodecane or pentane in a 15-mL hypo vial by vigorous shaking for 3 minutes. The head space was minimized by adding distilled water, and the vial was tightly sealed with a teflon-faced silicone rubber cap. After waiting 15 minutes for phase seperation, 2 μL of the separated solvent phase was injected into a gas chromatograph equipped with

an electron-capture detector (Hewlett-Packard Model 5710 A). A 60/80 Carbopack B, 0.1% sp-1000 glass column was used for halogenated aliphatics, and a 1% sp-1000 on 100/120 Supelcoport was used for the DCBs. The same extraction and injection procedure was applied for standard solutions used for calibration. Dodecane was a superior extractant for the halogenated aliphatics, while pentane was superior for the dichlorobenzenes.

H_2O_2 was determined using a titanium-chloride method (Parker 1928).

3.3.2 Results for Secondary Utilization Experiments

3.3.2.1 Removal of Halogenated Aliphatics in Denitrification Columns

Six halogenated aliphatic compounds were fed into the one-BAZ denitrification column, in which the liquid detention time after injection was varied from 50 to 500 minutes. The primary substrate (acetate) concentrations in the feed reservoir, influent, and effluent throughout the experiments are shown as SOC in Figure 3.32. During Run 1a, in which the detention time was not changed from the one used to establish the BAZ, the effluent SOC concentration was low and steady. The effluent SOC was lower than 0.2 mg/L, which corresponded to more than 97% removal. A representative sampling for halogenated-compound determination was made near the end of this period, as indicated by arrow in Figure 3.32.

In Run 1b, in which the detention time was increased by 2.5 times, the effluent SOC increased slightly and the concentrations were between 0.2-0.3 mg/L for most measurements. Because a lower effluent SOC concentration was expected with increased detention time, ^{14}C labelling of the feed acetate was removed for one week to help elucidate the phenomenon. In spite of no input of ^{14}C in the feed, the effluent ^{14}C level was not much changed (0.20 mg-SOC/L, on average). When the ^{14}C-labeling was restarted, the average effluent SOC was 0.23 mg/L. These results show that the portion of effluent SOC contributed by feed acetate was only 0.03 mg/L, while the majority (87%) came from another source, namely, previously labeled biofilm. The accumulated and labeled biomass was responsible for release of biomass-associated soluble microbial products (Namkung and Rittmann, 1986). With an increased

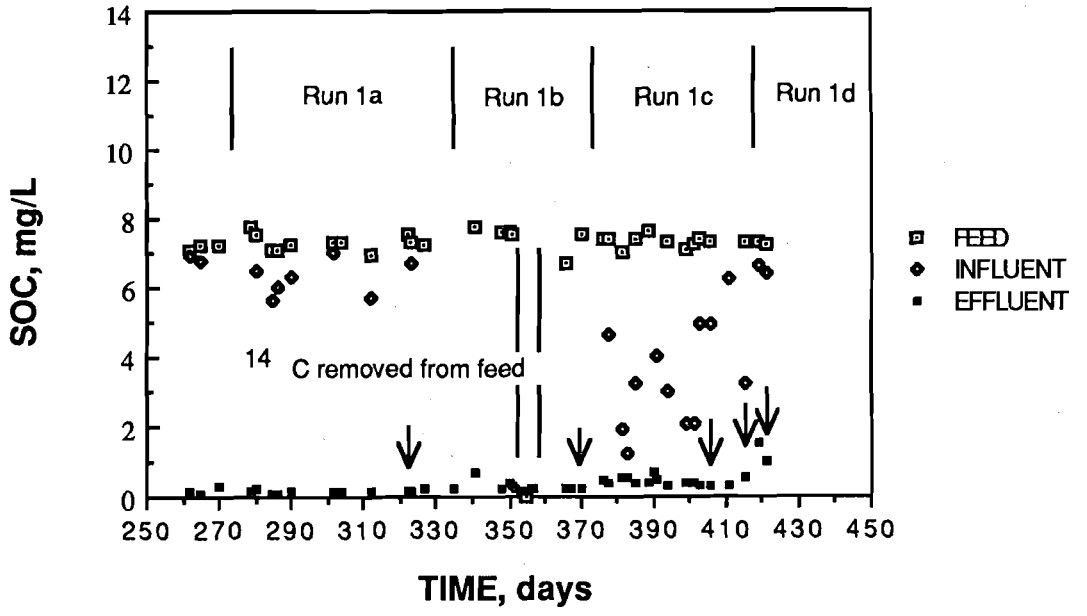

Figure 3.32. SOC concentrations during Run 1 in a denitrifying column. Arrows indicate samplings for halogenated organic compound determination.

detention time, the fed acetate was consumed only in the upstream portion of the BAZ, and the biofilm in the downstream portion of the BAZ was undergoing a starving condition. Therefore, the biofilm distribution in the column was not at a steady state.

Run 1c was initiated by increasing the liquid detention time by 10 times from the original. The effluent SOC increased even more at first (about 0.5 mg/L), and then gradually decreased to about 0.3 mg/L. Again, this increase was caused by soluble microbial product formation. The influent SOC dropped severely due to the increased retention time of liquid in the connection tubing between the reservoir and the column. Oxygen diffusion through the tubing was responsible for stimulating aerobic degradation of feed acetate before it reached the denitrifying BAZ. This drop of the influent SOC concentration was substantially eliminated by increasing the flow rate in the tubing and by diverting most of the flow to waste. As shown by the arrows for Run 1c in Figure 3.32, samplings made after the flow diversion had an improved SOC concentration entering the column.

In Run 1d, the detention time was decreased back to the level of Run 1a by increasing the flow rate through the column. The effluent quality deteriorated initially after the change, then recovered quickly. Due to a time constraint, the sampling was made before the column reached a new steady state.

The results for the halogenated aliphatics, as well as SOC, are shown in Figures 3.33 to 3.37 for Runs 1a to 1d, respectively. Sample concentrations are normalized to the measured concentration at the sampling port just upflow of the nitrate injection, and the initial concentrations of each compound are given in the figures. Since the concentration at the nitrate injection port could not be measured, it was assumed to be the same as the concentration of the immediate upstream port.

In Figure 3.33, which is for the original (50-minutes) detention time, out of six halogenated aliphatic compounds, only CTC showed significant removal (28%) through the BAZ. Losses in all the other compounds were not greater than usual experimental error.

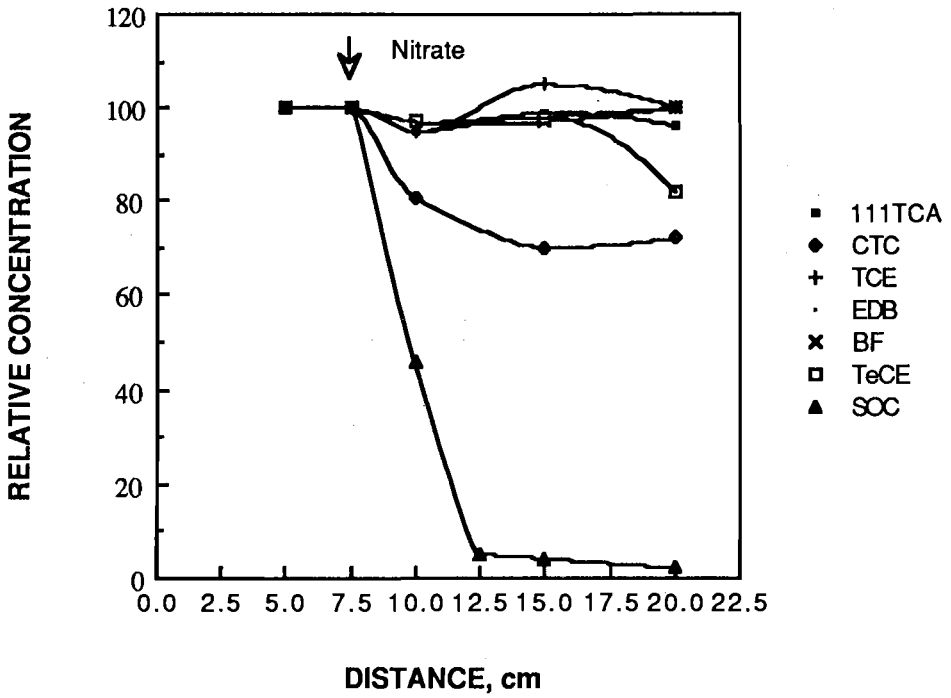

Figure 3.33. Profiles of halogenated aliphatic compounds in a denitrifying column at 50-min. detention time after nitrate injection (Run 1a). The initial concentrations for the compounds were (in µg/l) 84 for 1,1,1-TCA, 81 for CTC, 95 for TCE, 87 for EDB, 106 for BF, 79 for TeCE, and 6,600 for SOC.

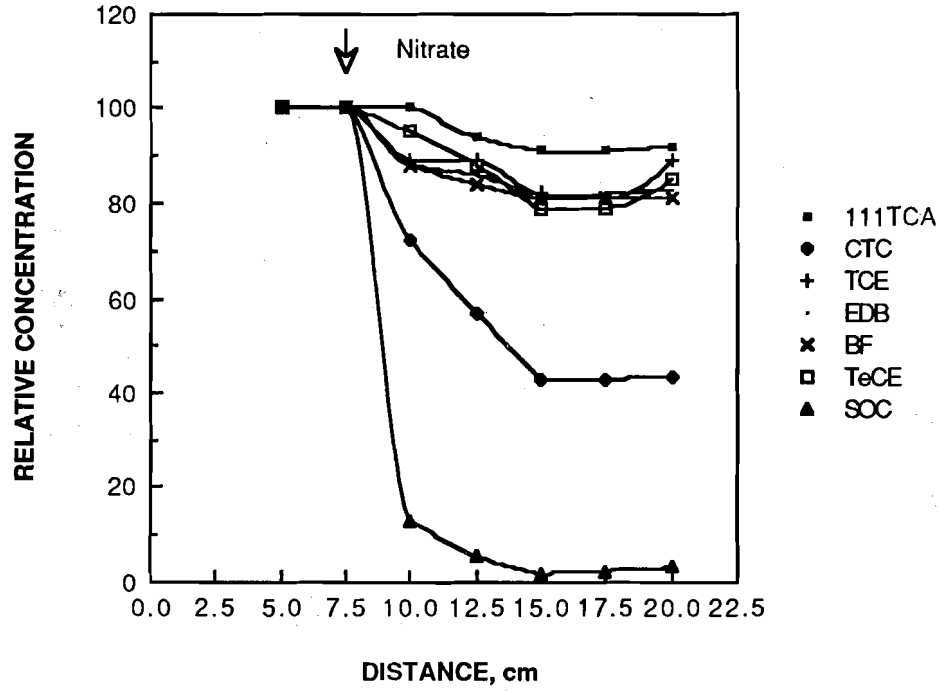

Figure 3.34. Profiles of halogenated aliphatic compounds in a denitrifying column at 125-min. detention time after nitrate injection (Run 1b). The initial concentrations for the compounds were (in µg/l) 99 for 1,1,1-TCA, 69 for CTC, 62 for TCE, 69 for EDB, 57 for BF, 55 for TeCE, and 5,100 for SOC.

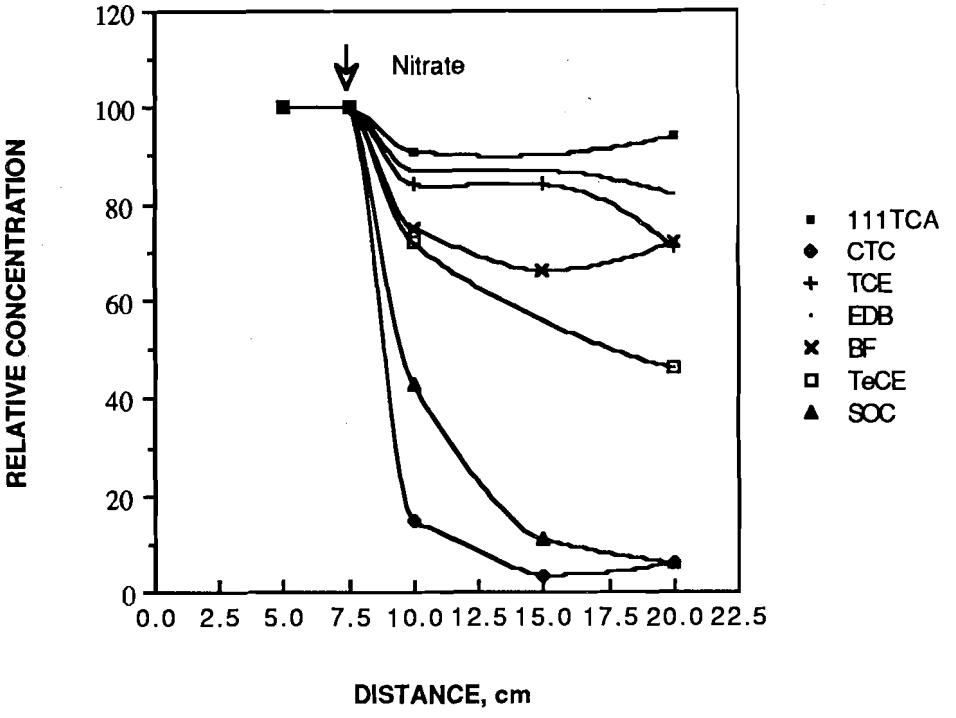

Figure 3.35. Profiles of halogenated aliphatic compounds in a denitrifying column at 500-min. detention time after nitrate injection (Run 1c, day 406). The initial concentrations for the compounds were (in μg/l) 112 for 1,1,1-TCA, 53 for CTC, 88 for TCE, 45 for EDB, 54 for BF, 50 for TeCE, and 4,900 for SOC.

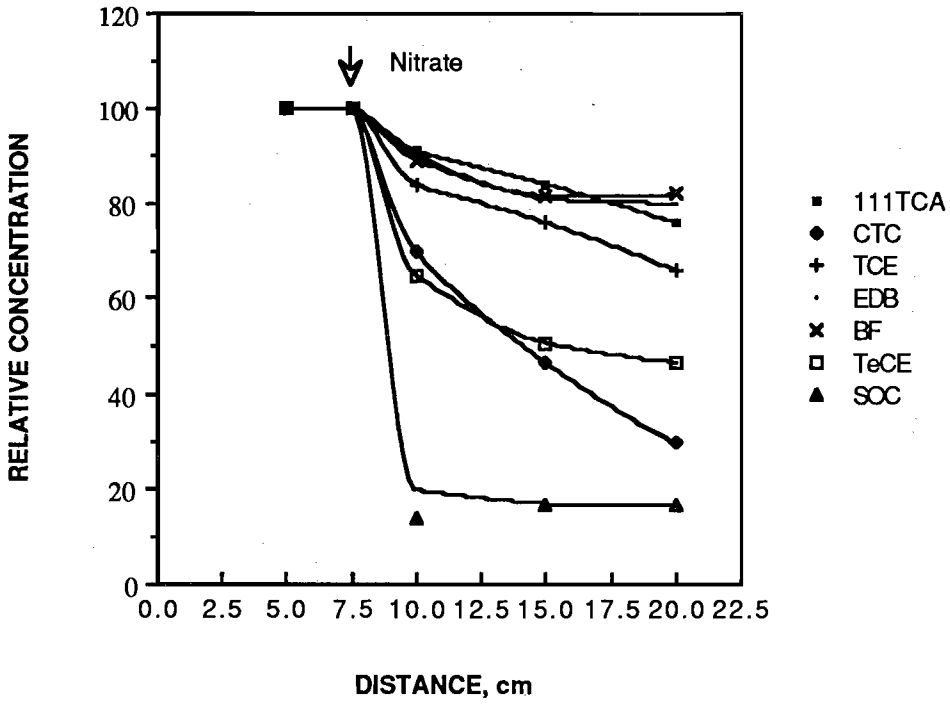

Figure 3.36. Profiles of halogenated aliphatic compounds in a denitrifying column at 500-min. detention time after nitrate injection (Run 1c, day 415). The initial concentrations for the compounds were (in µg/l) 96 for 1,1,1-TCA, 65 for CTC, 91 for TCE, 38 for EDB, 49 for BF, 84 for TeCE, and 3,200 for SOC.

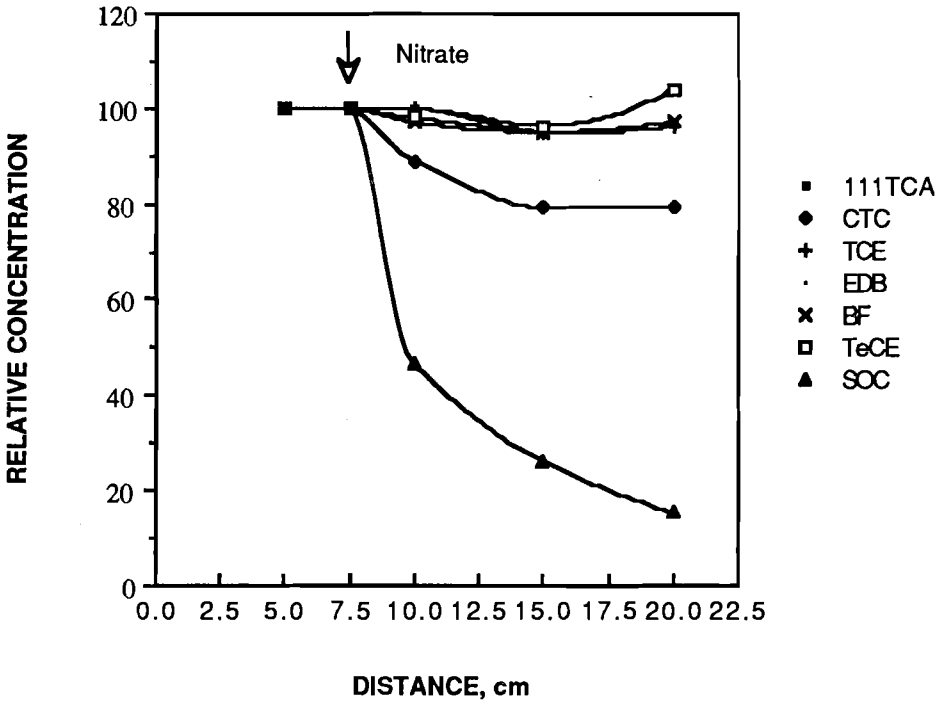

Figure 3.37. Profiles of halogenated aliphatic compounds in a denitrifying column at 50-min. detention time after nitrate injection (Run 1d). The initial concentrations for the compounds were (in µg/l) 94 for 1,1,1-TCA, 62 for CTC, 87 for TCE, 45 for EDB, 59 for BF, 66 for TeCE, and 6,300 for SOC.

The results of Run 1b, which had a detention time 2.5 times longer than Run 1a, are shown in Figure 3.34. The removal of CTC became more significant (around 60%), and the other compounds, except 1,1,1-TCA, had 15%-20% removal. 1,1,1-TCA had the lowest removal efficiency, about 10%. The concentrations of TCE and TeCE were shown to be higher at 20-cm location than at 15-17.5 cm. The percentage removals for these compounds dropped from 19 to 11 for TCE, and 21 to 15 for TeCE. Since the percentage removal of the primary substrate (acetate) was very stable (the coefficient of variation--100% (standard deviation/mean)--was in the range of 2-4%; data not shown), the variation of the percentage removal of these secondary substrates should be attributed to analytical error for these compounds.

Figure 3.35 shows the results of the day-406 sampling in Run 1c, which had 10 times longer detention time compared to Run 1a, or 4 times longer than that in Run 1b. CTC was removed almost completely (94%), and its concentration decreased from 53 μg/L to 3 μg/L. Significant removals of TeCE (50%), BF (30%), and TCE (15%-30%) occurred in response to the increased contact time between the compounds and the BAZ. EDB and 1,1,1-TCA, however, showed only comparable percentage removal (about 20% and 10%, respectively) to the previous detention time in Run 1b. Figure 3.36 shows the results in a subsequent sampling made on day 415. Similar or slightly increased removals were observed for TeCE (50%), TCE (30%), EDB (20%), and 1,1,1-TCA (20%), but, less removals were made for CTC (70%) and BF (20%). Even though there were some fluctuations in removal efficiency between the two samplings, overall trends of removal remained consistent, and the average removals for most compounds in this extended detention time were substantially higher than the removals in Run 1b. Another important finding in Run 1c was that all of the six halogenated aliphatics tested were degradable under denitrification conditions.

Figure 3.37 shows the results obtained from Run 1d, which had the same detention time as Run 1a. The overall trends for the halogenated compounds were very similar to those in Figure 3.33. Thus, it became clear that the increased removal in Runs 1b and 1c were not the effect of cell adaptation, but occurred because of the increased detention time.

The results in these experiments, especially the results shown in Figures 3.35 and 3.36, are partially consistent with, but still contain substantial contradictions to those of Bouwer (1987), who showed that CTC had the fastest removal, followed by BF, 1,1,1-TCA, and EDB, but TeCE was refractory. In this experiment, BF showed relatively slow removal, but TeCE was relatively rapidly degraded in the BAZ. Trace amounts of chloroform were produced after nitrate injection in this experiment, which demonstrated a reductive dehalogenation of CTC. Because no radioactive tracer study was performed, it was not demonstrated whether or not the removed portion of the halogenated compounds was converted to CO_2. Bouwer and McCarty (1983) demonstrated, however, that CTC was converted to CO_2 and cell mass in a denitrifying biofilm column.

Run 2 was conducted under identical operating conditions to Run 1a, except that this column had two BAZs, while Run 1a was performed in a one-BAZ column. The results were qualitatively similar to Run 1a, but showed less removal of CTC (see Figure 3.38). This was, probably, due to the gas accumulation, as explained in Section 3.2.3.

3.3.2.2 Removal of Dichlorobenzenes in Denitrification Columns

Profiles of 1,2-DCB and 1,3-DCB for the day-415 sampling from Run 1c are shown in Figure 3.39. 1,4-DCB could not be determined due to a technical problem: the peak for this compound overlapped with that for BF in the Supelcoport column which was used for DCB determination (BF was determined by a Carbopack column in which 1,4-DCB did not overlap). Figure 3.39 shows that 1,2-DCB decreased from 35 μg/L to 23 μg/L, having about 30% removal across the BAZ. A similar removal efficiency was observed in another sampling which was made on day 406 (data not shown). The removal of 1,3-DCB was slightly better than that of 1,2-DCB in Figure 3.39, but it was slightly less in the other sampling.

As with the halogenated aliphatics, detention time was a critical parameter in the extent of DCB removal. At the reduced detention time used in Runs 1a and 1d, no significant removal was observed. The result of Run 1d is shown in Figure 3.40.

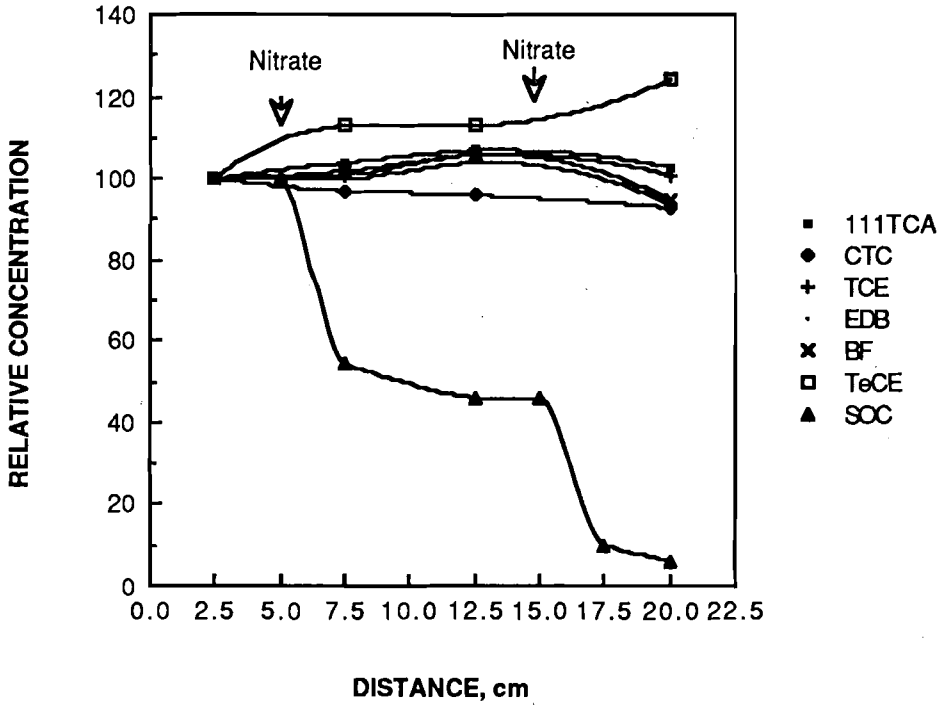

Figure 3.38. Profiles of halogenated aliphatic compounds in a denitrifying column at 50-min. detention time after nitrate injection (Run 2). The initial concentrations for the compounds were (in μg/l) 158 for 1,1,1-TCA, 158 for CTC, 152 for TCE, 130 for EDB, 119 for BF, 118 for TeCE, and 6,700 for SOC.

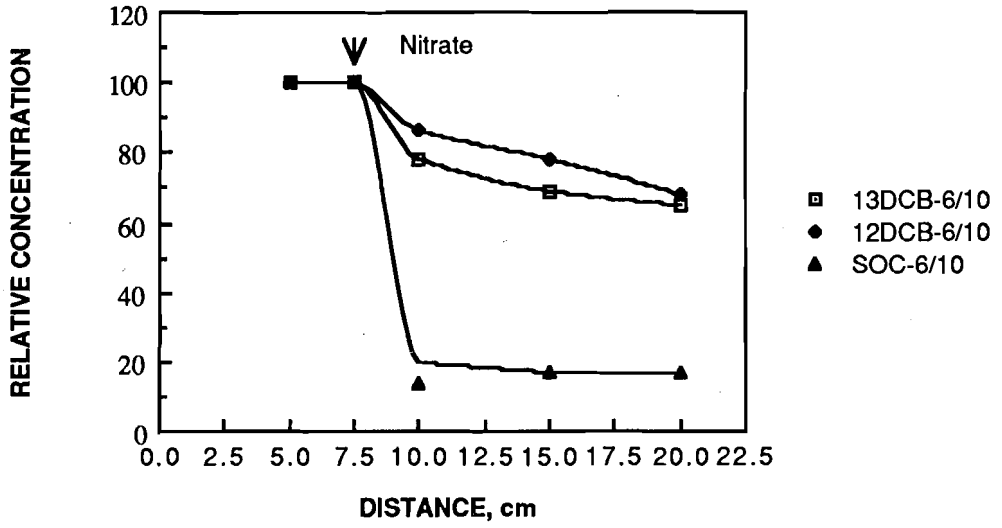

Figure 3.39. Profiles of 1,2- and 1,3-DCB in a denitrifying column at 500-minute detention time after nitrate injection (Run 1c, day 415). Influent concentrations were (in μg/l) 42 for 1,2-DCB, 29 for 1,3-DCB, and 7,300 for SOC.

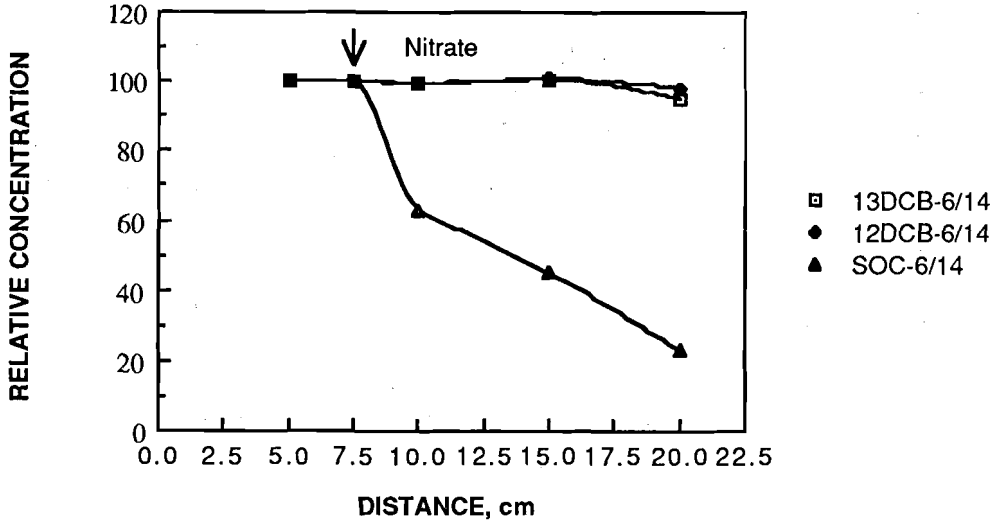

Figure 3.40. Profiles of 1,2- and 1,3-DCB in a denitrifying column at 50-minute detention time after nitrate injection (Run 1d). Influent concentrations were (in μg/l) 35 for 1,2-DCB, 23 for 1,3-DCB, and 7,200 for SOC.

The observation of DCB removal in a denitrifying column is very important, because these compounds were thought to be biologically persistent under anoxic conditions (Bouwer and McCarty 1983, Kuhn et al. 1985, Bouwer 1987). To investigate any non-biological reactions which might have been responsible for the removal, two potential alternative pathways were examined: sorption and volatilization.

DCBs have moderately high octanol-water partition coefficients, with a typical log K_{ow} value around 3.4 (Miller et al., 1985). Therefore, DCBs could adsorb onto or absorb into hydrophobic parts in cells produced from the primary substrate. This was, however, not the reason for the removal in this experiment. First, the liquid samples were not filtered before DCB extractions; thus, any DCBs sorbed to effluent cells would have been measured. Second and more important, the DCBs were fed continuously for the duration of the test. Any sorption capacity of the cells in the column would have been saturated long before samples were taken.

Volatilization of DCBs into the nitrogen gas, produced during the denitrification reaction, could take place. But, the gas production rate was trivial compared to the liquid flow rate (0.4% by volume) and would not explain the substantial removal of DCBs. Moreover, Section 3.3.2.1 showed that 1,1,1-TCA in Run 1c had a much lower percentage removal (15% on average of two samplings) than for the DCBs, even though it had one order of magnitude higher Henry's law constant (Lyman et al., 1982). Lack of volatilization loss of 1,1,1-TCA supported the insignificance of volatilization for DCBs.

As there was no significant alternative pathway for DCB removal in these experiments, the removal can be attributed to biodegradation. Further research is necessary to prove this rigorously.

3.3.2.3 Removal of Dichlorobenzenes with Hydrogen-Peroxide Injection

The feed, influent, and effluent concentrations of SOC in the column injected with H_2O_2 (Run 3 in Table 3.4) are shown in Figure 3.41. The effluent SOC concentration decreased quickly and reached a relatively stable concentration in a week. A slightly lower amount

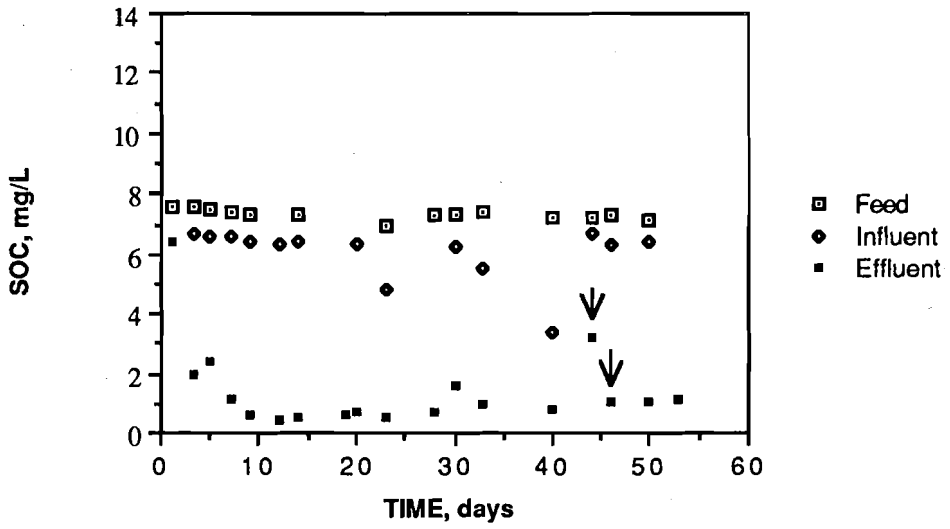

Figure 3.41. SOC concentrations in a H_2O_2 injection column (Run 3). Arrows indicate samplings for DCB determinations.

of H_2O_2 than required for SOC oxidation was fed in order to avoid toxicity from H_2O_2. Thus, the reaction was under H_2O_2 limitation, and the SOC degradation was not complete. The hydrogen peroxide disappeared faster than expected from the stoichiometry of SOC oxidation. It is likely that the enzyme catalase degraded H_2O_2 to O_2, in order to reduce H_2O_2 toxicity, at a more rapid rate than the O_2 was utilized.

DCB sampling was made on days 44 and 46, and results are shown in Figures 3.42 and 3.43, respectively. Figure 3.42 shows comparatively lower SOC removal, due to low H_2O_2 injection on that day. In both figures, the three DCBs were removed with the same pattern. 1,4-DCB showed the lowest removal (10%) among the three compounds, while the other two had comparable degrees of removal (20%-30%).

Most of the DCB removal took place immediately after the H_2O_2 injection. Because the SOC was removed beyond the first sampling port, while DCB removal occurred before that port, some role of H_2O_2 in the removal of DCBs is implicated. H_2O_2 was not directly responsible for this removal, since a series of batch experiments (see Figure 3.44) showed that a H_2O_2 addition into a non-biological reactor did not cause any greater removal of DCBs than occurred in a control. Although hydrogen peroxide did not play a direct role in DCB removal, it is still possible that the biologically mediated hydrogen peroxide decay to oxygen affected DCB removal, since hydrogen peroxide was degraded before the first sampling port. Therefore, it is not clear whether or not the normal aerobic degradation of DCBs, as seen by other authors (Bouwer and McCarty 1985, Bouwer 1987, Kuhn et al. 1985), was solely responsible for the DCB removals observed in the H_2O_2 injection column.

The results in this experiment differ considerably from those of Bouwer (1987), who employed a biofilm column with a 10-min detention time and aerobic conditions from contact with ambient oxygen. Bouwer (1987) showed that 10 μg/L of 1,2-DCB and 1,4-DCB were removed more than 97%, and the adaptation periods were less than 3 weeks. 1,3-DCB was removed 71%, but the adaptation period required was 500 days. The present study showed relatively lower percentage removals, but 1,3-DCB was removed with a much shorter adaptation period. These differences support the fact that the

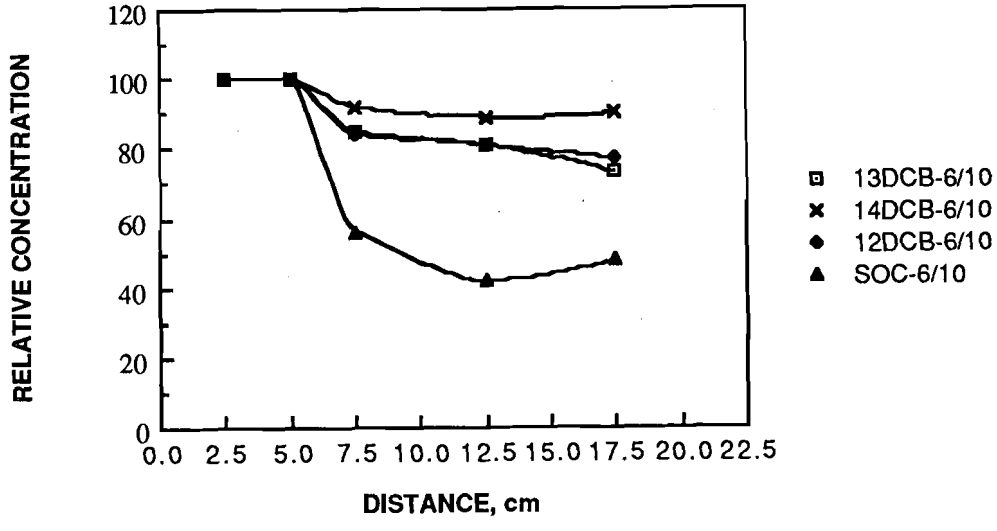

Figure 3.42. Profiles of DCBs in an H_2O_2-injection column at 50-minutes detention time (day 44 from Run 3). The initial concentrations were (in µg/l) 44 for 1,2-DCB, 43 for 1,3-DCB, 42 for 1,4-DCB, and 6,650 for SOC.

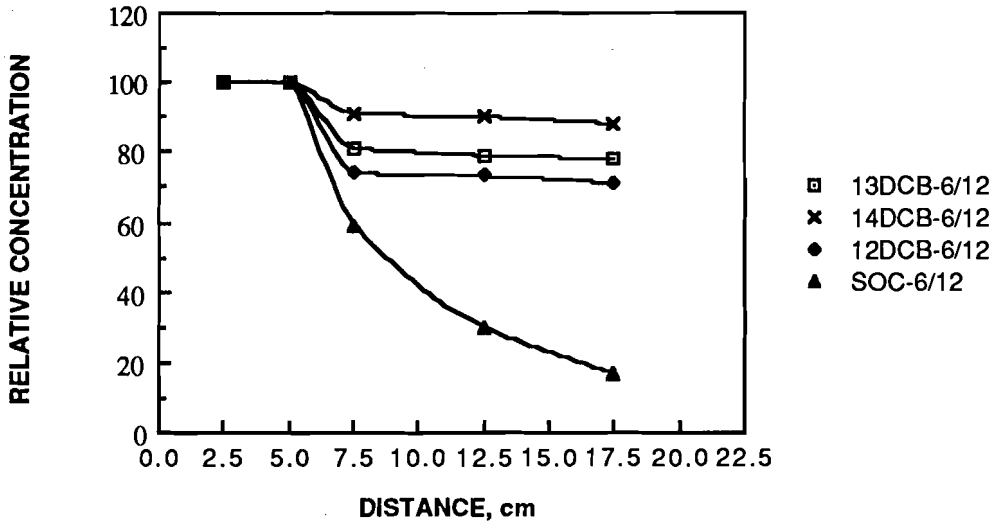

Figure 3.43. Profiles of DCBs in an H_2O_2-injection column at 50-minutes detention time (day 46 from Run 3). The initial concentrations were (in μg/l) 33 for 1,2-DCB, 35 for 1,3-DCB, 46 for 1,4-DCB, and 6,250 for SOC.

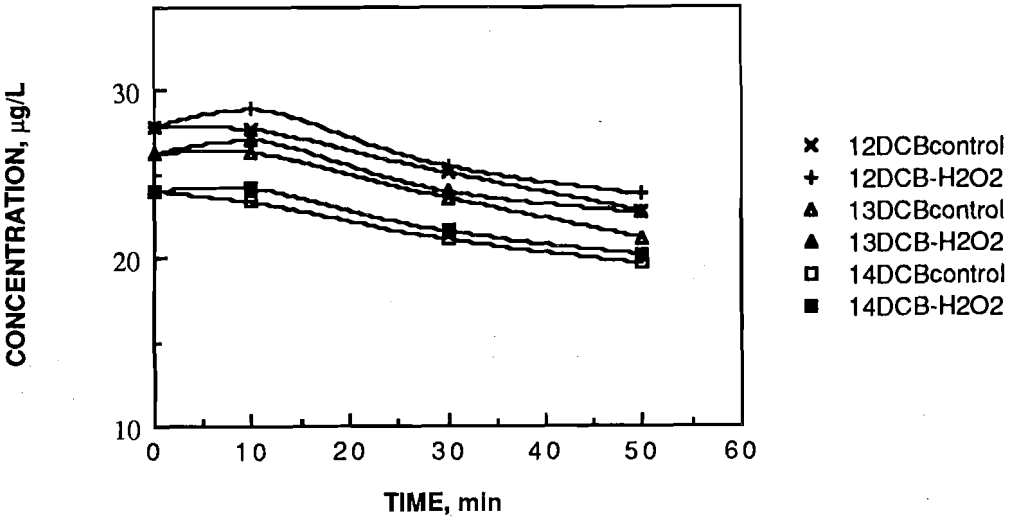

Figure 3.44. The effects of H_2O_2 on DCB removals in non-biological batch reactors. For this experiment, 15-mL extraction vials which were sealed with teflon-faced silicone septa were used as the batch reactors. A series of vials which contained 20 mg/L of H_2O_2, an equivalent concentration that the column reactor actually received, were filled with feed solution without leaving headspace and extracted at times 10, 30, and 50 minutes after initiation. The time of extraction was equivalent to the real detention times from the H_2O_2 injection port to the sampling ports in Figures 3.43 and 3.44. A series of control vials which did not contain H_2O_2 were prepared and extracted same way.

removal mechanism in this study might have differed from that in the aerobic column which Bouwer (1987) used. Future study is necessary to thoroughly evaluate the differences.

CHAPTER 4. COMPUTER MODELING

4.1 One-Dimensional Solute Transport Model

The governing mass balance on a biodegradable compound for steady-state flow through a homogeneous, one-dimensional column, such as that described in Chapter 2, has the form

$$\varepsilon \frac{\partial S}{\partial t} = D_H \frac{\partial^2 S}{\partial x^2} - v \frac{\partial S}{\partial x} - aJ + Q_S \qquad (4.1)$$

where S is the dissolved substrate concentration, ε is the porosity, D_H is the hydrodynamic dispersion coefficient, v is the specific discharge (superficial flow velocity), a is the specific surface area of the bed particles, J is the substrate flux into the biofilm, and Q_S is the substrate source term due to lateral input through the injection ports. Equation (4.1) can seldom be solved analytically to give S as a function of t and x. Hence numerical solution using a digital computer is necessary.

For numerical solution in general, equation (4.1) is discretized in time and space, and a finite difference approximation for both kinds of derivatives are straight forward. The difference equations can be solved at successive time steps until a given stopping point, as defined by a particular problem.

Equation (4.1) can be simplified for steady-state by setting the time derivative to zero. The resulting equation,

$$0 = D_H \frac{d^2 S}{dx^2} - v \frac{dS}{dx} - aJ + Q_S \qquad (4.2)$$

is an ordinary differential equation, as opposed to equation (4.1), which is a partial differential equation.

To discretize steady-state equation (4.2), no difference approximation is needed for time. The discretized steady-state equation was chosen for two reasons. First, it approximately describes realistic scenarios of enhanced <u>in situ</u> bioreclamation: namely, the steady-state input of a limiting factor (the electron acceptor here) into an aquifer containing a fairly constant pollutant source. Second, the numerical solution of equation (4.2) provided an

opportunity to develop new, highly efficient solution techniques for strongly non-linear ordinary differential equations. The numerical approach, based upon quasilinearization, also can be applied to other groundwater situations involving nonlinear reaction terms. The numerical quasilinearization with finite differences is presented in detail in Section 4.3.

4.2. Biofilm Phenomena and Kinetics

Because of the high specific surface area in an aquifer, almost all of the biological activity is associated with the solids as biofilms or microcolonies. This research utilizes the concept of a biofilm, which is generally defined as a layer-like aggregation of microorganisms attached to a solid surface. Modeling of biofilm kinetics has been achieved by considering an ideal biofilm that is locally homogeneous and planar. The processes affecting substrates and biomass are represented by a set of differential and algebraic equations which must be satisfied simultaneously.

Figure 4.1 shows the conceptual basis of the biofilm model. The biofilm, having thickness L_f, is composed of an idealized homogeneous matrix of cells at a density of X_f. The substrate concentration changes nonlinearly across the biofilm thickness from S_s to S_w at the attachment surface.

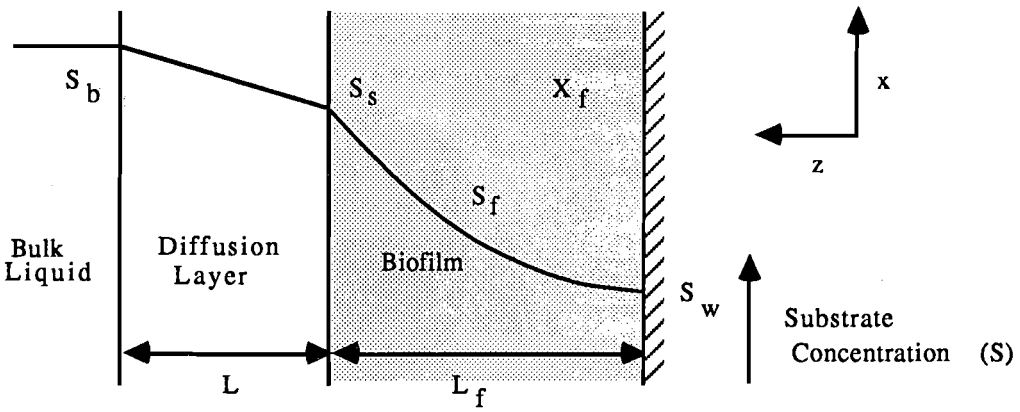

Figure 4.1. Conceptual basis of the biofilm model (after Rittmann and McCarty, 1980a).

The substrate is transported from the bulk liquid across an idealized layer, L, through which all the resistance to mass transfer lies. This layer is referred to as the diffusion layer and represents the resistance to mass transfer from the liquid to the biofilm. There have been several published correlations for relating L to reactors and substrate variables (Rittmann, 1982a). The substrate concentration varies linearly across this layer according to Fick's first law

$$J = \frac{D}{L}(S_b - S_s) \tag{4.3}$$

Substrate utilization within the biofilm is assumed to follow a Monod relationship and is defined by the following equation

$$r_{ut} = \frac{-k\ X_f\ S_f}{K_s + S_f} \tag{4.4}$$

where r_{ut} is the rate of substrate uptake per unit biofilm volume, k is the maximum specific rate of substrate utilization, and K_s is the half-maximum-rate substrate concentration. Equation (4.4) represents the accumulation of substrate in the biomass due to utilization, and it has a negative sense.

Molecular diffusion within the biofilm is described by Fick's second law and is represented by

$$r_{diff} = D_f \frac{\partial^2 S_f}{\partial z^2} \tag{4.5}$$

where r_{diff} is the rate of substrate accumulation due to diffusion, and D_f represents the molecular diffusion coefficient of the substrate within the biofilm. The total time rate of change of substrate within the biofilm can be written as

$$\frac{\partial S_f}{\partial t} = D_f \frac{\partial^2 S_f}{\partial z^2} - \frac{k\ X_f\ S_f}{K_s + S_f} \tag{4.6}$$

If the substrate profile is at steady-state, equation (4.7) simplifies to

$$0 = D_f \frac{\partial^2 S_f}{\partial t^2} - \frac{k\ X_f\ S_f}{K_s + S_f} \qquad (4.7)$$

and is subject to the following boundary conditions:

1. No substrate flux into the solid attachment surface

$$\frac{\partial S_f}{\partial z} = 0 \quad @\ z = 0 \text{ and } t \geq 0 \qquad (4.8)$$

2. Continuity of flux at the biofilm/diffusion layer interface

$$S_f = S_s \quad @ \quad z = L_f \text{ and } t \geq 0 \qquad (4.9)$$

There are three basic substrate concentration profiles that are generally used to categorize biofilms. A deep biofilm is defined as one in which the substrate concentration drops to zero at some point within the biofilm. A deep biofilm has the maximum substrate flux for a given S_s value. The other extreme case is that of a fully penetrated biofilm, or one in which the substrate concentration equals S_s at all points within the biofilm. For all cases between fully-penetrated and deep, a biofilm is defined as shallow.

The remaining major aspect of the biofilm model is coupling mass transport from the bulk liquid to the surface of the biofilm, equation (4.3), with substrate utilization and diffusion in the biofilm, equation (4.7). The coupling and solution of the governing equations complete the basics of biofilm modeling.

A steady-state biofilm is defined as one where all the time derivatives are set to zero (Sáez and Rittmann, 1988). A mass balance on the biofilm requires that cell losses are balanced by cell growth. The growth rate of a biofilm per unit surface area is defined by YJ, where Y is the cell yield coefficient and J is the substrate flux into the biofilm. The biofilm loss rate per unit surface area is defined as $-L_f X_f b_T$, where L_f is the biofilm thickness, X_f is the biofilm density, and b_T is the overall first-order loss coefficient. The overall first-order loss coefficient is comprised of two components, as expressed in the following equation

$$b_T = b + b_s \qquad (4.10)$$

where b is the cell maintenance and decay coefficient and b_s is the shear loss coefficient. The shear loss is a result of shear forces of the flow passing by the biofilm and stripping pieces of it away with the flow. Rittmann (1982b) presented a simple model in which an estimate of the shear loss coefficient can be made with knowledge of the biofilm thickness and reactor parameters. The equations developed by Rittmann (1982b) are used in this research to estimate the shear-loss coefficient.

A final concept of steady-state biofilm modeling is a definition of a threshold concentration below which no steady-state biofilm can occur. The threshold concentration is defined as S_{min}, and concentrations below it give a biofilm that is continuously losing mass, which violates the steady-state assumption. S_{min} is computed as

$$S_{min} = \frac{K_s\, b_T}{Y\, k - b_T} \qquad (4.11)$$

Steady-state-biofilm modeling involves the solutions of equations (4.3) and (4.7), as well as the mass balance on biofilm mass. Originally, complicated and time consuming numerical techniques were used to solve the coupled equations. The resulting solution determined the flux, J, into the biofilm for a given set of kinetic parameters (K_s, k, b_T, Y, X_f, L, D, and D_f) and a bulk substrate concentration, S_b. Such a solution technique encompasses all the biofilm profiles i.e. deep, shallow, and fully-penetrating.

Repetitious use of these sophisticated numerical models for solving the governing equations for steady-state flux determination is not practical when the goal is to model a large system, such as for aquifer bioreclamation. As a result of this, several researchers developed pseudo-analytical techniques that fit the numerical results with algebraic equations (Rittmann and McCarty, 1980a; 1981; Sáez and Rittmann, 1988)

The solution presented by Sáez and Rittmann (1988) is the most recent and accurate method available among the several in existence. More accurate over a large range of substrate concentration than

previous methods, the new pseudo-analytical technique is the best option for steady-state biofilm modeling. A short summary of the model's structure is presented here for clarity; the reader is referred to the original manuscript for complete details.

The first premise behind the pseudo-analytical technique is that the actual flux to a steady-state biofilm is a fraction, f, of the flux into a deep biofilm. This is represented mathematically by

$$J = f\, J_{deep} \qquad (4.12)$$

where J_{deep} is the flux into a deep biofilm exposed to the same concentration, S_b.

The second premise is that the solution is presented most efficiently with dimensionless parameters. The efficiency comes about because the many dimensional parameters can be lumped together to form a smaller number of dimensionless parameters, which are indicated by an asterisk. The key dimensionless parameters are

$$S_s^* = \frac{S_s}{K_s} \; ; \; S_b^* = \frac{S_b}{K_s}$$

$$S^*_{min} = \frac{b_T}{Yk - b_T}$$

$$J^* = \frac{J}{(K_s k X_f D_f)^{1/2}}$$

$$K^* = \left(\frac{D}{L}\right) \left[\frac{K_s}{(kX_f D_f)}\right]^{1/2}$$

For example, equation (4.12) can be rewritten in the dimensionless regime as

$$J^* = f\, J^*_{deep} \qquad (4.13)$$

Sáez and Rittmann (1988) found the value of f could be expressed algebraically as

$$f = \tanh[\alpha (\frac{S_s^*}{S_{min}^*} - 1)\beta] \quad (4.14)$$

where α and β are defined by

$$\alpha = 1.5739 + 0.32075 (- \log S_{min}^*)^{0.15213} \quad 10^{-4} \leq S_{min}^* \leq 1 \quad (4.15)$$

$$\alpha = 1.5739 + 0.37149 (\log S_{min}^*)^{0.31344} \quad 1 \leq S_{min}^* \leq 10^3 \quad (4.16)$$

$$\beta = 0.5014 + 0.01985 (-\log S_{min}^*)^{0.19476} \quad 10^{-4} \leq S_{min}^* \leq 1 \quad (4.17)$$

$$\beta = 0.5014 + 0.02726 (\log S_{min}^*)^{0.52256} \quad 1 \leq S_{min}^* \leq 10^3 \quad (4.18)$$

Because S_s^*, the dimensionless substrate concentration at the biofilm surface, is not known <u>apriori</u>, it must be computed iteratively, using a Newtons root finding technique, from

$$S_b^* = S_s^* + \frac{\tanh[\alpha(\frac{S_s^*}{S_{min}^*} - 1)\beta] \sqrt{2 [S_s^* - \ln (1 + S_s^*)]}}{K^*} \quad (4.19)$$

Once the appropriate S_s^* value is converged upon, the flux is calculated by Fick's first law

$$J^* = (S_b^* - S_s^*) K^* \quad (4.20)$$

which is easily transferred into the dimensional flux using the definition of the non-dimensional flux

$$J = J^* [K_s k X_f D_f]^{1/2} \quad (4.21)$$

4.3 The Quasilinearization Technique

The objective of this section is to present a summary of the quasilinearization technique coupled with the finite-difference solution technique. The equation to be solved is the steady-state one-dimensional transport equation with a biological reaction term, which was presented in a previous section as equation (4.2).

Traditional approaches (Rittmann, 1982a) involve solving the transient problem, equation (4.1), until steady-state is achieved. Here the time derivative, in addition to the spatial derivatives, is approximated using finite differences. The time dimension adds many more computations than are necessary if the steady-state solution can be obtained directly. Thus, the traditional approaches are computationally inefficient and are not feasible for extension to more complex problems. Here, a technique which bypasses all of the intermediate calculations and solves directly for the steady-state is developed. Handling the non-linearity of the reaction rate term (J) is the focus of computational strategy, because the biofilm reaction rate term approaches infinite reaction order at (S) values close to S_{min}.

The problems of non-linearity can be overcome by quasilinearization (Lee, 1968). The quasilinearization process involves the use of a first-order Taylor's series approximation for the non-linear substrate flux term. If S^m is assumed to be the known substrate concentration at an iteration level m, then the substrate flux at the next iteration level can be approximated as

$$J(S^{m+1}) = J(S^m) + \frac{dJ}{dS}(S^{m+1} - S^m) \qquad (4.22)$$

Equation (4.22) can be substituted into equation (4.2) to yield a linear ordinary differential equation for S^{m+1},

$$D_H \frac{d^2}{dx^2} S^{m+1} - v \frac{d}{dx} S^{m+1} - a\frac{dJ}{dS} S^{m+1} = -Q_s + aJ(S^m) - a\frac{dJ}{dS} S^m \qquad (4.23)$$

Finite differences are used to approximate the spatial derivatives and yield a system of simultaneous linear algebraic equations which can be solved for S^{m+1}. In one dimension, the system of equations has a tridiagonal matrix structure. The spatial domain is divided into n grid-points (i = 1, n), where n is defined as

$$n = \frac{L_T}{\Delta x} \qquad (4.24)$$

where L_T is the total length of the column and Δx is the grid spacing. A three-point finite difference approximation was used for the dispersion term, which takes the form

$$\frac{d^2S}{dx^2} = \frac{S_{i+1} - S_i + S_{i-1}}{\Delta x^2} \qquad (4.25)$$

where i is the grid point at which the term was evaluated. The advective term is approximated by a central difference

$$\frac{dS}{dx} = \frac{S_{i+1} - S_{i-1}}{2\Delta x} \qquad (4.26)$$

Substitution of equations (4.25) and (4.26) into equation (4.23) to yield the discrete finite difference equation for a grid point i is given by

$$(cS_{i+1} + dS_i + eS_{i-1})^{m+1} = \left[aJ(S_i) - a\frac{dJ}{dS}S_i\right]^m \qquad (4.27)$$

where

$$c = \frac{D_H}{\Delta x^2} - \frac{v}{2\Delta x}; \qquad d = \frac{-2D_H}{\Delta x^2} - a\frac{dJ}{dS}; \qquad e = \frac{D_H}{\Delta x^2} + \frac{v}{2\Delta x}$$

The discrete equations are subject to two appropriate boundary conditions for the numerical method to be implemented. The influent condition (at x = 0) is

$$vS^{in} = vS - D_H\frac{dS}{dx} \qquad (4.28)$$

in which S^{in} is the substrate concentration at the inlet of the reactor Rittmann (1982a). The boundary condition at the effluent end (x = L) is

$$\frac{dS}{dx} = 0 \qquad (4.29)$$

When equation (4.27) is written for each grid point and the appropriate boundary conditions are imposed, the system of equations for S^{m+1} results.

The key to implementing the numerical technique with quasilinearization is an efficient and accurate evaluation of the dJ/dS term. The new pseudo-analytic equations developed by Sáez and

Rittmann (1988) can be differentiated to yield an expression for dJ/dS for the entire range of concentrations. Once the S_s value has been converged upon, the expression is given by

$$\frac{dJ^*}{dS_b^*} = K^* \left(1 - \frac{dS_s^*}{dS_b^*} \right) \tag{4.30}$$

where

$$\frac{dS_b^*}{dS_s^*} = 1 + \frac{1}{K^*} \left\{ \sqrt{2[S_s^* - \ln(1+S_s^*)]}\ \mathrm{sech}^2\left[\alpha \left(\frac{S_s^*}{S^*_{min}} - 1 \right)^{\beta} \cdot \right. \right.$$

$$\left. \left. \frac{\alpha\beta}{S^*_{min}} \left(\frac{S_s^*}{S^*_{min}} - 1 \right)^{\beta-1} \right] + \frac{\tanh\left[\alpha \left(\frac{S_s^*}{S^*_{min}} - 1 \right)^{\beta} \right] \cdot \left(\frac{S_s^*}{1 + S_s^*} \right)}{\sqrt{2(S_s^* - \ln(1 + S_s^*))}} \right\} \tag{4.31}$$

One interesting feature is the behavior of dJ/dS as the substrate concentration approaches S_{min}, where the reaction order approaches infinity. The expression dJ/dS can be simplified to a finite value at S_{min}: the result is simply

$$\left. \frac{dJ}{dS} \right|_{S_{min}} = \frac{D}{L} \tag{4.32}$$

Equation (4.32) can be understood on intuitive terms. Since the biofilm must be fully penetrated when S is near S_{min}, there should only be external mass transfer resistance to control the flux. Thus, the flux is a first-order function of S, with D/L as the reaction constant.

The method of quasilinearization was implemented and proved to be very accurate and efficient compared to previous methods. Figure 4.2 demonstrates the accuracy of the new technique, when no Q_s terms are included, by comparing the results to the previous method of time stepping. Table 4.1 shows the parameters used for the comparison of techniques. The new technique also was tested with several other sets of kinetic and reactor parameters and had similarly good accuracy and convergence. A comparison of the computational efficiency for the techniques is demonstrated in Table 4.2. The convergence criterion was defined for both algorithms with the following equation

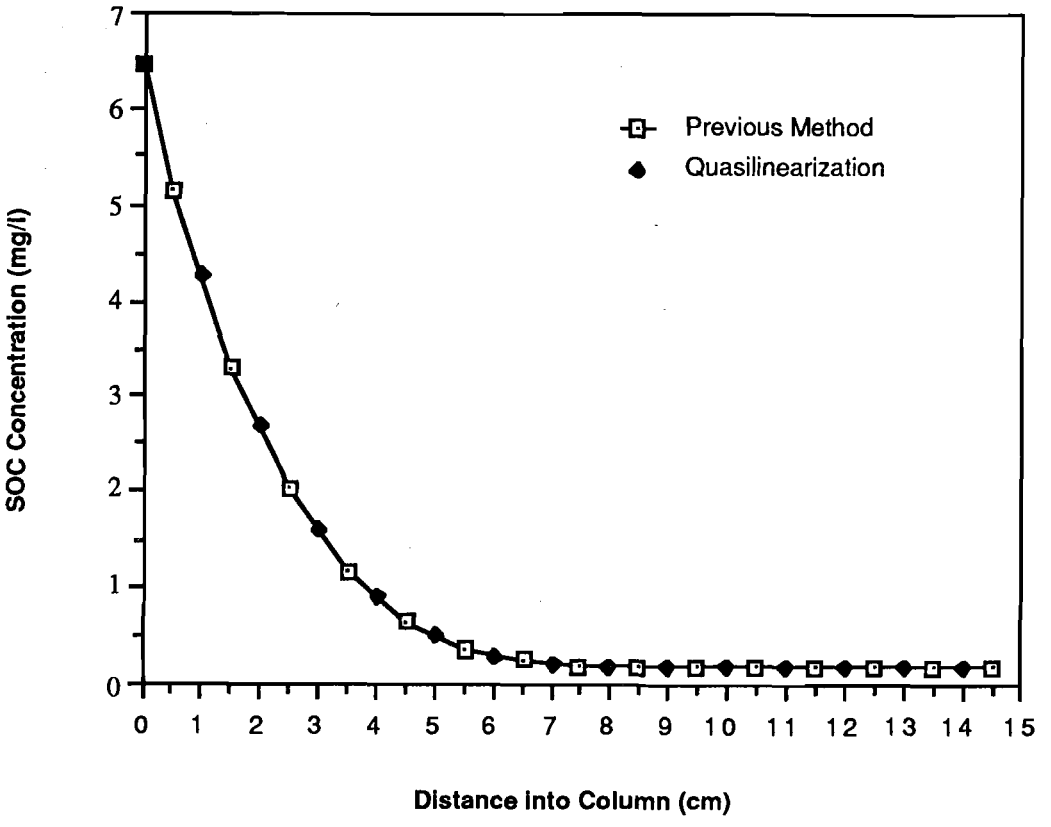

Figure 4.2. Comparison of traditional methods and quasilinearization for numerical solution of equation (4.2) with the parameters given in Table 4.1.

$$| (S^{m+1} - S^m)/S^m | < \Omega \qquad (4.33)$$

where m is the current iteration level and Ω is the defined convergence criteria (typically 0.1 to 0.001 %). Equation (4.33) had to be satisfied for all grid points in the numerical domain. Computational efficiency was characterized by the number of iterations required to converge to the steady-state solution and by the amount of execution time required to converge when a Micro-Vax computer was used. Table 4.2 shows typical values for both efficiency measures. The new technique was at least an order of magnitude more efficient for modeling a one-dimensional problem.

Table 4.1 Parameters used for the Comparison of Numerical Methods

Parameters	Value
k	0.023 g SOC/gVSS-day
K_s	0.50 mg SOC/l
L	0.0220 cm
v	360 cm/day
Δx	1.0 cm
ε	0.30
Δt	0.0001 day
a	14 cm^{-1}
S^o	7.2 mg SOC/l
Convergence on S	0.5%

Table 4.2. Comparison of Efficiency for Traditional Time-Stepping and Quasilinearization Techniques

Technique	Number of Iterations	Execution Time, secs
Time-Stepping	182	19.4
Quasilinearization	11	2.6

The computational advantage of quasilinearization should increase dramatically as the problem is increased in size and complexity, such as by including two and three dimensions.

4.4 Treatment of Lateral Injection Ports

The object of having multiple injections of the electron acceptor is to spread out the biologically active zone, thus reducing the potential for clogging. The Q_s terms in equations (4.1) and (4.2) represents injections along the flow path. Accurate and efficient solution of the finite-difference equations becomes a more difficult problem when lateral injections are allowed, because the inputs create local numerical instabilities. Therefore, special treatment is necessary to incorporate the multiple lateral injections.

The approach used in the numerical formulation is to implement local upstream weighting of the advection term at the lateral injection port. This technique is a commonly used method to smooth out numerical oscillations (Lapidus and Pinder, 1982). Instead of equation (4.26), the new finite difference approximation of the advection term takes the form

$$v(S^{i+1} - S^i) \tag{4.34}$$

at all segments which have inputs. The discrete equation is modified for the grid point of lateral injection

$$(c'S_{i+1} + d'S_i + e'S_{i-1})^{m+1} = \left[aJ(S_i) - a\frac{dJ}{dS}S_i\right]^m \tag{4.35}$$

where

$$c' = \frac{D_H}{\Delta x^2}\ ; \qquad d' = \frac{-v}{Dx} - \frac{2D_H}{\Delta x^2} - a\frac{dJ}{dS}\ ; \qquad e' = \frac{D_H}{\Delta x^2} + \frac{v}{\Delta x}$$

Local upstream weighting corrects most of the problem of upstream numerical dispersion; however, instability is still evident to some degree. Figure 4.3 compares the results with and without local upstream weighting for a sample situation. The parameters used are the same as those shown in Table 4.1, with a lateral injection, Q_s, of

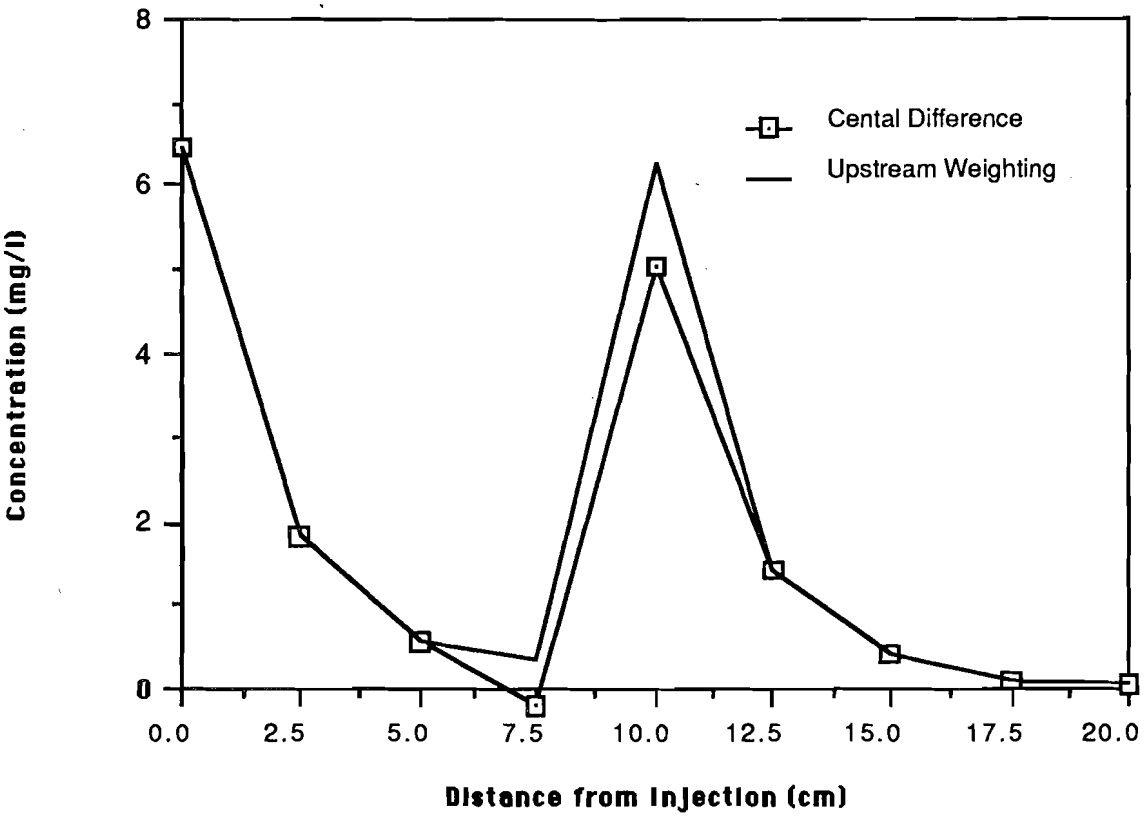

Figure 4.3. Comparison of upstream weighting and central finite differencing on the lateral injection prediction ability.

6.5 mg/l at the same velocity of the main flow at grid point 4, which is 10 cm. downstream from the first injection of NO_3^-.

4.5 Development of the Secondary Utilization Model

Secondary utilization is a concept which says that a trace-level organic compound can be degraded by a biomass, even when the concentration of the trace-level compound is less than its S_{min}. The degradation is possible because the biomass is grown and sustained by its utilization of a more plentiful primary substrate (electron donor), which allows and governs the accumulation of biomass (Kobayashi and Rittmann, 1982; Namkung, et.al., 1983). Namkung et.al.(1983) demonstrated how to model the utilization of a secondary substrate. Such a model requires knowledge of the kinetic parameters of the secondary substrate, as well as the distribution of biomass, which is determined by primary-substrate utilization.

The flux of secondary substrate is determined by its kinetic parameters and the biofilm thickness. A secondary substrate does not effect the biomass thickness, the primary substrate controls L_f. The secondary substrate enters the column at a certain concentration and is subject to the same physical processes as the electron donor and acceptor. Therefore, another mass balance equation on each individual secondary substrate must be performed. The steady-state solute transport equation, equation (4.2), must be solved for each of the secondary substrates. The same numerical technique, quasilinearization and finite-differences, can be utilized with certain modifications.

Because secondary substrates do not affect L_f, the steady-state-biofilm model is not appropriate for determining its flux. Instead, the pseudo-analytical solution of Rittmann and McCarty (1981), which was built upon the work of Atkinson and How (1974), must be utilized to estimate the flux of the secondary substrate into the biofilm. The distribution of biomass must be determined previously from the method presented in Section 4.3 and is a necessary input requirement for flux estimation for the secondary substrate. The details of the pseudo-analytical solution are presented in the original paper; however a short summary is presented here for clarity.

The following dimensionless parameters are defined for use with the pseudo-analytical solution of Rittmann and McCarty(1981), which is appropriate for biofilms at any thickness:

$$L_f^* = L_f\,[(kX_f)/(D_fK_s)]^{1/2}\ ;\ L^* = L/\tau\ ;\ D_f^* = D_f/D;\quad \tau=\sqrt{2K_sD_f/kX_f},$$

Other dimensionless parameters that appear were defined in Section 4.2

The basic equation for the flux is given by equation (4.36)

$$J^* = 2D_f^*L_f^*\eta\,\frac{S_s^*}{S_s^* + 1} \qquad (4.36)$$

where η = the effectiveness factor.

1. A starting estimate of an effectiveness factor η is required Rittmann and McCarty (1981) suggested starting from

   $$\eta = \tanh\{\sqrt{2}\,L_f^*\}/\sqrt{2}\,L_f^*$$

2. A trial S_s^* is estimated from

   $$S_S^* = 1/2\left[(S^*-1-2L^*L_f^*D_f^*\eta) + \sqrt{(S^*-1-2L^*L_f^*D_f^*\eta)^2 + 4S^*}\ \right]$$

3. A trial flux is calculated from S_s^*.

   $$J^* = 2D_f^*L_f^*\eta\,\frac{S_s^*}{S_s^* + 1}$$

4. A checking $S_s^{*'}$ is calculated from the external mass transport requirement

   $$S_s^{*'} = S^* - J^*L^*$$

5. A value ϕ is computed from

   $$\phi = \frac{\sqrt{2}\,L_f^*}{(1 + 2S_s^{*'})^{1/2}}$$

6. Checking η' is calculated from ϕ

$$1 - \frac{\tanh(\sqrt{2}L_f^*)}{\sqrt{2}L_f^*}\left(\frac{\phi}{\tanh\ \phi} - 1\right) \qquad \text{if } \phi \leq 1$$

or

$$1/\phi - \frac{\tanh(\sqrt{2}L_f^*)}{\sqrt{2}L_f^*}\left(\frac{\phi}{\tanh\ \phi} - 1\right) \qquad \text{if } \phi \geq 1$$

7. If η' and η are within 0.1% of each other , then η has converged to an acceptable value, and it is proper to proceed to the next step. If not, it is necessary to go back to step 3 and repeat the process.

8. When an acceptable value of η is found, J^* is calculated from

$$J^* = 2\eta D_f^* L_f^* \frac{S_s^*}{1 + S_s^*}$$

9. The dimensional flux is then

$$J = J^* (K_s D/\tau)$$

The η iteration usually converges in no more than five iterations.

The internal iteration and complexity of the presented algorithm does not permit an explicit expression for dJ/dS. However, the value of dJ/dS at a particular bulk substrate concentration was estimated using finite differences. Forward differencing was used with an interval, ΔS, of 0.1 to 0.01% of S_b. The finite difference equation used for the dJ/dS evaluation for the secondary substrate was

$$\frac{dJ}{dS} = \frac{J(S + \Delta S) - J(S)}{\Delta S} \qquad (4.37)$$

The solute transport equation for the secondary substrate was solved using the L_f distribution calculated from the primary substrate at every grid point. The secondary substrate was assumed not to affect the overall growth rate of the biomass, which was controlled solely by the primary substrate. The method of quasilinearization and finite differences was used identically as

before with the dJ/dS estimate given by equation (4.37). The concentration of secondary contaminant and its kinetic parameters as well as the reactor parameters, were necessary inputs for the model. The convergence and accuracy of the secondary utilization model were very similar to those of the primary-substrate model presented in Section 4.3.

CHAPTER 5. APPLICATION OF COMPUTER MODELING

5.1 SOC and NO_3^- Profiles

The one-dimensional model presented in Chapter 4 was evaluated for its ability to describe the laboratory results on SOC and NO_3^- removal through the BAZs. The laboratory results were presented in detail in Chapter 3. The assumptions used for applying the one-dimensional solute transport equation to the laboratory column are that wall effects were negligible and the surface area due to the sides of the column (less than one percent of the area of the glass beads). need not be included.

The kinetic parameters (k, K_s, Y, b, and X_f) were determined independently, as explained in Section 3.2.5. The kinetic and reactor parameters used to model the laboratory results are presented in Table 5.1. The value of S_{min} determined from the kinetic parameters is slightly less than the plateau concentration of SOC measured in the laboratory. This can be explained by the formation of soluble microbial products (SMP) (Namkung and Rittmann, 1986) which contained C^{14}. Thus, SOC measurements toward the downstream end of the column contained residual substrate and some SMP, while the model predictions are only for residual substrate.

5.1.1 One-BAZ Column

The modeling procedure was a two-step process. First the SOC profile was solved by assuming SOC was the rate-limiting substrate. This yielded steady-state profiles of SOC concentration and J_{SOC}, the flux of SOC into the biofilm. Then, the NO_3^- profile was obtained by solving the solute-transport equation for NO_3^- when the rate of NO_3^- removal was equal to the flux of SOC multiplied by a stiochiometric coefficient. The stoichiometry was found in the laboratory to be 0.67 mg NO_3^--N/mg Acetate as SOC. That is, equation (4.2) was solved for the NO_3^- concentration profile with $J_{NO3} = 0.67\ J_{SOC}$. The numerical values for flux of NO_3^- were computed from stored values of the SOC obtained with the primary substrate model and were calculated for each grid point. Since the rates of NO_3^- were determined by multiplying the flux of SOC at each grid point by 0.67 mg NO_3^-/mg SOC, the governing transport equation was linear, so that

quasilinearization was not required. In other words, dJ/dS was zero for NO_3^-, because J was a predetermined constant.

Table 5.1. Parameters used in Solute-Transport Modeling of One-BAZ column

Parameter	Units	Value Used in Model	Value with Alternative Units
Acetate	as SOC	-	
S^o	mgSOC/l	6.5	
L	cm	0.02195	
S_{min}	mgSOC/l	0.0131	
k	mgSOC/mgcell-day	2.22	4.17 mgSOC/mgcellC-d
K_s	mgSOC/l	0.218	
X_f	mg cells/cm^3	15.	8.0 mg cell C/cm^3
Y	mg cells/mg SOC	0.678	0.36 mg cell C/mgSOC
b	day^{-1}	0.07	
D_{SOC}	cm^2/day	1.07	
D_H	cm^2/day	120.58	
v	cm/day	144.	
a	cm^{-1}	20.0	
ε	cm^3/cm^3	0.30	
NO_3^-	as N	-	
S^o	mg NO_3^--N/l	7.32	
D_N	cm^2/day	1.40	

The model results are compared with the experimental results in Figure 5.1. The model and laboratory results compare very well. Both substrates were removed rapidly in the first 5.0 cm downstream of the injection. They then approached a plateau concentration beyond about 10 cm, as the SOC primary substrate approached its S_{min}. The correspondence between model and experimental results for both substrates verifies that SOC was rate limiting and that the stoichiometry between NO_3^- and SOC removals was correct. While there is nearly perfect agreement for the electron acceptor, NO_3^-, small deviations for SOC occur at 5.0 and 7.5 cm

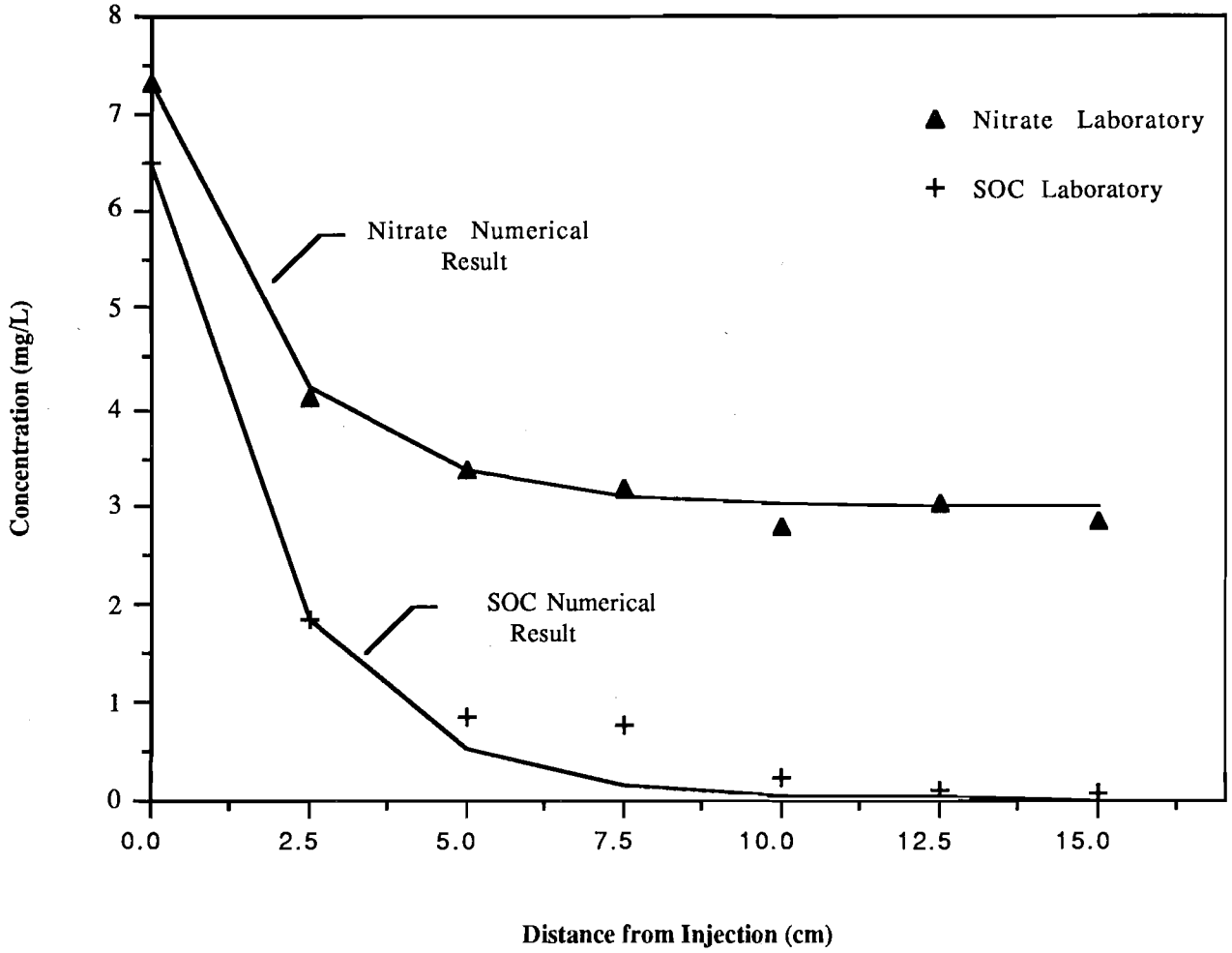

Figure 5.1. Comparison of laboratory and numerical results for the one-BAZ column. Zero distance indicates the injection port.

downstream of the injection port. These deviations may be the result of short circuiting due to nitrogen gas build-up, or they may be caused by sampling error.

5.1.2 Two-BAZ Column

The two BAZ column was modeled using the solute transport model and the same reactor and kinetic parameters as for the one-BAZ column. The same influent SOC concentration was used as in the one BAZ experiment; however, the electron acceptor was injected in two locations, the second injection being ten centimeters downstream from the first. The same total amount of electron acceptor was injected into both columns, but the two BAZ column received 25% through the first port and the remaining 75% through the second port, this corresponds to 1.92 and 5.52 mg NO_3^--N/l respectively. This two-injection strategy caused NO_3^- to be the rate limiting substrate in the first BAZ, where it was depleted to close to its S_{min} just before the second injection. At this point, there was approximately 50 % removal of acetate. After the second injection, NO_3^- was in ample supply, and SOC (acetate) became the rate-limiting substrate.

The change of rate-limiting substrate after the second injection of NO_3^- presented an interesting modeling situation. If the electron acceptor had limited the growth throughout the length of the column, the modified model with lateral injection ports could have been used directly. In the case of a change of limitation, however, two coupled solute-transport equations had to be used.

In the section of the column after the first injection, quasilinearization and finite differences were used to solve the solute transport equation for NO_3^-, the rate limiting substrate. Then, the profile for SOC was obtained from the NO_3^- fluxes and stoichiometry, as reported in the previous section. At the point of the second injection of nitrate a new solute transport equation had to be solved. For the points downstream of the second injection, this new solute transport equation was solved using SOC as the primary substrate; it was coupled to the upstream segment of the column by considering the continuity of SOC flux at the injection port. For NO_3^-, the upstream flux of NO_3^- was added to the flux through the injection port, as it represented only approximately 0.18% of the flux through

the port. The NO_3^- profile after the second injection was obtained from the SOC fluxes and stoichiometry.

Table 5.2 shows the parameters used in the solute transport modeling. The kinetic parameters for NO_3^- were not independently measured in the laboratory and had to be estimated. The maximum specific rate of substrate utilization, k, was taken from the k of SOC, adjusted by stoichiometry. The K_s value was varied until proper fit of the laboratory data was obtained. The low value for K_s for NO_3^- is consistent for electron acceptors (Rittmann and Langeland, 1985). The kinetic parameters for SOC, the primary substrate after the second NO_3^- injection, were averaged from those measured independently at different locations in the column.

Figure 5.2 shows the numerical results compared to the laboratory data. The numerical results are in extremely good agreement with the laboratory data. The stoichiometric values used in the numerical work, 1.5 mgSOC/mgNO_3^- and 0.67 mgNO_3^-/mgSOC for the first and second BAZ, respectively, allowed proper representation of both substrate profiles in both BAZs. Thus, the choice of which substrate was rate-limiting seems justified.

Comparison of Figures 5.1 and 5.2 demonstrates that having two NO_3^- injections spread out the distance over which a BAZ was present. With two injections, the BAZ covered about 12.5 cm, while it covered about 7.5 cm for one injection.

5.2 Secondary Substrate Profiles

The laboratory profiles of the secondary substrates presented in Chapter 3 for the one-BAZ column were modeled using the framework summarized in Chapter 4. The primary substrate profile was modeled first. From the results for the primary substrate, the steady-state biofilm thickness was calculated at each grid point from the following equation (Rittmann and McCarty, 1980a)

$$L_{fi} = \frac{J_i Y}{b X_f} \qquad (5.1)$$

where J_i is the flux into the biofilm at grid point i. The result was a profile of biofilm thickness throughout the length of the column. The L_f values then served as key inputs to the model to estimate the

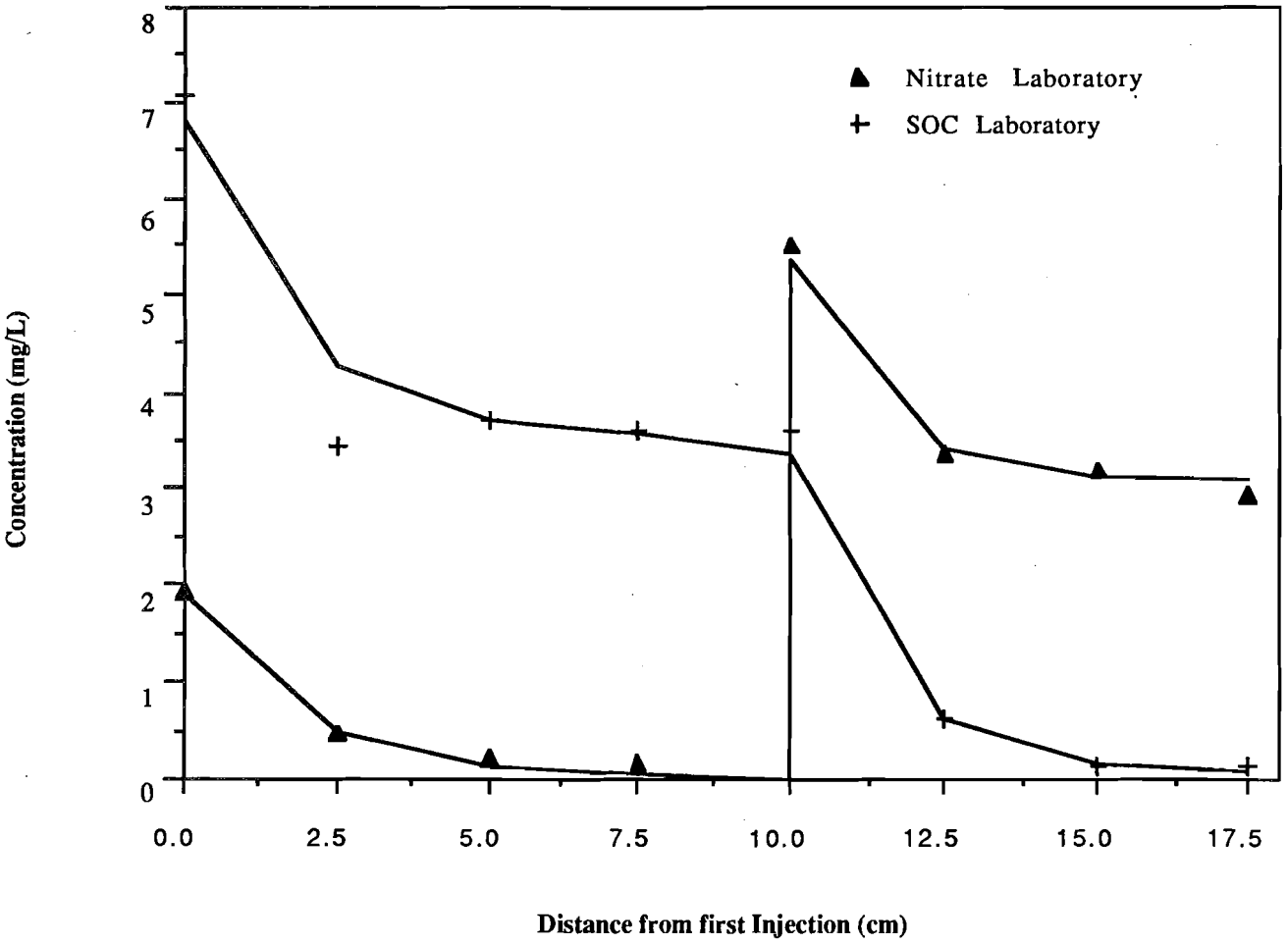

Figure 5.2. Comparison of laboratory and numerical results for the two-BAZ column. Nitrate injections are at 0.0 and 10.0 cm. Lines represent model prediction.

flux of a particular secondary substrate into the biofilm (Rittmann and McCarty, 1981; Namkung et al., 1983).

Table 5.2. Parameters Used in Solute-Transport Modeling of Two-BAZ column

Parameter	Units	Value
Nitrate	as NO_3^-- N	-
S^o	mg NO_3^-/l	1.92, 5.52
L	cm	0.02195
S_{min-N}	mg NO_3^-/l	0.0090
k	mg NO_3^-/mg cell-day	1.45
K_s	mg NO_3^-/l	0.146
X_f	mg cells/cm^3	15.
Y_N	mg cells/mg NO_3^-	1.02
b	day^{-1}	0.07
D_N	cm^2/day	1.07
D_{HN}	cm^2/day	120.58
v	cm/day	144.
ϵ	cm^3/cm^3	0.30
Acetate	as SOC	-
S^o	mg SOC/l	7.09
k	mgSOC/mgcell-day	2.00
K_s	mgSOC/l	0.80
X_f	mg cells/cm^3	15.
Y	mg cells/mg SOC	0.678
S_{min}	mgSOC/l	0.0497
D	cm^2/day	1.40

The strategy for modeling the secondary substrates was to choose k and K_s values that provided a good fit to the experimental results for one experiment. This fitting exercise was needed, because the k and K_s values of these secondary substrates were not known independently for the denitrification system. The appropriate reactor parameters and the kinetic parameters of the primary substrate.were known independently. The fitted k and K_s values

were used to predict the results for different experiments with the same secondary substrates.

As explained in Section 3.3, several secondary substrates were fed continuously into the laboratory column. The original detention time of 50 minutes showed only slight removal of one compound, CTC. To obtain better removals, the detention time was increase at first to 125 minutes and then to 500 minutes. Most of the compounds showed significantly greater percentage removal as the detention time increased. Three categories of compounds resulted: (1) CTC was rapidly removed, (2) BF, EDB, TeCE, and TCE were removed less rapidly, and (3) TCA was not removed. To evaluate the secondary-substrate modeling, CTC, BF, EDB, TeCE, and TCE were modeled.

5.2.1 Carbon Tetrachloride

The first secondary substrate modeled was CTC, which entered the first BAZ at a concentration of 81.0 μg/l. The k and K_S values which gave a good fit for a detention time of 50 minutes were 0.030 μg/mg cell-day and 4.5 μg/l, respectively. Figure 5.3 shows the results of the numerical fitting for the 50 minute detention time. Clearly, all of the points are well represented by the numerical result. In order to demonstrate the predictive ability of the numerical model, the profiles at the two other detention times (125 and 500 min.) were calculated using the same k and K_S values. The superficial velocity and influent concentration are suitably modified for each of the other runs.

The 125-min. detention time was modeled by changing the superficial velocity and influent concentration to 0.04 cm/min and 69 μg/l, respectively. Figure 5.4 shows the results of the numerical prediction compared to the laboratory data. The two curves fit well and show removal through all of the BAZ (~ 7.5 cm.). The 500-min. detention time column was modeled using the laboratory obtained concentration of 53 μg/l and an adjusted superficial velocity of 0.01 cm/min. Figure 5.5 shows the results of the numerical prediction. The results are encouraging, because the numerical and experimental results have the same trends of rapid decrease and approach a plateau concentration. The absolute values of the plateau

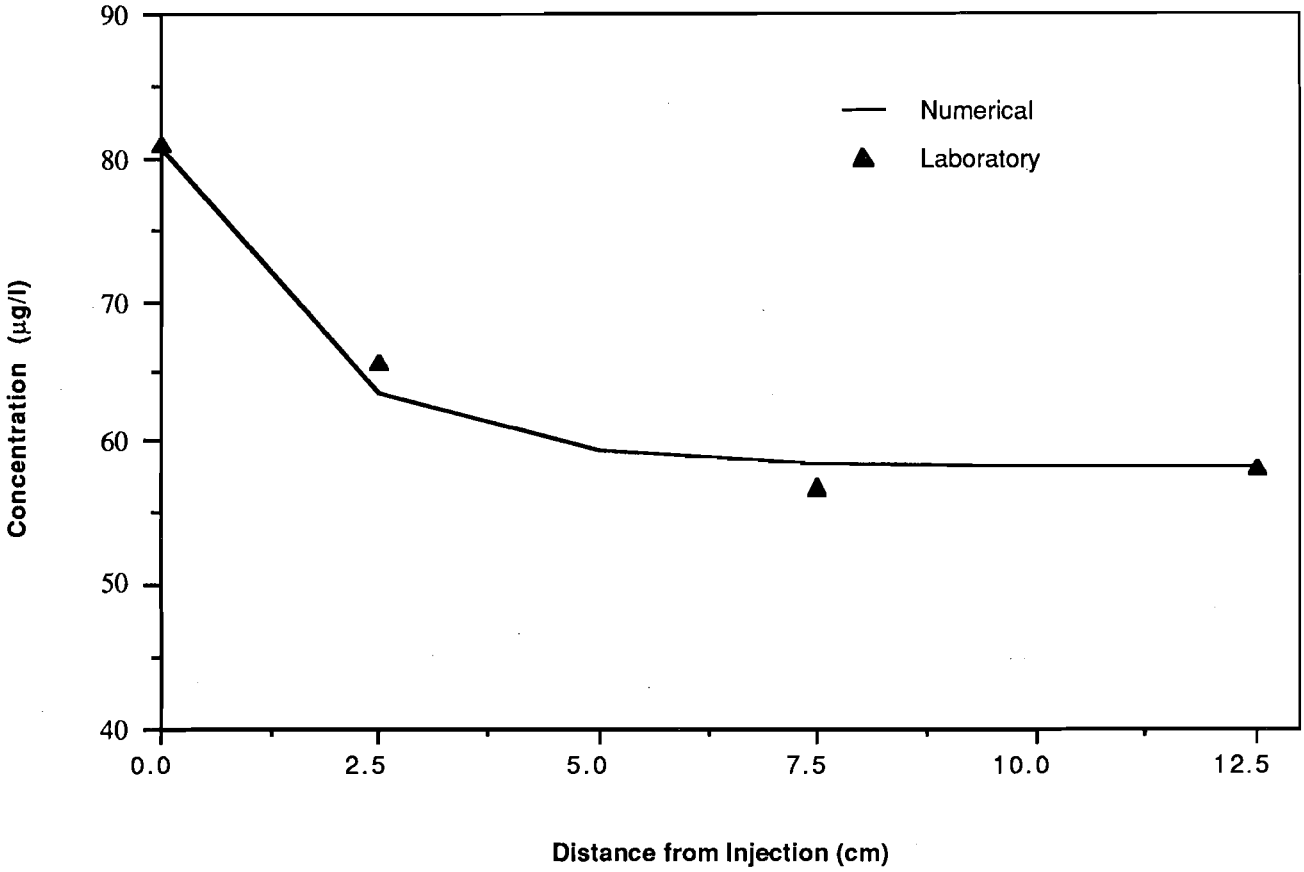

Figure 5.3. Numerical curve fit to the CTC profile at a detention time of 50.0 min. The k and K_s are 0.030 µg/mg cell-day and 4.5 µg/l, respectively.

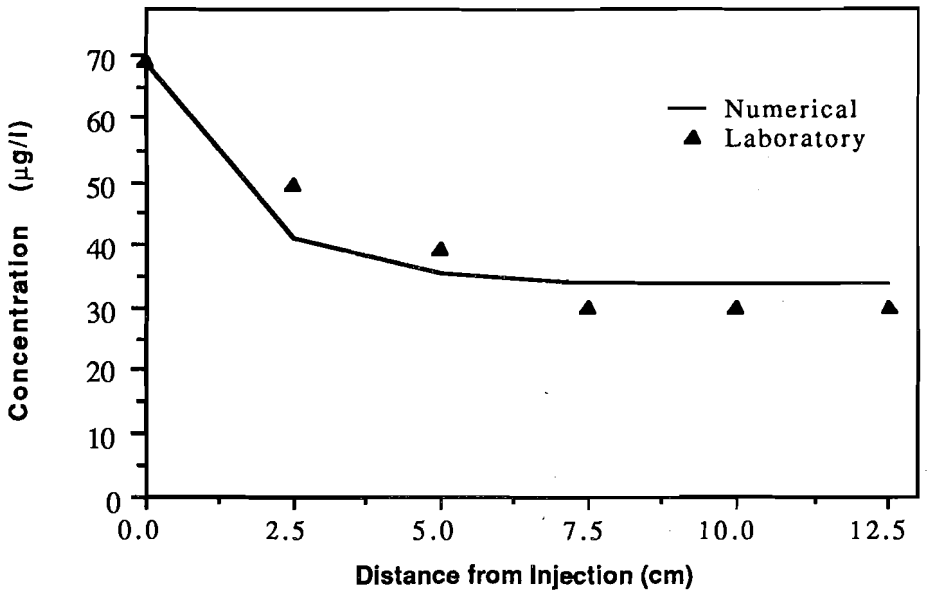

Figure 5.4. Prediction of the CTC profile at a detention time of 125. min. and with k = 0.030 µg/mg cell-day and K_s = 4.5 µg/l.

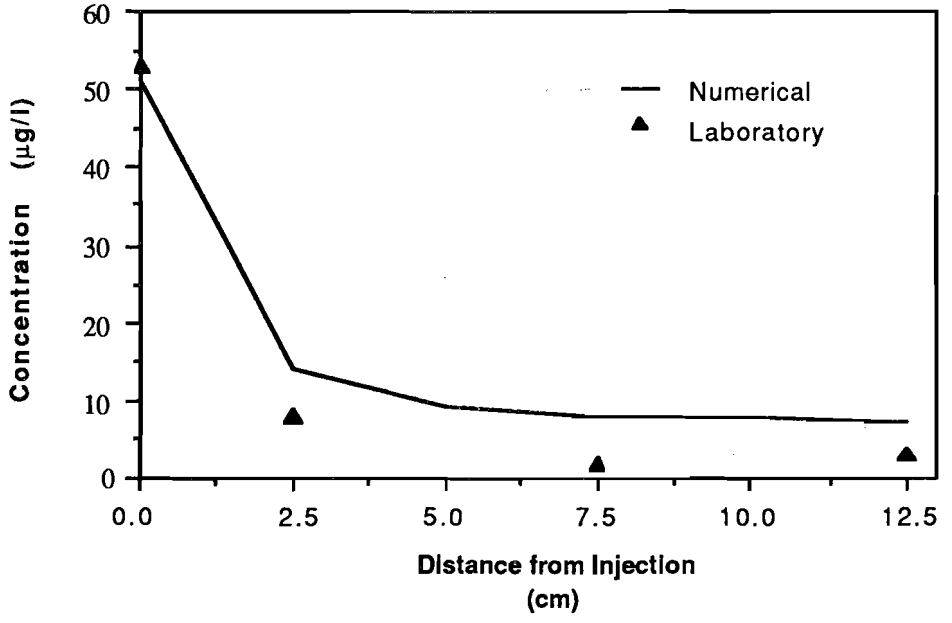

Figure 5.5. Prediction of the CTC profile at a detention time of 500 min and with k = 0.030 µg/mg cell-day and K_s = 4.5 µg/l.

concentration are slightly different, but are in the same order of magnitude.

Before the secondary-substrate experiments were started, the one BAZ column had been operated for over one year at approximately the same detention time and concentration of substrates. By the time the secondary substrates were added to the column, a steady-state biomass distribution had been attained throughout the length of the BAZ. One possibility is that the biomass distribution changed during the experiments at longer detention times and, to some degree, with different influent SOC concentrations. Reduction of the detention time reduced the substrate (SOC) input to the BAZ and should have created a situation of slower biological activity in the BAZ. The time that the new detention times were maintained before sampling of the profiles of the secondary substrates is a major factor in the assumption made about the biomass distribution for the secondary-substrate measurements. Because of the long time used to establish the steady-state biofilm and the relatively short times the reactors were run at the new detention times (6 weeks at 125 min. and 5 weeks at 500 min.), it was assumed that the biomass distribution remained the same as that calculated for the 50 minute detention time. Nevertheless, it is possible that the BAZ lost active biomass during the detention-time experiments. The data shown in Figures 5.3 - 5.5 suggest that the loss of activity for CTC removal was negligible.

5.2.2 Bromoform, Ehtylene Dibromide, Tetrachloroethene, and Trichloroethene

The second secondary substrate modeled was bromoform (BF), which entered the column at a concentration of 106 μg/l at a detention time of 50 min. As opposed to CTC, BF had no detectable removal at the 50 min detention time. This was due to insufficient contact time with the biomass, and as a result, the detention time of the column was increased. The 125-min. detention time had an influent concentration of BF of 57 μg/l, and BF removal was observed. In this case, the kinetic parameters, k and K_S, were found for this detention time. Figure 5.6 shows the results of the numerical fitting between the experimental values and the model results using k and K_S values of 0.013 μg/mg-day and 9.5 μg/l, respectively.

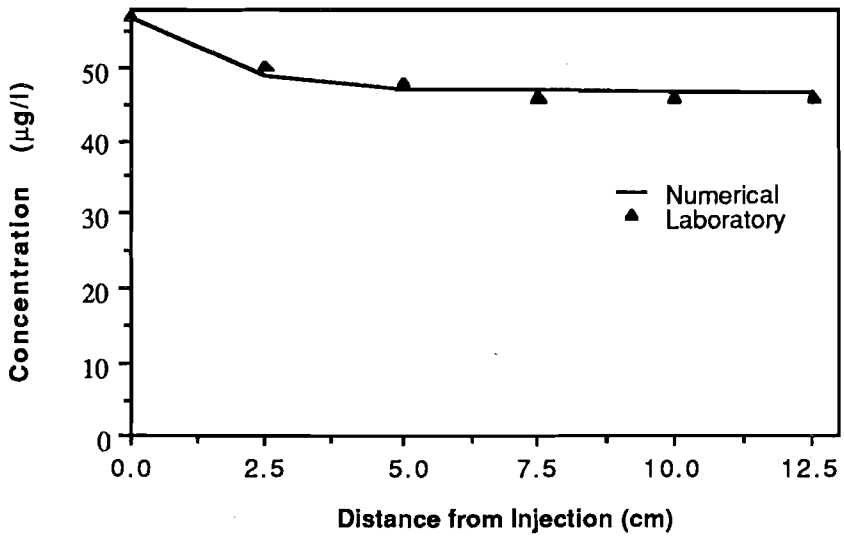

Figure 5.6 Numerical fit to the BF profile at a detention time of 125 min. The k and K_s are 0.013 µg/mg cell-day and 9.5 µg/l, respectively.

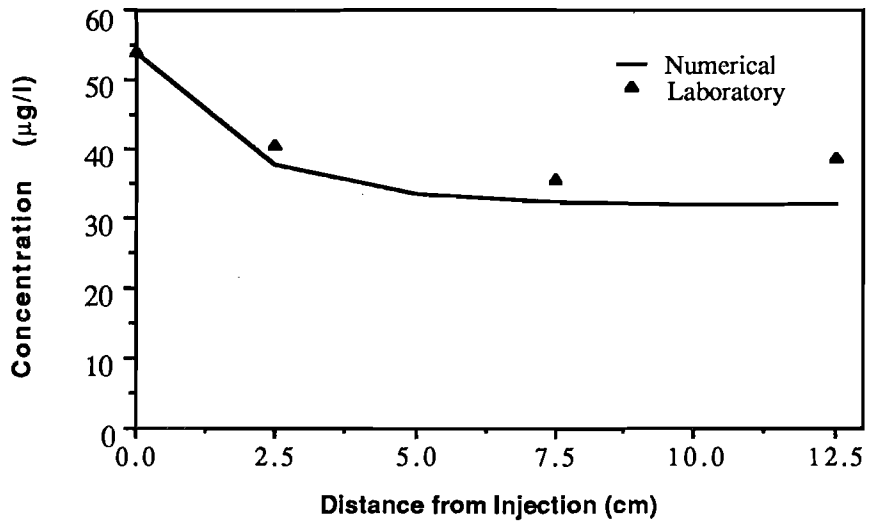

Figure 5.7. Prediction of the BF profile at a detention time of 500 min. and with k = 0.013 µg/mg cell-day and K_s = 9.5 µg/l.

The 500-min. detention time column had an influent concentration of 54 µg/l of BF. Figure 5.7 shows the results of the numerical model using the kinetic parameters from the 125 minute detention time. The numerical model predicted a slightly lower plateau concentration than was measured in the laboratory. This difference in removals perhaps can be attributed to biofilm loss between the two sampling periods. The assumption made was that the biomass distribution remained constant throughout the duration of the secondary-utilization experiments, even though some biomass loss probably took place.

Modeling predictions for the 50-min. detention time gave a prediction of only 1.5% removal of BF (results not shown). This negligible predicted removal was consistent with the undetectable removal for the experiments. The kinetic parameters of tetrachloroethene (TeCE), ehtylene dibromide (EDB), and trichloroethene (TCE) were measured at the intermediate detention time of 125 min. Again, there were no detectable removals of these compounds at the lowest detention time of 50 min. The numerical model was fit to the laboratory data to obtain the k and K_S values of each compound. These values are shown in Table 5.3. Because the numerical fit to laboratory data was similar to that shown for BF in Figure 5.6, these curves are not presented. The same trend of somewhat greater removals of substrate predicted by the numerical model than measured in the laboratory applied to the greater detention time results for these three compounds. The differences are hypothesized to be the result of biomass loss.

Table 5.3. K_S and k Values of TeCE, EDB, and TCE Obtained From Numerical Curve Fitting.

Compound	Ks (mg/l)	k (mg/mg-day)
TeCE	8.0	0.01760
EDB	9.0	0.00900
TCE	8.5	0.00935

5.3 Simulation of Bioreclamation Strategies

There are several possible strategies that can be used to achieve maximum performance of a bioreclamation site. Two very interesting strategies are presented in this chapter in the form of hypothetical examples. One strategy is to minimize the clogging from biomass growth. A clogging problem is exacerbated by injection of an excess amount of electron acceptor through one well or port. If the electron-donor concentration is relatively large compared to that of the electron acceptor, clogging is likely to develop in a region close to the point of injection. In order to reduce the potential for clogging, lower concentrations of the electron acceptor can be added at several locations along the flow path.

The clogging potential can be demonstrated by presenting an example problem. A model problem compares one injection of nitrate at 10.0 mg/l to a multiple injection of an equivalent amount of nitrate. For this example, SOC is assumed to be present in excess, so that nitrate is assumed to limit the growth throughout the length of the column. The concentration of SOC is assumed to be 20.0 mg SOC/l as it enters the column. Kinetic parameters for denitrification limited by NO_3^-, found in Table 5.2, were used for the model problem. The reactor parameters used in this example are shown in Table 5.3

Table 5.4. Parameters Used in Clogging Example Problem

Parameter	Units	Value
Nitrate	as NO_3^-- N	-
S^o	mg NO_3^-/l	3.3, 3.3, 3.3
L	cm	0.0289
v	cm/day	180.
ε	cm^3/cm^3	0.30
d_p	cm	0.12
a	cm^{-1}	50.0
Acetate	as SOC	-
S^o	mg SOC/l	20.00

Figure 5.8 shows the nitrate and SOC profiles when the NO_3^- is injected through one or three ports. It is evident that the net removal of SOC is nearly equivalent for either case, although it is slightly better with three injections. A relative measure of clogging potential can be estimated by considering the relative biofilm thickness throughout the length of the column. The relative biofilm thickness is the film thickness at a point in the reactor divided by the particle diameter. It is clear by comparing the relative biofilm thicknesses of the two scenarios, given in Figure 5.9, that the multiple injection gives much less potential for clogging.

The second strategy involves enhancing the removal of organic contaminants when the total available primary substrate is low. Injection of additional SOC when the original SOC is depleted should extend the BAZ and allow increased consumption of individual secondary substrates.

In order to demonstrate the advantage of an additional injection of carbon, a simple example was developed. Consider a situation such as the SOC profile in the one-BAZ column (see Figure 5.1). The SOC was rate limiting throughout the length of the column. The injected electron acceptor was removed approximately 50%. At this point, if additional acetate were added to the column, the BAZ could be extended. This configuration was modeled numerically using the laboratory kinetic parameters. The initial concentration of nitrate was 10.0 mg NO_3^--N/l, and the SOC was 6.5 mg SOC/l. At a distance of ten centimeters downstream from the nitrate injection, 10.0 mg SOC/l was injected. Figure 5.10 shows the resulting nitrate and SOC profiles. The BAZ was extended another 7.5 cm from the second injection.

The advantage of adding the SOC injection can be demonstrated further by considering the fate of CTC applied to the column at a concentration of 100 µg/l (using the same k and K_s values obtained in Section 5.2.1). Figure 5.11 shows the profile of CTC throughout the length of the column. There is approximately 43% removal in the first ten centimeters of the column. An additional 40 % removal is calculated for the last ten centimeters and is due to the injection of SOC. Thus, extension of the BAZ by addition of more biodegradable SOC significantly enhanced removal of CTC.

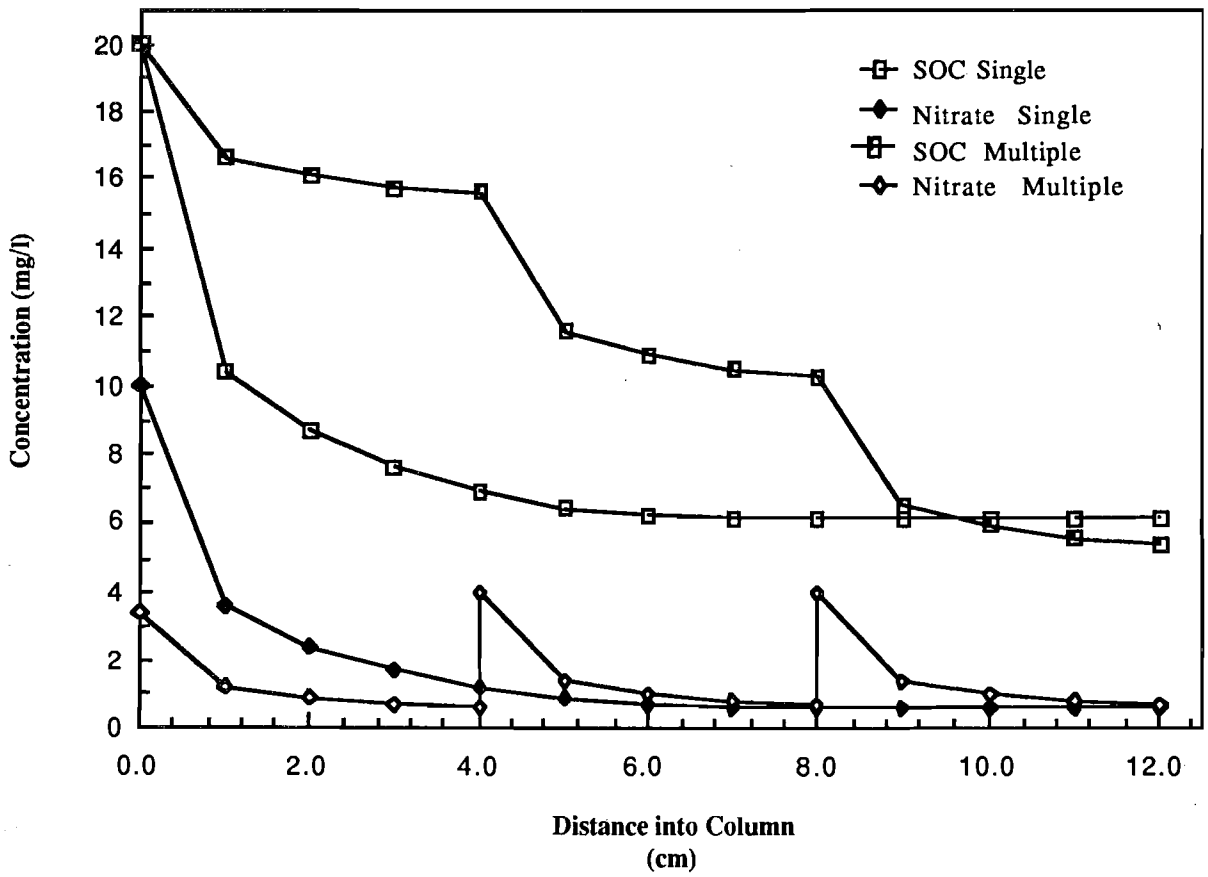

Figure 5.8. SOC and nitrate profiles for one and three injections of NO_3^-.

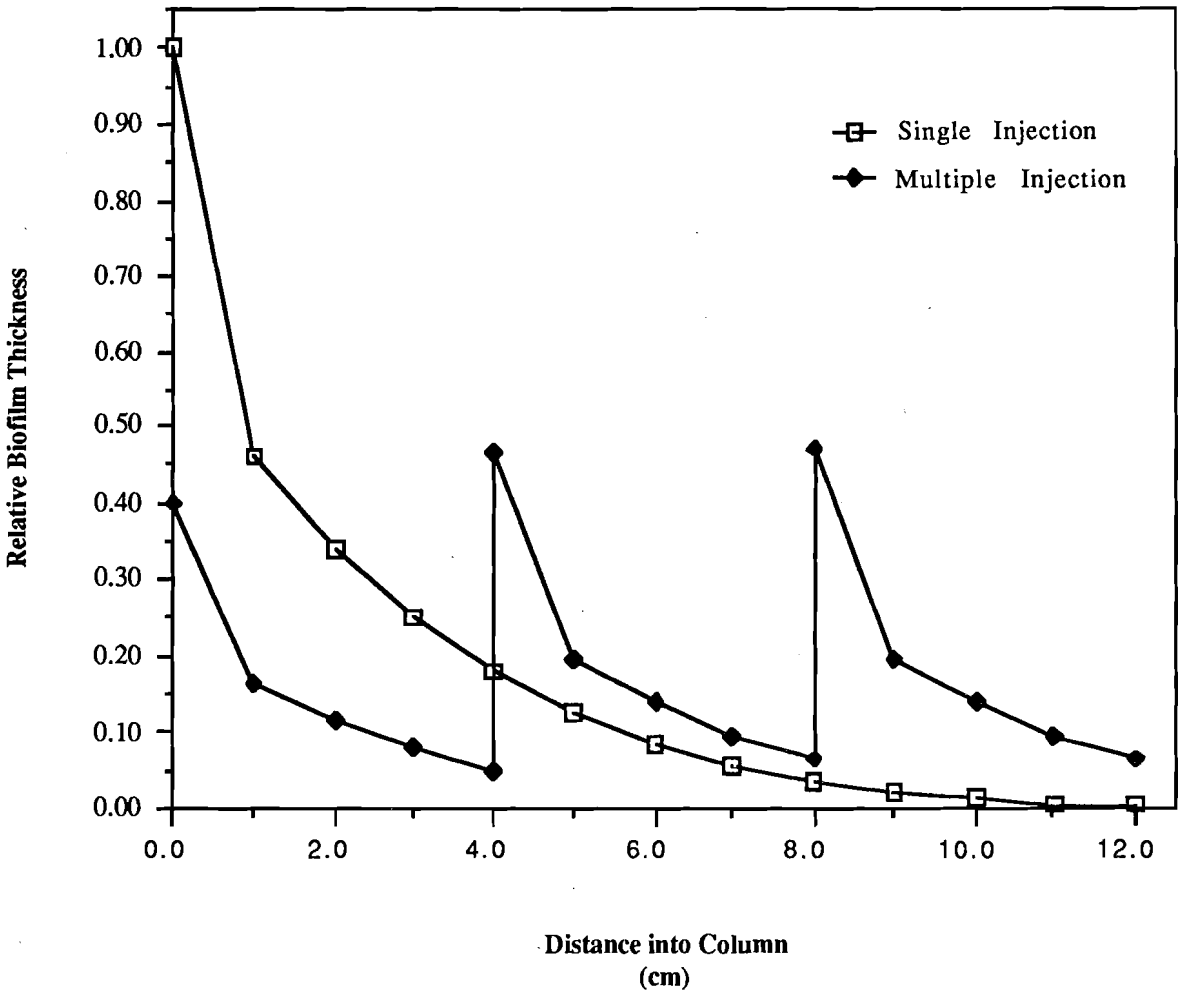

Figure 5.9. Relative biofilm thicknesses comparing single and multiple nitrate injections.

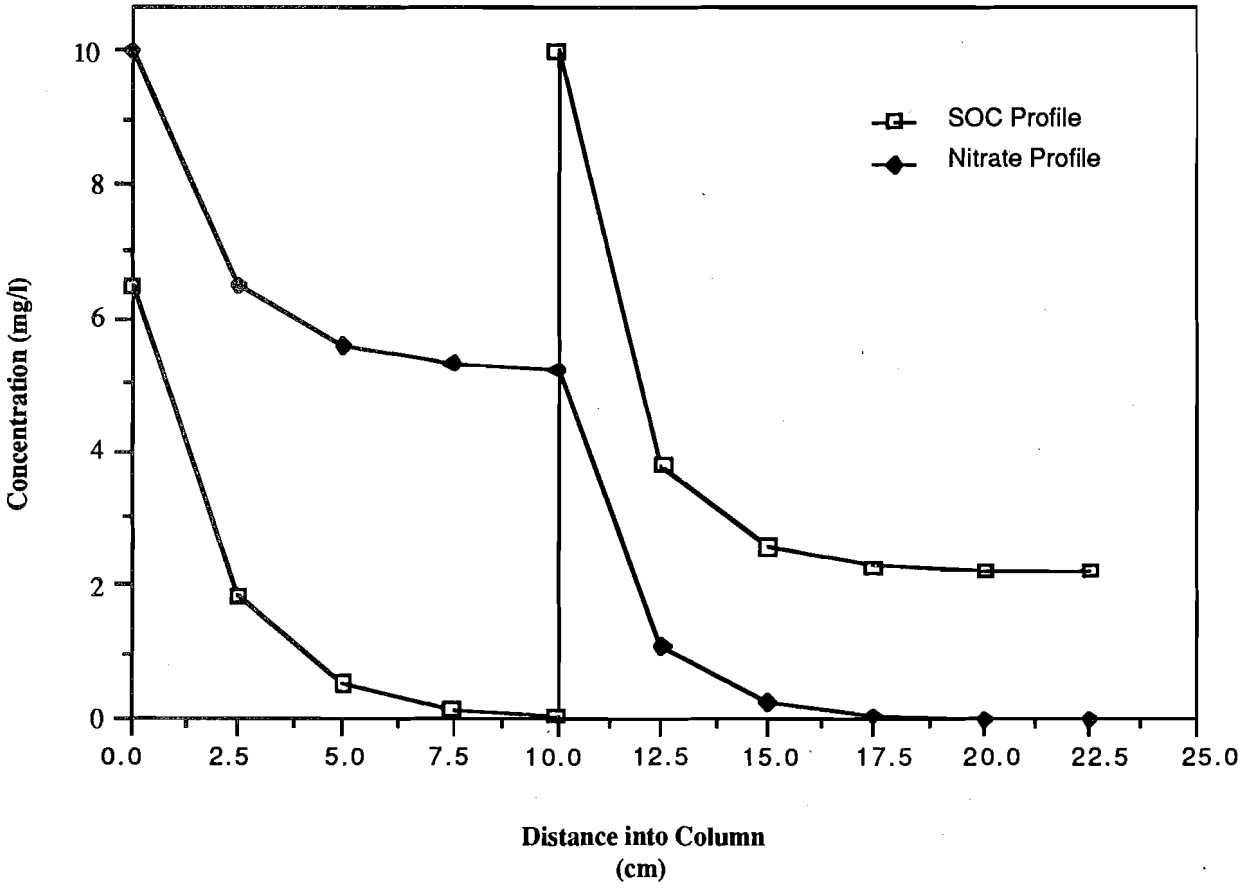

Figure 5.10. Profiles of SOC and nitrate after being injected alternately.

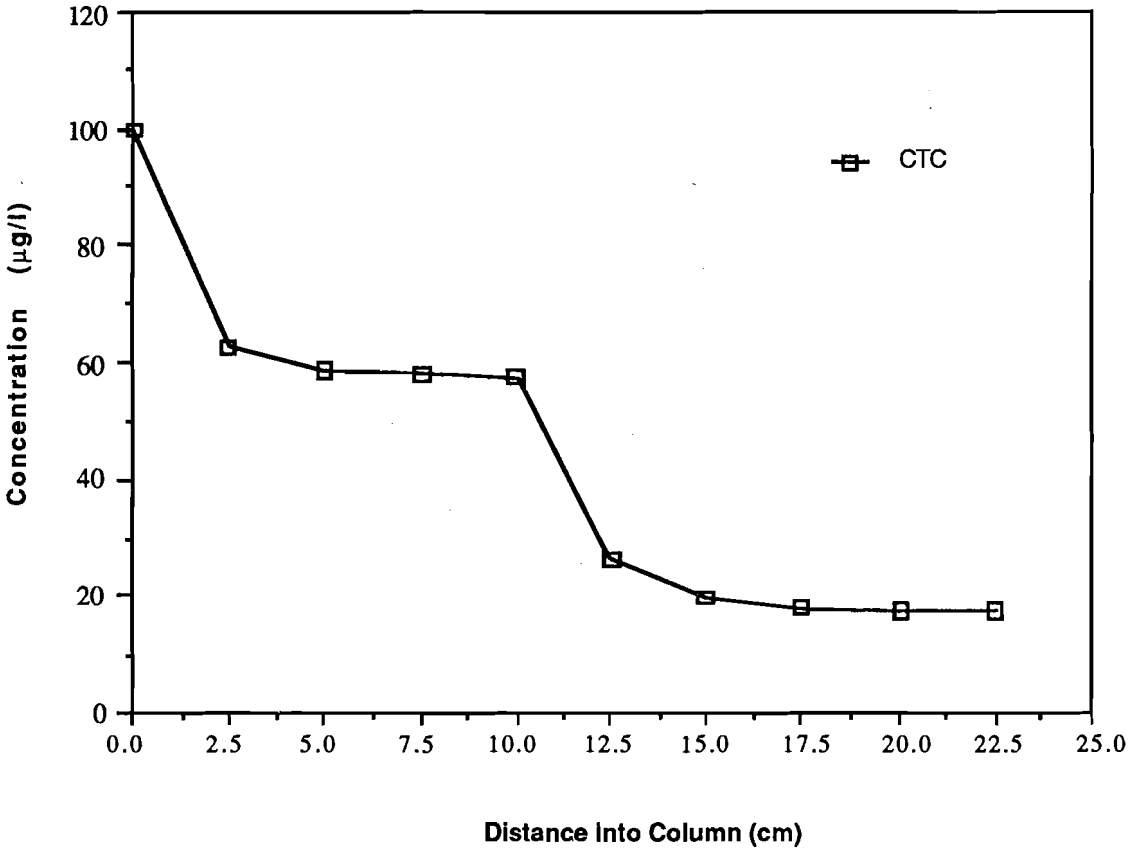

Figure 5.11. Profile showing additional secondary utilization of CTC after SOC is added by a second injection at 10 cm.

CHAPTER 6. CONCLUSIONS AND RECOMMENDATIONS

This research project investigated the fundamental mechanisms that can act when an electron acceptor is injected along the flow path of an electron-donor-rich groundwater to establish a biologically active zone (BAZ) for degradation of pollutants that serve as primary and secondary substrates. The research methodology consisted of laboratory column experiments that were coupled with computer modeling.

The laboratory experiments demonstrated that lateral injection of NO_3^- could be successfully utilized to control the location and extent of BAZs in systems where acetate was fed as the sole carbon source. Columns containing one and two BAZs were successfully operated, and profiles of acetate and NO_3^- were determined. Additional measurements of steady-state biofilm thicknesses and densities gave further evidence of the value of lateral injection for spreading out biological activity along the flow path, which leads to enhanced biodegradation capability and diminished clogging potential. These experiments also demonstrated the deleterious effects of N_2 gas accumulation; N_2 gas bubbles that occurred as a result of denitrification tended to accumulate in the BAZs, resulting in reduced liquid contact times and lowered acetate removal efficiencies.

Laboratory experiments evaluating the secondary utilization of eight trace-concentration halogenated solvents were also conducted. Results of these experiments indicate that carbon tetrachloride was removed most completely by denitrifying BAZs, while tetrachloroethene, bromoform, dibromoethane, and trichloroethene were removed to lesser degrees. Trichloroethane removal was slight. A significant result was that 1,2 and 1,3 dichlorobenzene were 20-30% removed; these compounds have previously been considered refractory under denitrifying conditions.

A highly efficient numerical model that couples solute transport mechanisms and biofilm kinetics was developed. Employing a quasilinearization technique for the biofilm reaction term, the model is capable of solving directly for the steady-state profiles of limiting substrate, biofilm thickness, non-limiting substrates, and secondary substrates. The predictive ability of the model was successfully verified by simulating the results of the laboratory experiments

using independently determined kinetic parameters. Independently determined kinetic parameters did not exist for the secondary substrates; in this case, one set of results from the column experiments was used to obtain a best-fit set of kinetic parameters, which were then used to predict the results for experiments conducted with different liquid flow velocities. The model predictions correctly described all trends. Absolute deviations between predicted and experimental results were very small for cases involving acetate and nitrate; systematic deviations for some of the secondary substrates occurred and probably were due to a loss of biomass during the experiments conducted at the higher detention times.

The steady-state models were applied to investigate possible strategies to be used in field bioreclamations. The use of multiple injection wells was studied for its ability to decrease aquifer clogging potential by spreading out the distance over which the limiting substrate is added. Modeling results verified that the strategy of multiple injections could reduce high densities of biofilm accumulation near the injection well. Also investigated was the strategy of adding a supplemental carbon source to extend the length of a BAZ. The modeling illustrated that such an extension of the BAZ could be accomplished and could result in longer contact times for a secondary substrate in the BAZ, thereby increasing the removal of the secondary substrate.

The results of this research demonstrate that injection of limiting substrates along the groundwater flow path is a viable means of establishing spatially distributed BAZs for enhanced in situ bioreclamation. Trace-levels of hazardous secondary substrates can be degraded as groundwater flows through the BAZs. The phenomena of formation of BAZs and substrate utilization within BAZs can be quantitatively interpreted and predicted at the laboratory scale by rigorous mathematical models that couple principles of solute transport and biofilm kinetics.

An ultimate goal is to develop the fundamental understanding of coupled biological and hydrological processes to a level sufficiently great that field-scale in situ bioreclamation systems can be designed reliably. A critical need is to extend the research reported here to

include transient and multi-dimensional aspects. In particular, the following areas of additional research are recommended:

1. Use the combined experimental and modeling approach to study transient biofilm kinetics and dual-substrate limitation.

2. Examine the use of alternative electron acceptors to establish specialized BAZs capable of degrading specific pollutants.

3. Conduct further study of the basic mechanisms of dichlorobenzene degradation under denitrifying conditions.

4. Examine the fundamental mechanisms of bacterial transport and attachment and their role in the establishment and extension of BAZs.

5. Study the effect of biological activity upon the hydraulic properties of aquifers.

6. Extend the computer modeling to consider transient, heterogeneous, multi-dimensional flow fields, as well as transient biofilms.

7. Study the phenomena controlling the biodegradation of organic contaminants which are strongly adsorbed or which form a nonaqueous phase.

REFERENCES

American Public Health Association, Inc. 1981. Standard Methods for the Examination of Water and Wastewater. 15th ed. Washington D.C.

Atkinson, B. and S.Y. How. 1974. "The Overall Rate of Substrate Uptake (Reaction) by Microbial Films. Part II. Effect of Concentration and Thickness with Mixed Microbial Films." Transactions, Inst. Chem. Engrs. 52: 260-272.

Bouwer, E.J. 1987. "Biotransformations of Contaminants in Groundwater." Paper presented at the Third National Water Conference, Philadelphia, PA, January.

Bouwer, E.J. and P.L. McCarty. 1983. "Transformation of Halogenated Organic Compounds Under Denitrification Conditions." Appl. Environ. Microb. 45: 1295-1299.

Bouwer, E.J. and P.L. McCarty. 1985. "Utilization Rates of Trace Halogenated Organic Compounds in Acetate-Grown Biofilms." Biotech. and Bioengr. 27: 1564-1571.

Casolari, A. 1988. "Microbial Death." In Physiological Models in Microbiology, Vol. II. edited by M.J. Bazin and J.I. Prosser. 1-44. Boca Raton, FL: CRC Press, Inc.

Chang, H.T. 1985. Mathematical Modeling and Scanning Electron Microscopic Study of Biofilms on Adsorptive Media. Ph.D. Dissertation. Department of Civil Engineering, University of Illinois, Urbana, IL.

Daugherty, R. L. and J. B. Franzini. 1977. Fluid Mechanics with Engineering Applications. New York: McGraw-Hill.

Flathman, P.E. et al. 1983. Biological Spill Cleanup. Proc. Technical Seminar on Chemical Spills; October 25-27; Toronto. 117-130.

Flathman, P.E., J.R. Quince, and L.S. Bottomley. 1984. Biological Treatment of Ethylene Glycol-Contaminated Groundwater at Naval Air Engineering Center, Lakehurst, New Jersey. Proc. 4th National

Symposium on Aquifer Restoration and Ground Water Monitoring; May 23-25; Columbus, Ohio. 23-25.

Freeze, R.A. and J.A. Cherry. 1979. Groundwater. Englewood Cliffs, N.J.: Prentice-Hall.

Ghiorse, W.C. and D.L. Balkwill. 1983. "Enumeration and Morphological Characterization of Bacteria Indigenous to Subsurface Environments." Dev. Ind. Microb. 24.

Kobayashi, H. and B.E. Rittmann. 1982. "Microbial Removal of Hazardous Organic Compounds." Environ. Sci. Technol. 16: 170A-181A.

Kuhn, E.P., P.J. Colberg, J.L. Schnoor, O. Wanner, A.F.B. Zehnder, and R.P. Schwarzenbach. 1985. "Microbial Transformations of Substituted Benzenes during Infiltration of River Water to Groundwater: Laboratory Column Studies." Environ. Sci. Technol. 19: 961-968.

Lapidus, L. and G. F. Pinder. 1982. Numerical Solution of Partial Differential Equation in Science and Engineering. New York: J. Wiley and Sons, Inc.

Lee, E. S. 1968. Quasilinearization and Invariant Imbedding. New York: Academic Press.

Lyman, W.J., W.F. Reehl, and D.H. Rosenblatt. 1982. Handbook of Chemical Property Estimation Methods. New York: McGraw-Hill Book Co.

McCarty, P.L. 1972. "Energetics and Bacterial Growth." In Organic Compounds in Aquatic Environments. edited by S.D. Faust and J.V. Hunter. New York: Marcel Dekker, Inc.

McCarty, P.L., B.E. Rittmann, and M. Reinhard. 1981. "Trace Organics in Groundwater." Environ. Sci. Technol. 15: 40-51.

Miller, M.M., S. P. Wasik, G.-L. Huang, W.-Y. Shiu, and D. Mackay. 1985. "Relationship between Octanol-Water Partition Coefficient and Aqueous Solubility." Environ. Sci. Technol. 19: 522-529.

Nagel, G., W. Kuehn, P. Werner, and H. Sontheimer. 1982. "Sanitation of Groundwater by Infiltration of Ozone Treated Water." GWF-Wasser/Abwasser. 123: 399-407.

Namkung, E. 1985. Kinetics and Mechanisms of Low-Concentration Multisubstrate Utilization by Biofilms. Ph.D. Dissertation. Department of Civil Engineering, University of Illinois, Urbana, IL.

Namkung, E. and B.E. Rittmann. 1986. Soluble Microbial Products (SMP) Formation Kinetics by Biofilms. Water Research.20: 795-806.

Namkung, E., R.G. Stratton, and B.E. Rittmann. 1983. "Predicting Removal of Trace-Organic Compounds by Biofilms." J. Water Poll. Control Fed. 55: 1366-1372.

Parker, G.A. 1928. In Colorimetric Determination of Nonmetals, edited by D.R. Boltz and Z.A. Howell. New York: J. Wiley and Sons.

Rittmann, B.E. 1982a. "Comparative Performance of Biofilm Reactor Types." Biotech. and Bioengr 24: 1341-1370.

Rittmann, B.E. 1982b. "The Effect of Shear Loss on Biofilm Loss Rate." Biotech. and Bioengr. 24: 501-506.

Rittmann, B.E. and W.E. Langeland. 1985. "Simultaneous Denitrification with Nitrification in Single Channel Oxidation Ditches." J. Water Poll. Control Fed. 57: 300-308.

Rittmann, B.E. and P.L. McCarty. 1980a. "Evaluation of Steady-State Biofilm Kinetics." Biotech. and Bioengr. 22: 2359-2373.

Rittmann, B.E. and P.L. McCarty. 1980b. "Model of Steady-State Biofilm Kinetics." Biotech. and Bioengr. 22: 2343-2357.

Rittmann, B.E. and P.L. McCarty. 1981. "Substrate Flux into Biofilms of any Thickness." J. Environ. Engr. 107: 831-849.

Rittmann, B.E., P. L. McCarty, and P.V. Roberts. 1980. Trace-Organics Biodegradation in Aquifer Recharge. Ground Water. 18: 236-243.

Sáez, P.B. and B.E. Rittmann. 1988. An Improved Pseudo-Analytical Solution for Steady-State Biofilm Kinetics. Biotech. and Bioengr. 32: 362-368.

Stratton, R., E. Namkung, and B.E. Rittmann. 1983. "Biodegration of Trace-Organic Compounds by Biofilms on Porous Media." J. Amer. Water Works Assn. 75: 463-469.

Werner, P. 1985. "A New Way for the Decontamination of Polluted Aquifers by Biodegradation." Water Supply. 3: 41-47.

APPENDIX--NOMENCLATURE

Fundamental quantities

L	length
M	mass, in general
M_S	mass of substrate
M_X	mass of bacteria
T	time

English symbols

a	surface area per reactor volume (L^{-1})
b	specific decay or maintenance-respiration coefficient (T^{-1})
b_S	coefficient of specific biofilm loss due to shearing (T^{-1})
b_T	overall first-order biofilm loss coefficient (T^{-1})
d_p	particle diameter (L)
D	molecular diffusion coefficient of substrate in water (L^2T^{-1})
D_H	hydrodynamic diffusion coefficient (L^2T^{-1})
D_f	molecular diffusion coefficient of substrate in biofilm (L^2T^{-1})
f	ratio between the fluxes in actual and deep biofilms
J	substrate flux into biofilm ($M_SL^{-2}T^{-1}$)
J_{deep}	minimum substrate flux into a deep steady-state biofilm ($M_SL^{-2}T^{-1}$)
$J(S^m)$	substrate flux at a gridpoint and iteration level m ($M_SL^{-2}T^{-1}$)
k	maximum specific rate of substrate utilization ($M_SM_X^{-1}T^{-1}$)
K_S	half-maximum-rate substrate concentration (M_SL^{-3})
L	thickness of effective diffusion layer (L)
L_f	biofilm thickness (L)
L_{fi}	biofilm thickness at a gridpoint i (L)
L_T	total length of reactor (L)
n	number of gridpoints used in numerical model
Q_S	substrate source due to lateral input through injection ports ($M_SL^{-3}T^{-1}$)
r_{diff}	rate of substrate accumulation due to diffusion ($M_SL^{-3}T^{-1}$)
r_{ut}	rate of substrate accumulation due to substrate utilization ($M_SL^{-3}T^{-1}$)
S	rate-limiting substrate concentration (M_SL^{-3})
S_b	bulk-liquid substrate concentration (M_SL^{-3})
S_i	rate-limiting substrate concentration at gridpoint i (M_SL^{-3})

S^{in} substrate concentration at the inlet of reactor ($M_S L^{-3}$)

S_{min} minimum bulk substrate concentration of the rate-limiting substrate able to sustain a steady-state biofilm ($M_S L^{-3}$)

S_o initial substrate concentration at time=0 ($M_S L^{-3}$)

S^o influent concentration of rate-limiting substrate ($M_S L^{-3}$)

S_s substrate concentration at liquid-biofilm interface ($M_S L^{-3}$)

S_t substrate concentration at time=t ($M_S L^{-3}$)

S^m rate-limiting substrate concentration at iteration level m ($M_S L^{-3}$)

ΔS change in substrate concentration ($M_S L^{-3}$)

t time (T)

Δt change in time (T)

v superficial flow velocity (LT^{-1})

x longitudinal distance into the reactor (L)

Δx grid-spacing for the numerical model (L)

X_f biomass density in the biofilm ($M_x L^{-3}$)

X_o biomass concentration at time=0 ($M_x L^{-3}$)

X_t biomass concentration at time=t ($M_x L^{-3}$)

ΔX change in biomass concentration ($M_x L^{-3}$)

Y true yield of bacterial mass per unit substrate mass utilized ($M_x M_s$)

z distance normal to biofilm surface (L)

Dimensionless symbols

D_f^* dimensionless molecular diffusion coefficient of substrate in biofilm [= D_f/D]

J^* dimensionless substrate flux into the biofilm $\left[= \frac{J}{(K_s k X_f D_f)^{1/2}}\right]$

J^*_{deep} dimensionless substrate flux into a deep biofilm $\left[= \frac{J_{deep}}{(K_s k X_f D_f)^{1/2}}\right]$

K^* dimensionless kinetic parameter $\left[= \left(\frac{D}{L}\right) \left[\frac{K_s}{(kX_f D_f)}\right]^{1/2}\right]$

L^* dimensionless diffusive layer thickness [= L/τ]

L_f^* dimensionless biofilm thickness [= $L_f [(kX_f)/(D_f K_s)]^{1/2}$]

S_s^* dimensionless substrate concentration at the liquid-biofilm interface [= (S_s/K_s)]

S_{min}^* dimensionless minimum bulk substrate concentration of the rate-limiting substrate able to sustain a steady-state biofilm $\left[=\frac{b_T}{Yk - b_T}\right]$

S_b^* dimensionless bulk substrate concentration [= (S_b/K_s)]

Greek symbols

α product coefficient in the factor f

β exponential coefficient in the factor f

ε porosity or bed voidage

η effectiveness factor, ratio of actual and fully-penetrated substrate fluxes at a given S_s

μ_m maximum specific cell growth rate (T^{-1})

μ specific cell growth rate (T^{-1})

τ standard biofilm depth dimension (L) $[=\sqrt{2K_sD_f/kX_f}]$,

ϕ coefficient used in flux estimation of secondary substrates $\left[= \frac{\sqrt{2}\ L_f^*}{(1 + 2S_s^{*'})^{1/2}}\right]$

Ω convergence criteria of numerical method